Sub-Nyquist artifacts and sampling moiré effects Part 2: Spectral-domain analysis

Isaac Amidror

IC-LSP, EPFL
1015 Lausanne
Switzerland

ABSTRACT

Sampling moiré effects occur due to aliasing (foldover) when a continuous periodic signal $g(x)$ is sampled using a sampling frequency that does not respect the Nyquist condition. However, visible beating artifacts may also occur when $g(x)$ is sampled using sampling frequencies which fully respect the Nyquist condition. These moiré-like effects, that we call *sub-Nyquist artifacts*, are more difficult to analyze since they are not visible by our main moiré investigation tool, the Fourier theory. In a recent publication we have addressed this difficulty by bypassing spectral-domain considerations, and studying these phenomena using a signal-domain approach. In the present contribution we go further ahead, and show how, in spite of this difficulty, we can still interpret the phenomena in question from the spectral-domain point of view. This also leads us to new interesting connections between sampling-related phenomena in the discrete world and modulation (beating) phenomena which occur in the purely continuous world, known in acoustics as "beats of mistuned consonances".

Keywords: sampling, reconstruction, moiré effects, sub-Nyquist artifacts, modulation, beats

1. Introduction

In a previous publication [1] we have reviewed the beating artifacts that may occur when sampling a periodic signal $g(x)$ of frequency f using a sampling frequency f_s. Obviously, when the sampling frequency f_s does not respect the Nyquist condition of the sampling theorem (i.e. when f_s is not at least twice the highest frequency contained in $g(x)$), various moiré or aliasing artifacts may appear in the resulting sampled signal $g(x_k)$ (see, for example, Figs. 1 and 2). But we have also seen, as already mentioned in [2], [3, p. 642] or [4, pp. 222, 225], that some beating artifacts (pseudo moirés) may still appear in the sampled signal $g(x_k)$ even when f_s *does* respect the Nyquist condition.

These beating artifacts are intriguing for several reasons: (a) They appear where the Nyquist condition is fully satisfied, so that no aliasing or moiré artifacts should be present. (b) Their periods (or frequencies) are not represented in the Fourier spectrum, although they are clearly visible in the sampled signal. (c) Furthermore, in the signal domain, the beating effect in question does not really correspond to a smooth low-frequency signal, but rather to a highly oscillating signal that is only *modulated* by low-frequency envelopes. For these reasons, the phenomena in question are not considered

as true sampling moiré effects. And yet, as described in [1], in many aspects their behaviour is very similar to that of true moirés.

The fact that these moiré-like artifacts are not visible by our main moiré investigation tool, the Fourier theory (see point (b) above), makes them more difficult to analyze. This difficulty was addressed in [1] by means of a theorem that explains these phenomena from the signal-domain point of view, i.e. in terms of the sampled points themselves. For the sake of completeness, this theorem is presented below in Appendix C, Remark 9.

This signal-domain approach provides, indeed, a good explanation of the sub-Nyquist artifacts and the sampling moiré effects. Nevertheless, it is well known (both in signal processing and in the moiré theory) that spectral-domain considerations may often offer a new, wider perspective on the phenomena in question. It may be asked, therefore, whether or not this general rule applies to our case, too, even though sub-Nyquist artifacts are not directly visible in the Fourier spectrum.

In the present contribution we answer this question in the affirmative, and show how the phenomena in question can be understood from the point of view of the Fourier spectral domain, in spite of the inherent difficulties. This spectral-domain approach will shed a new light on the sub-Nyquist artifacts, their origins, their properties, and their relationship with the true sampling moiré effects. In particular, this approach will provide new interesting connections between the phenomena which occur in the discrete world due to the sampling process, and modulation (beating) phenomena which occur in the purely continuous world, known in acoustics as “beats of mistuned consonances”.

The present work is structured as follows: Sec. 2 provides our initial background, and sets up the basic notions that will be used in the sequel. Then, in Sec. 3 we develop our spectral-domain strategy, starting with the simple case of the cosine signal. In Sec. 4 we extend this spectral-domain approach to any general periodic signals. In Sec. 5 we discuss, based on the spectral-domain point of view, the effect of poor reconstruction on the visibility of sub-Nyquist artifacts. And finally, we present our conclusions in Sec. 6.

Figure 1: The artifact that occurs when $f \approx (1/1)f_s$ (which is, in fact, a true (1,-1)-order sampling moiré). Each row shows in the left-hand column the periodic signal $g(x) = \cos(2\pi fx)$ having frequency f, as well as its sampled version after being sampled with a sampling frequency of $f_s = 8.0$ (i.e. with a sampling interval of $\Delta x = 1/f_s = 1/8$). The right-hand column shows the respective CFT (continuous Fourier transform) of the continuous signal $g(x)$, along with the DFT (discrete Fourier transform) of its sampled version (after having applied the required reorganizations and scalings; see, for example, [5]). The only difference between the 5 rows is in the frequency f of the original signal $g(x)$: (a) $f = f_s$ (the singular state). (b) $f = f_s - 1/32$. (c) $f = f_s - 1/16$. (d) $f = f_s - 1/8$. (e) $f = f_s - 1/4$. Note that the new low frequency of this sampling moiré effect is clearly visible both in the sampled signal and in its DFT (although it does not exist in the original continuous signal and in its CFT).

Signal domain $\boxed{\frac{m}{n}=\frac{1}{1}}$ Spectral domain

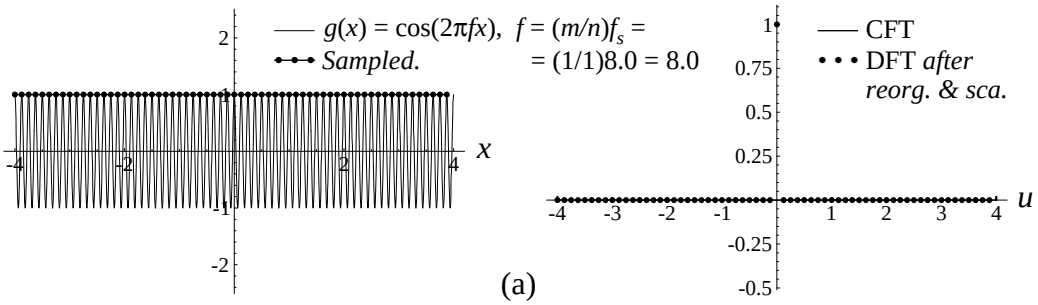

(a)

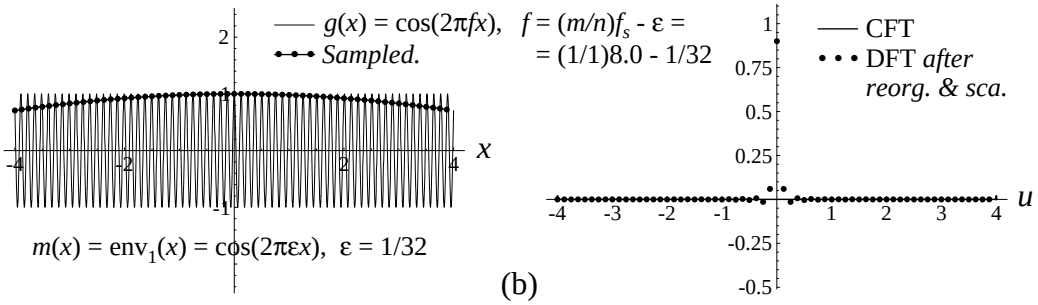

(b)

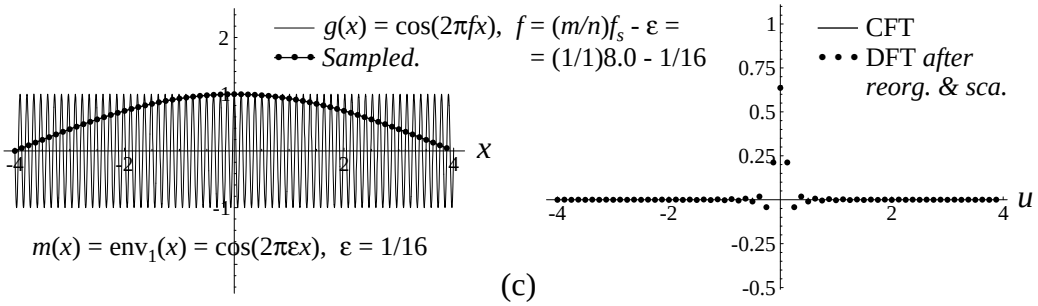

(c)

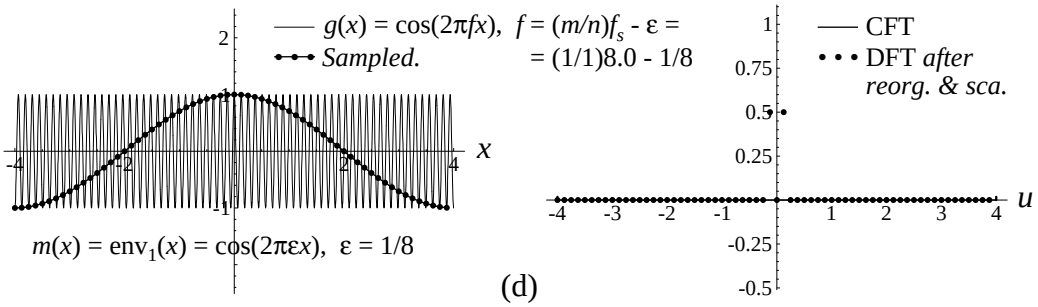

(d)

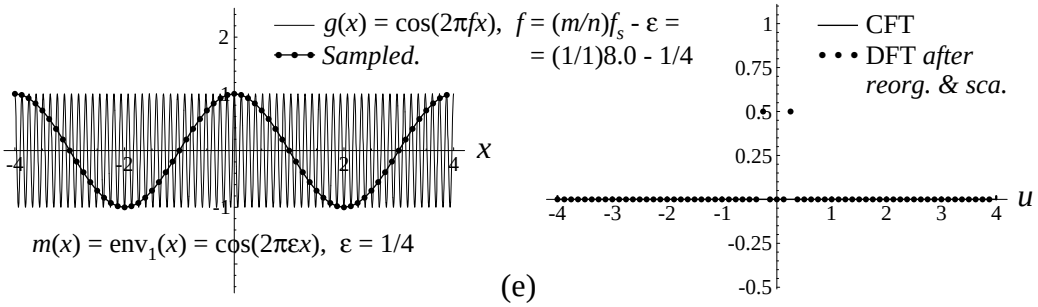

(e)

2. Background: sub-Nyquist artifacts vs. true sampling moiré effects

As we have seen in [1], when sampling a periodic function $g(x)$ of frequency f using a sampling frequency f_s, sampling artifacts may occur whenever f and f_s satisfy $f \approx \frac{m}{n} f_s$, where m and n are integer numbers. When $n = 1$ the resulting artifact is a true sampling moiré effect: a $(m,-1)$-moiré that occurs when $mf_s - f \approx 0$, and whose frequency is $f_M = mf_s - f$. But when $n > 1$ the resulting artifact is a (m/n)-order sub-Nyquist artifact, a beating artifact (pseudo moiré) that is modulated by n interlaced envelopes having the frequency $\varepsilon = \frac{m}{n} f_s - f$.

A sampling moiré effect occurs in a sampled signal due to aliasing. It appears in the signal domain as a new visible low-frequency signal having frequency f_M that passes through the very same sampling points $g(x_k)$ and mimics the original signal $g(x)$ (see, for example, Figs. 1 and 2). A sampling moiré effect is visible in the Fourier domain, too, where it appears as a new, false folded-over low-frequency f_M that did not exist in the original continuous signal before sampling. On the other hand, although a sub-Nyquist artifact is clearly visible in the sampled signal as a new low-frequency beating effect, this new low frequency ε is not directly represented in the Fourier spectrum.

To better illustrate this difference, let us compare the spectra of the sampled signals in Figs. 1 and 2, which show true sampling moiré effects, with those in Figs. 3-5, which show sub-Nyquist artifacts. In Figs. 1 and 2, the DFT (Discrete Fourier Transform) of the sampled signal $g(x_k)$ contains new low frequencies near the spectrum origin, which did not exist in the CFT (Continuous Fourier Transform) of the original signal $g(x)$. These new frequencies in the spectral domain correspond to the new low-frequency sampling moiré effect which is generated in the sampled signal due to aliasing (foldover).[1] However, in Figs. 3-5, which correspond to sub-Nyquist artifacts, no such new low frequencies appear in the DFT of the sampled signal, in spite of the new low-frequency beating artifacts that are clearly visible in the sampled signal itself.[2] This spectral-domain contrast between true sampling moiré effects and sub-Nyquist artifacts may seem surprising at first sight, but in fact it can be understood quite intuitively as

Figure 2: The artifact that occurs when $f \approx (2/1)f_s$ (which is, in fact, a true (2,-1)-order sampling moiré). This figure is similar to Fig. 1, except for the signal-frequency f being used in each row: (a) $f = 2f_s$ (the singular state). (b) $f = 2f_s - 1/32$. (c) $f = 2f_s - 1/16$. (d) $f = 2f_s - 1/8$. (e) $f = 2f_s - 1/4$. Like in Fig. 1, the new low frequency of this sampling moiré effect is clearly visible both in the sampled signal and in its DFT (although it does not exist in the original continuous signal and in its CFT).

---

[1] Note that the spectra in our figures show both the CFT of the original continuous signal $g(x)$ and the DFT of the sampled signal $g(x_k)$. All the required DFT normalizations (reorganizations and scalings) have been applied, as explained, for example, in Chapters 3 and 4 of [5].

[2] In fact, as we will see later on, this difference between true sampling moiré effects and sub-Nyquist artifacts also exists in the *CFT of the sampled signal*, which is shown in Figs. 6-8 but not in Figs. 1-5.

Signal domain $\boxed{\frac{m}{n} = \frac{2}{1}}$ Spectral domain

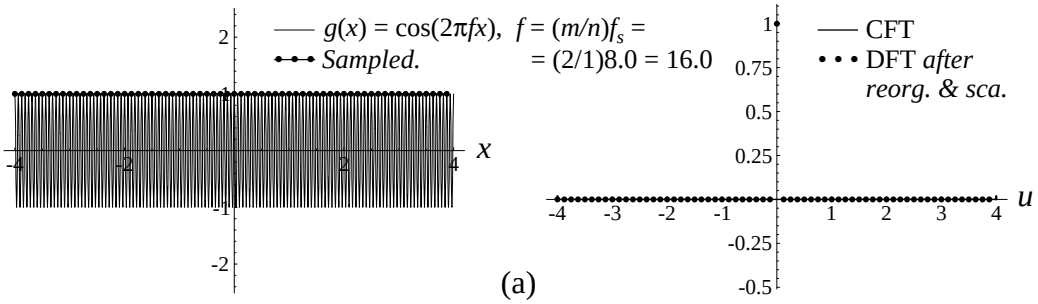

(a)

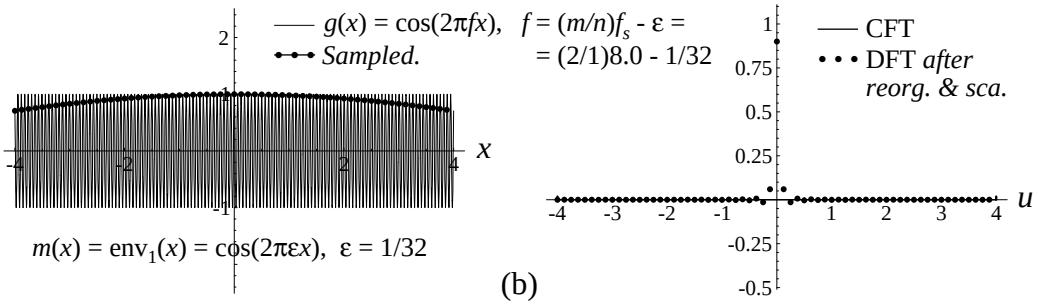

$m(x) = \text{env}_1(x) = \cos(2\pi\varepsilon x)$, $\varepsilon = 1/32$

(b)

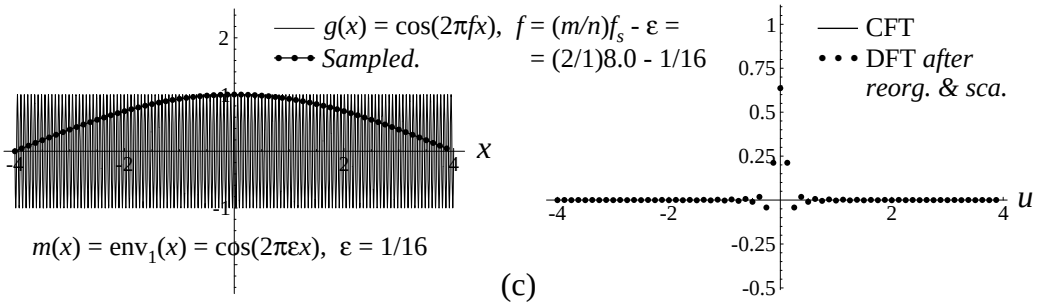

$m(x) = \text{env}_1(x) = \cos(2\pi\varepsilon x)$, $\varepsilon = 1/16$

(c)

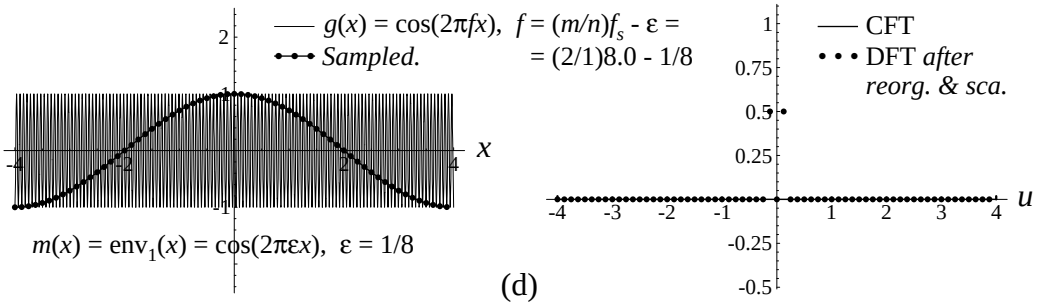

$m(x) = \text{env}_1(x) = \cos(2\pi\varepsilon x)$, $\varepsilon = 1/8$

(d)

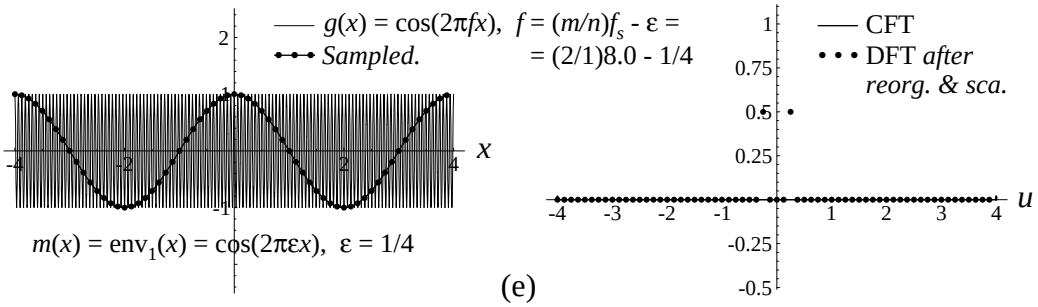

$m(x) = \text{env}_1(x) = \cos(2\pi\varepsilon x)$, $\varepsilon = 1/4$

(e)

follows: If we apply to our sampled signal $g(x_k)$ in Figs. 1 and 2 a smoothing filter (such as a moving average of $g(x_k)$ [6, pp. 277-280]), the results will indeed show a low-frequency signal which did not exist in the original continuous signal $g(x)$ before sampling. But if we apply the same smoothing (moving average) to our sampled signal in Figs. 3-5, the resulting signal will be identically zero. This means that in this case no new low-frequency content really exists in the sampled signal. In other words, the beating artifact we see in the sampled signal in this case is not a true low-frequency component (a moiré effect), but rather a modulation effect.[3]

So how can we explain the low-frequency beating artifacts that are clearly visible in the sampled signal in cases like Figs. 3-5, although they are not represented in the corresponding spectra? A signal-domain explanation was already presented in [1]. In the following sections we will show that a spectral-domain interpretation can be also given, in spite of the apparent difficulties. Moreover, we will see that the spectral-domain approach sheds new light on the phenomena in question and illuminates them from a completely different angle.

3. Spectral-domain explanation of the sub-Nyquist artifacts in cosine functions

For the sake of simplicity, we start our spectral-domain analysis with the simplest setting, in which the continuous-world function being sampled is $g(x) = \cos(2\pi fx)$. Let us first study the spectral-domain situation in two simple examples, that will give us a deeper insight and guide us to the explanation of the general case.

3.1 The case of the (1/2)-order sub-Nyquist artifact

A (1/2)-order sub-Nyquist artifact appears in the sampled signal when we sample at the sampling rate f_s an original cosine function $g(x) = \cos(2\pi fx)$ whose frequency f is close to $\frac{1}{2}f_s$, namely $f \approx \frac{1}{2}f_s$ or:

$$f = \tfrac{1}{2}f_s - \varepsilon \qquad (1)$$

Figure 3: The (1/2)-order sub-Nyquist artifact. This figure is similar to Figs. 1-2, except for the signal-frequency f being used in each row: (a) $f = \frac{1}{2}f_s$ (the singular state). (b) $f = \frac{1}{2}f_s - 1/32$. (c) $f = \frac{1}{2}f_s - 1/16$. (d) $f = \frac{1}{2}f_s - 1/8$. (e) $f = \frac{1}{2}f_s - 1/4$. The highly visible (1/2)-order sub-Nyquist artifact is generated because consecutive points $g(x_k)$ of the sampled signal alternately jump between the $n = 2$ modulating envelopes (each of the two modulating envelopes being simply a stretched and shifted version of $g(x)$). These two interlaced modulating envelopes are highlighted in the figure in different colours. Note that their new low frequency is not visible in the DFT of the sampled signal.

[3] This intuitive explanation will be treated more rigorously in Sec. 4.2. We will see there the precise meaning of the "moving average", and discuss its role as a centreline of the rapid oscillations in the sub-Nyquist artifact.

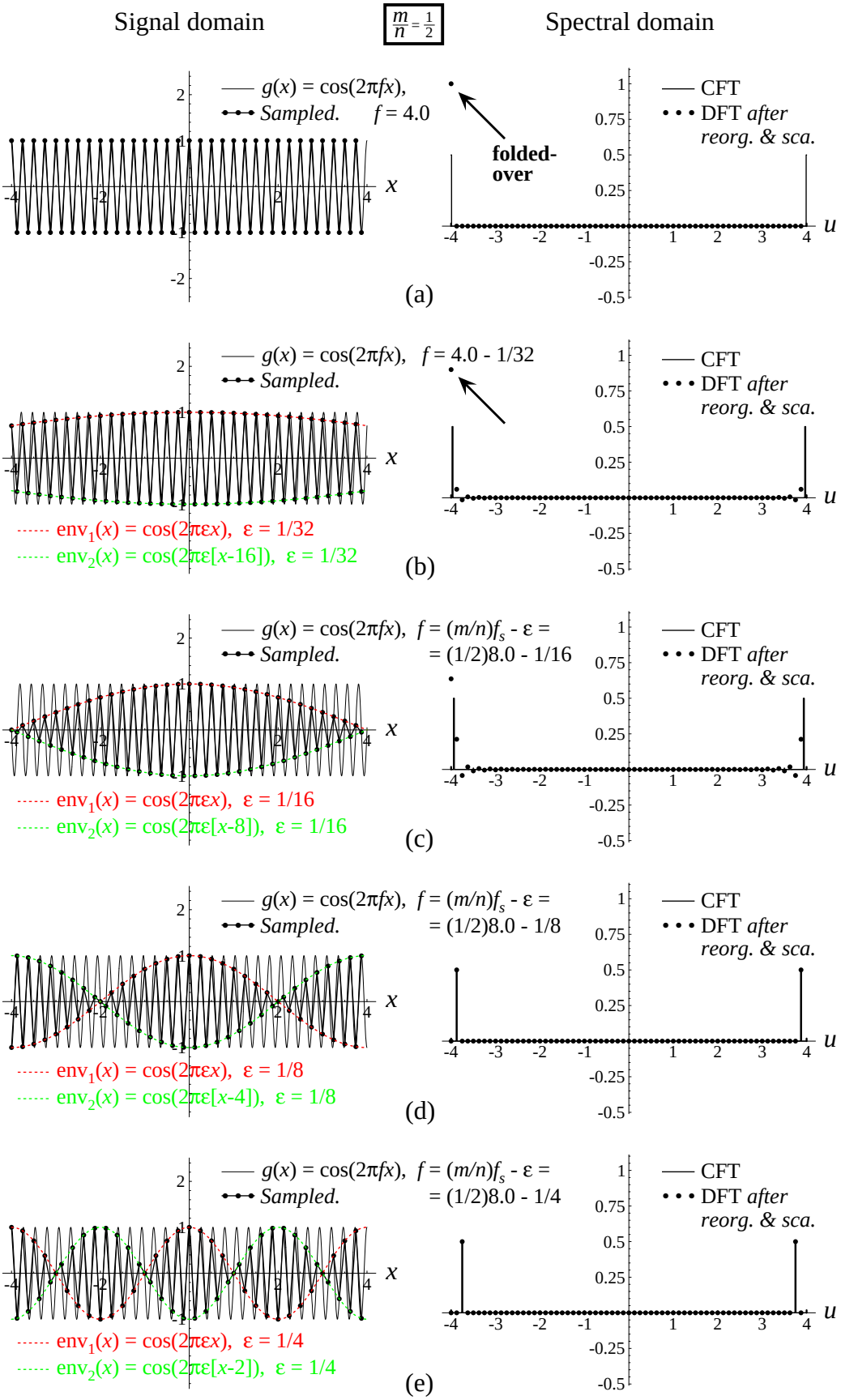
Signal domain
m/n = 1/2
Spectral domain
g(x) = cos(2πfx),
Sampled.
f = 4.0
folded-over
CFT
DFT after reorg. & sca.
x
u
(a)
g(x) = cos(2πfx), f = 4.0 - 1/32
Sampled.
CFT
DFT after reorg. & sca.
env1(x) = cos(2πεx), ε = 1/32
env2(x) = cos(2πε[x-16]), ε = 1/32
(b)
g(x) = cos(2πfx), f = (m/n)fs - ε =
= (1/2)8.0 - 1/16
Sampled.
CFT
DFT after reorg. & sca.
env1(x) = cos(2πεx), ε = 1/16
env2(x) = cos(2πε[x-8]), ε = 1/16
(c)
g(x) = cos(2πfx), f = (m/n)fs - ε =
= (1/2)8.0 - 1/8
Sampled.
CFT
DFT after reorg. & sca.
env1(x) = cos(2πεx), ε = 1/8
env2(x) = cos(2πε[x-4]), ε = 1/8
(d)
g(x) = cos(2πfx), f = (m/n)fs - ε =
= (1/2)8.0 - 1/4
Sampled.
CFT
DFT after reorg. & sca.
env1(x) = cos(2πεx), ε = 1/4
env2(x) = cos(2πε[x-2]), ε = 1/4
(e)

This is illustrated in Fig. 3, which shows the resulting beating artifact for several values of f around the frequency $\frac{1}{2}f_s$ (i.e. for several values of ε). The sampling frequency used in Fig. 3 (as well as in all our figures here) is $f_s = 8$, so that the maximum frequency allowed by the sampling theorem without causing aliasing is $\frac{1}{2}f_s = 4$.[4]

Consider for instance the (1/2)-order sub-Nyquist artifact that is shown in Fig. 3(e). The frequency of the continuous cosine function being sampled in this case is $f = 3.75$, which is indeed lower by $\varepsilon = 0.25$ than the maximum frequency $\frac{1}{2}f_s$ allowed by the sampling theorem. As we can see in the figure, the resulting sampled signal has a beating effect with an envelope period of length 4, i.e. an envelope frequency of $\varepsilon = 0.25$.

In order to understand this beating effect from the spectral-domain point of view, consider the two first rows of Fig. 6. These two rows show in the *continuous-world spectrum* what happens when we sample a continuous cosine function $g(x) = \cos(2\pi fx)$ having the frequency $f = \frac{1}{2}f_s - \varepsilon$ using the sampling frequency f_s. The reason we prefer to use here the continuous-world spectrum (CFT) of the sampled signal is that CFT spectra are easier to understand than DFT spectra (such as in Fig. 3): Their frequency range is not limited, and they do not suffer from wraparound and foldover of higher frequencies as DFT spectra do.[5]

Fig. 6(a) shows the continuous-world spectrum $G(u)$ of our original, unsampled cosine function $g(x)$. This spectrum consists of an impulse pair at the frequencies $\frac{1}{2}f_s - \varepsilon$ and $-\frac{1}{2}f_s + \varepsilon$. Fig. 6(b) shows the continuous-world spectrum of $g(x_k)$, the sampled counterpart of our cosine $g(x)$. As we know from sampling theory, if the CFT of $g(x)$ is $G(u)$, then the continuous-world spectrum of the sampled version of $g(x)$ consists of infinitely many replicas of the original spectrum $G(u)$, which are centered about all the integer multiples of the sampling frequency f_s (see, for example, [7, p. 222] or [5, p. 92]). Fig. 6(b) shows only five of these replicas, namely, the original one (which is identical, up to a certain amplitude scaling factor, to row (a) of the figure) plus its two nearest neighbours to each direction, that are centered about f_s, $2f_s$, $-f_s$, and $-2f_s$. As we can see in Fig. 6(b), these new sampling-induced replicas add to the continuous-world spectrum infinitely many new impulses. In particular, note that a new impulse pair is added just slightly beyond the impulse pair of our original cosine, i.e. at the frequencies $\frac{1}{2}f_s + \varepsilon$ and $-\frac{1}{2}f_s - \varepsilon$. This new impulse pair corresponds to a newly added cosine in the signal domain, whose frequency is $\frac{1}{2}f_s + \varepsilon$.

Thus, the central part of the spectrum shown in Fig. 6(b) corresponds in the signal domain to a sum of two cosines: our original continuous cosine, whose frequency $f = \frac{1}{2}f_s - \varepsilon$ is slightly below $\frac{1}{2}f_s$, and a new continuous cosine, whose frequency $f' = \frac{1}{2}f_s + \varepsilon$ is slightly above $\frac{1}{2}f_s$. Let us denote the sum of these two cosines (with halved amplitudes, for reasons we will soon see below) by $g_A(x)$:

---

[4] Note that this is also the maximum frequency in the DFT spectrum; see, for example, Eq. (4.10) in [5, p. 73].

[5] Note that the spectral domain in each row of Figs. 1-5 shows only the CFT of the original continuous function $g(x)$, and the DFT of the sampled signal $g(x_k)$. The CFT of the sampled signal is not shown there due to lack of room, but some particular cases are shown separately in Figs. 6-8.

$$g_A(x) = \tfrac{1}{2}\cos(2\pi fx) + \tfrac{1}{2}\cos(2\pi f'x)$$

$$= \tfrac{1}{2}\cos(2\pi[\tfrac{1}{2}f_s - \varepsilon]x) + \tfrac{1}{2}\cos(2\pi[\tfrac{1}{2}f_s + \varepsilon]x) \qquad (2)$$

The spectrum $G_A(u)$ of this continuous-world sum of cosines is shown in Fig. 6 in a separate panel (a′). Now, we claim that the continuous-world spectrum shown in row (b) of Fig. 6 is also the spectrum of the sampled version of $g_A(x)$, using the same sampling frequency f_s. To see this, note that the spectrum in row (b) can be also considered as an infinite replication of the spectrum $G_A(u)$, where the replicas are located, once again, about all the integer multiples of f_s: Because the impulse pairs of every two neighbouring replicas of $G_A(u)$ fall exactly at the same points along the u axis, their halved amplitudes simply add up on top of each other, giving back precisely the spectrum shown in row (b). This means that the continuous-world spectrum in row (b) belongs not only to the sampled version of our original cosine function $g(x) = \cos(2\pi fx)$, but also to the sampled version of the cosine sum $g_A(x)$. This means, in turn, that the *sampled* version of our original cosine $g(x)$ is identical to the *sampled* version of the cosine sum $g_A(x)$ (although obviously $g(x)$ and $g_A(x)$ themselves are different):

$$g(x_k) = g_A(x_k) \qquad \text{at all the sampling points } x_k \qquad (3)$$

Let us try to figure out the shape of the continuous cosine sum $g_A(x)$, in order to deduce therefrom the shape of its sampled version $g_A(x_k)$ and hence the shape of our sampled cosine $g(x_k)$. As reminded in Appendix A, the sum of two continuous cosines with close frequencies f_1 and f_2 gives a continuous-world beating effect (pseudo moiré) whose envelope frequency is $f_{\text{env}} = \frac{1}{2}(f_2 - f_1)$. In our present case the two close cosine frequencies in the sum $g_A(x)$ are $f_1 = f$ and $f_2 = f' = f + 2\varepsilon$ (see Fig. 6(b)), and therefore we have $f_{\text{env}} = \frac{1}{2}(f_2 - f_1) = \varepsilon$. Since this frequency (the envelope frequency of the continuous-world beats in $g_A(x)$) is very low with respect to our sampling frequency f_s, it is clear that the beating effect will be captured by the sampled signal $g_A(x_k)$, and hence by our sampled cosine, $g(x_k)$. And indeed, a glimpse at Fig. 3 confirms that the beating effect we obtain in our sampled cosine has the envelope frequency of $f_{\text{env}} = \varepsilon$. For example, in the case shown in Fig. 3(e) this beating effect has the envelope frequency of $\varepsilon = \frac{1}{4}$, i.e. an envelope period of 4. Note that this low-frequency artifact in our sampled signal is more prominent than the original cosine itself. But this beating effect is a sub-Nyquist artifact and not an aliasing or sampling-moiré artifact, since the frequency of the original continuous cosine being sampled here, $f = \frac{1}{2}f_s - \varepsilon = 3.75$, is lower than the maximum frequency allowed by the sampling theorem, $\frac{1}{2}f_s = 4$.

In conclusion, the spectral-domain explanation of our (1/2)-order sub-Nyquist artifact is quite straightforward: The beating effect we get when sampling an original continuous signal $g(x) = \cos(2\pi fx)$ whose frequency is $f = \frac{1}{2}f_s - \varepsilon$ is simply the sampled version of the continuous-world beating modulation effect that occurs in the continuous cosine sum $g_A(x)$. This is clearly illustrated in Fig. B1 of Appendix B. Now, as stipulated by Theorem A.1 in Appendix A, this continuous-world modulation effect consists of two interlaced low-frequency cosinusoidal envelopes, each of which being a stretched and shifted version of our original cosine $g(x)$. These two interlaced envelopes, which are highlighted in Fig. 3 by different colours, are expressed by:

$$\begin{aligned} \mathrm{env}_1(x) &= \cos(2\pi f_{\mathrm{env}} x) = \cos(2\pi\varepsilon x) \\ \mathrm{env}_2(x) &= \cos(2\pi\varepsilon[x + a]) \end{aligned} \tag{4}$$

where the envelope frequency is $\varepsilon = \frac{1}{2}f_s - f$, and the shift a equals half of the envelope's period $1/\varepsilon$, i.e. $a = 1/(2\varepsilon)$. Because the frequency ε is much lower than the frequency f of the original cosine signal $g(x)$ being sampled, this sampling-induced artifact may be quite visible, and distort our perception of the true nature of the original signal. And yet, the low frequency ε itself is not present in the CFT or DFT of our sampled signal.

3.2 The case of the (1/3)-order sub-Nyquist artifact

We have seen above the spectral-domain explanation of the (1/2)-order sub-Nyquist artifact. But as already mentioned in [2] and later in [1], similar sub-Nyquist artifacts may also appear at other alias-free combinations of signal and sampling frequencies, i.e. in cases with other m,n combinations. Before we proceed to the spectral-domain explanation of the general (m/n)-order sub-Nyquist artifact, let us first consider the particular case with (m/n) = (1/3).

Suppose we sample at the rate of f_s an original cosine function $g(x) = \cos(2\pi fx)$ whose frequency f is close to $\frac{1}{3}f_s$, namely $f \approx \frac{1}{3}f_s$ or:

$$f = \tfrac{1}{3}f_s - \varepsilon \tag{5}$$

This time, a (1/3)-order sub-Nyquist artifact will appear in the sampled signal. This is illustrated in Fig. 4, which shows the resulting beating artifact for several values of f around the frequency $\frac{1}{3}f_s$ (i.e. for several values of ε). As we can see in the figure, in this case, too, the beating artifact has an envelope frequency of ε, i.e. an envelope period of length $1/\varepsilon$. To better understand this from the spectral-domain point of view, consider Fig. 7(d), which shows the continuous-world spectrum of our sampled signal $g(x_k)$. As we can see, the situation in this spectrum is very similar to the situation in Fig. 6(b): In both cases, the continuous-world spectrum of the sampled cosine signal $g(x_k)$ consists of an infinite replication of the spectrum of the original cosine $g(x) = \cos(2\pi fx)$, $G(u) = \frac{1}{2}\delta(u-f) + \frac{1}{2}\delta(u+f)$, where the replicas are centered about all the integer multiples of the sampling frequency f_s. And in both cases, these new sampling-induced replicas add to the original continuous-world spectrum a new impulse pair that is located just slightly

Figure 4: The (1/3)-order sub-Nyquist artifact. This figure is similar to Figs. 1-3, except for the signal-frequency f being used in each row: (a) $f = \frac{1}{3}f_s$ (the singular state). (b) $f = \frac{1}{3}f_s - 1/32$. (c) $f = \frac{1}{3}f_s - 1/16$. (d) $f = \frac{1}{3}f_s - 1/8$. (e) $f = \frac{1}{3}f_s - 1/4$. The highly visible (1/3)-order sub-Nyquist artifact is generated because consecutive points $g(x_k)$ of the sampled signal alternately jump between the $n = 3$ modulating envelopes (each of these modulating envelopes being simply a stretched and shifted version of $g(x)$). These three interlaced modulating envelopes are highlighted in the figure in different colours. Note that their new low frequency is not visible in the DFT of the sampled signal.

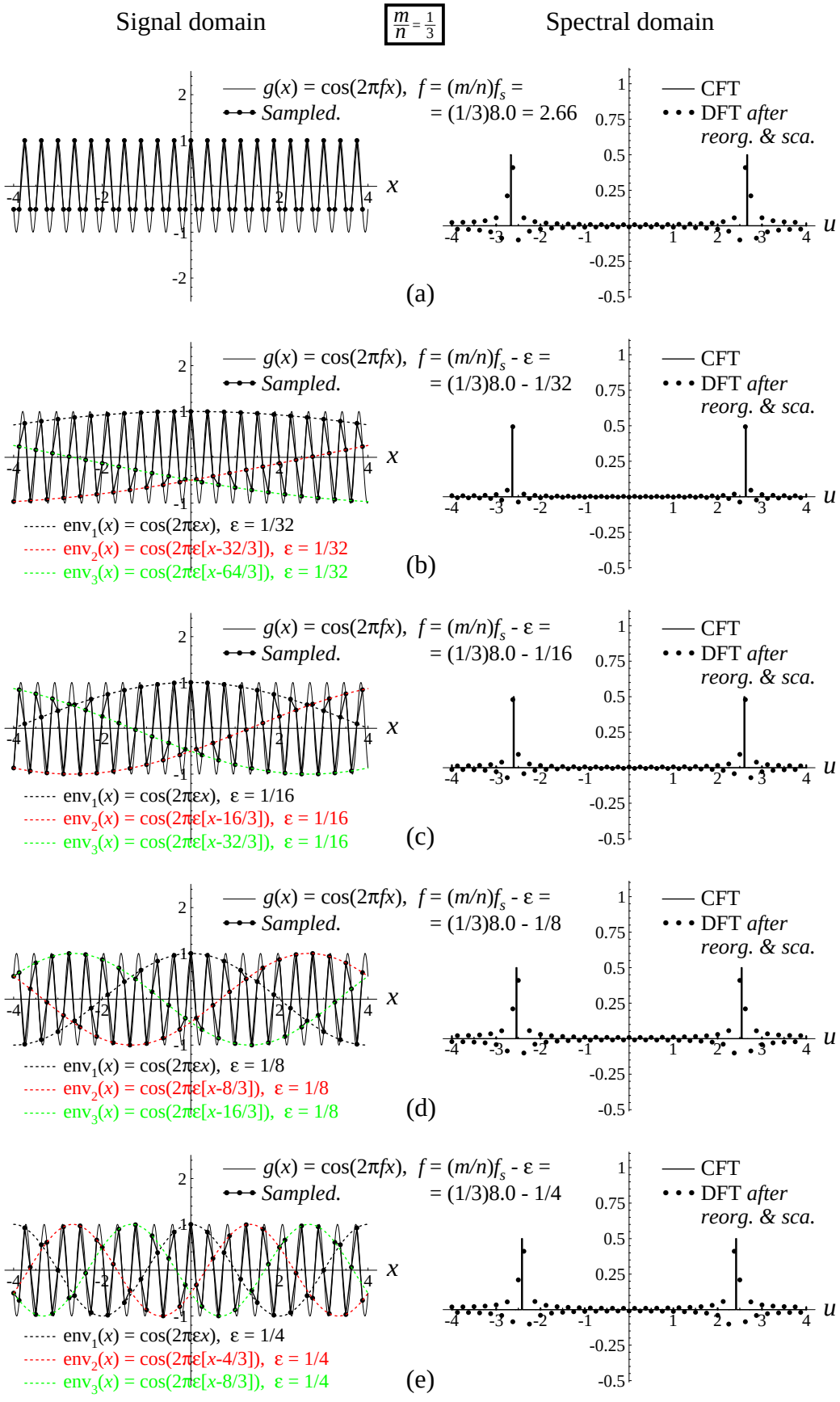
Signal domain
m/n = 1/3
Spectral domain
g(x) = cos(2πfx), f = (m/n)f_s =
= (1/3)8.0 = 2.66
Sampled.
CFT
DFT after reorg. & sca.
x
u
(a)
g(x) = cos(2πfx), f = (m/n)f_s - ε =
= (1/3)8.0 - 1/32
env1(x) = cos(2πεx), ε = 1/32
env2(x) = cos(2πε[x-32/3]), ε = 1/32
env3(x) = cos(2πε[x-64/3]), ε = 1/32
(b)
g(x) = cos(2πfx), f = (m/n)f_s - ε =
= (1/3)8.0 - 1/16
env1(x) = cos(2πεx), ε = 1/16
env2(x) = cos(2πε[x-16/3]), ε = 1/16
env3(x) = cos(2πε[x-32/3]), ε = 1/16
(c)
g(x) = cos(2πfx), f = (m/n)f_s - ε =
= (1/3)8.0 - 1/8
env1(x) = cos(2πεx), ε = 1/8
env2(x) = cos(2πε[x-8/3]), ε = 1/8
env3(x) = cos(2πε[x-16/3]), ε = 1/8
(d)
g(x) = cos(2πfx), f = (m/n)f_s - ε =
= (1/3)8.0 - 1/4
env1(x) = cos(2πεx), ε = 1/4
env2(x) = cos(2πε[x-4/3]), ε = 1/4
env3(x) = cos(2πε[x-8/3]), ε = 1/4
(e)

beyond the impulse pair of the original continuous cosine. Now, just as we did in the previous case, we consider the sum of the two corresponding cosine functions back in the signal domain (with halved amplitudes):

$$g_A(x) = \tfrac{1}{2}\cos(2\pi f x) + \tfrac{1}{2}\cos(2\pi f' x)$$

and show, exactly in the same way, that its sampled version at the sampling rate of f_s satisfies Eq. (3).

But while in the previous case (Fig. 6(b)) the frequency of the original cosine and the frequency of the newly added cosine were $f = \frac{1}{2}f_s - \varepsilon$ and $f' = \frac{1}{2}f_s + \varepsilon$, respectively, in our present case the frequency of the original cosine is $f = \frac{1}{3}f_s - \varepsilon$ and the frequency of the newly added cosine is $f' = f_s - (\frac{1}{3}f_s - \varepsilon) = \frac{2}{3}f_s + \varepsilon$ (see Fig. 7(d)). Although these two cosine frequencies are slightly farther apart than in the previous case, it turns out that a similar modulation effect is generated in $g_A(x)$ in our present case, too. To see this, note that this time we have $f' = 2f + 3\varepsilon$. If we denote here $f_1 = f$ and $f_2 = f'$, we obtain:

$$f_2 = 2f_1 + \delta \tag{6}$$

with $\delta = 3\varepsilon$. But according to Theorem A.1 in Appendix A, the sum of two continuous cosines with frequencies f_1 and f_2 that satisfy $f_2 = 2f_1 + \delta$ gives a continuous-world beating effect (pseudo moiré) whose envelope frequency is $f_{env} = [1/(2+1)]\delta = \varepsilon$. Now, turning back to our sampled signal $g(x_k)$, we see by virtue of Eq. (3) that $g(x_k)$ has the same beating effect as $g_A(x_k)$, i.e. an envelope frequency $f_{env} = \varepsilon$. And indeed, this is clearly confirmed in Fig. 4: For example, in the particular case shown in Fig. 4(e) this beating modulation effect has the envelope frequency of $\varepsilon = \frac{1}{4}$, i.e. an envelope period length of 4. Furthermore, as stipulated by Theorem A.1, this modulation effect consists of 2+1 = 3 interlaced low-frequency cosinusoidal envelopes, each of which being a stretched and shifted version of our original cosine $g(x)$. These 3 envelopes, which are highlighted in Fig. 4 by different colours, are expressed by:

$$\begin{aligned} \mathrm{env}_1(x) &= \cos(2\pi f_{env} x) = \cos(2\pi\varepsilon x) \\ \mathrm{env}_2(x) &= \cos(2\pi\varepsilon[x + a]) \\ \mathrm{env}_3(x) &= \cos(2\pi\varepsilon[x + 2a]) \end{aligned} \tag{7}$$

where the envelope frequency is $\varepsilon = \frac{1}{3}f_s - f$, and the shift a equals $\frac{1}{3}$ of the envelope's period $1/\varepsilon$, i.e. $a = 1/(3\varepsilon)$. Because the envelope frequency ε is much lower than the frequency f of the original cosine signal $g(x)$ being sampled, this sampling-induced artifact may be clearly visible and distort our perception of the true nature of the original signal. But this beating effect is a sub-Nyquist artifact and not an aliasing or sampling-moiré artifact, since the frequency of the original continuous cosine being sampled here, $f = \frac{1}{3}f_s - \varepsilon$, is lower than the maximum frequency allowed by the sampling theorem, $\frac{1}{2}f_s = 4$. And once again, the low frequency ε itself is not present in the spectral domain.

This spectral-domain consideration explains, indeed, the 3 interlaced modulation envelopes we get in a (1/3)-order sub-Nyquist artifact, like in Fig. 4.

3.3 The case of the general (*m*/*n*)-order sub-Nyquist artifact

Having understood the cases of the (1/2)- and (1/3)-order sub-Nyquist artifacts, we are ready now to proceed to the most general case, that of the (*m*/*n*)-order sub-Nyquist artifact. As a simple illustration we will refer to the (2/5)-order sub-Nyquist artifact that is shown in Fig. 5 and in Fig. 7(e).

In order to obtain a (*m*/*n*)-order sub-Nyquist artifact, let us sample at the rate of f_s an original cosine function $g(x) = \cos(2\pi fx)$ whose frequency f is close to $\frac{m}{n}f_s$, namely $f \approx \frac{m}{n}f_s$ or:

$$f = \tfrac{m}{n}f_s - \varepsilon \tag{8}$$

This is illustrated for the case of $(m/n) = (2/5)$ in Fig. 5, which shows the resulting beating artifact for several values of f around the frequency $\frac{m}{n}f_s$ (i.e. for several values of ε). Consider now Fig. 7(e), which shows for the case of $(m/n) = (2/5)$ the continuous-world spectrum of the sampled signal $g(x_k)$. The situation in this spectrum is very similar to the situation in the two previous cases: Here, too, the new sampling-induced replicas of the impulse pair $G(u)$ add to the original continuous-world spectrum a new impulse pair that is located slightly beyond the impulse pair of the original continuous cosine. Therefore, just as we did in the previous cases, we consider the sum of the two corresponding cosine functions back in the signal domain (with halved amplitudes):

$$g_A(x) = \tfrac{1}{2}\cos(2\pi fx) + \tfrac{1}{2}\cos(2\pi f'x) \tag{9}$$

and show exactly in the same way that its sampled version at the sampling rate of f_s satisfies Eq. (3).

In our general case the frequency of the original cosine is $f = \frac{m}{n}f_s - \varepsilon$ and the frequency of the newly added cosine is $f' = f_s - (\frac{m}{n}f_s - \varepsilon) = \frac{n-m}{n}f_s + \varepsilon$ (see Fig. 7(e) for the case of $(m/n) = (2/5)$). This means that $f' = \frac{n-m}{m}f + \frac{n}{m}\varepsilon$. Thus, if we denote here $f_1 = f$ and $f_2 = f'$, we obtain:

$$f_2 = \tfrac{n-m}{m}f_1 + \delta \tag{10}$$

with $\delta = \frac{n}{m}\varepsilon$. But according to Theorem A.1 in Appendix A, the sum of two continuous cosines with frequencies f_1 and f_2 that satisfy $f_2 = \frac{n-m}{m}f_1 + \delta$ gives a continuous-world beating effect (pseudo moiré) whose envelope frequency is $f_{\text{env}} = \frac{m}{n}\delta = \varepsilon$. Therefore, turning back to our sampled signal $g(x_k)$, we see by virtue of Eq. (3) that $g(x_k)$ has the same beating effect as $g_A(x_k)$, i.e. an envelope frequency of $f_{\text{env}} = \varepsilon$. For example, in the particular case shown in Fig. 5(e) the beating effect has the envelope frequency of $\varepsilon = \frac{1}{4}$, i.e. an envelope period length of 4.

In conclusion, the beating effect we get when sampling the original continuous signal $g(x) = \cos(2\pi fx)$ whose frequency is $f = \frac{m}{n}f_s - \varepsilon$ is simply the sampled version of the continuous-world beating modulation effect that is generated in the continuous cosine sum $g_A(x) = \frac{1}{2}\cos(2\pi fx) + \frac{1}{2}\cos(2\pi f'x)$. This is clearly illustrated for the case of $(m/n) = (2/5)$ in Fig. B3 of Appendix B. As stipulated by Theorem A.1, this modulation effect consists of $k+j = (n-m) + m = n$ interlaced low-frequency cosinusoidal envelopes, each

of which being a stretched and shifted version of our original cosine $g(x)$. These n envelopes are expressed by:

$$\begin{aligned} \text{env}_1(x) &= \cos(2\pi f_{\text{env}} x) = \cos(2\pi\varepsilon x) \\ \text{env}_2(x) &= \cos(2\pi\varepsilon[x + a]) \\ \text{env}_3(x) &= \cos(2\pi\varepsilon[x + 2a]) \\ &\ldots \\ \text{env}_n(x) &= \cos(2\pi\varepsilon[x + (n-1)a]) \end{aligned} \tag{11}$$

where the envelope frequency is $\varepsilon = \frac{m}{n} f_s - f$, and the shift a equals $\frac{m}{n}$ of the envelope's period $1/\varepsilon$, i.e. $a = \frac{m}{n\varepsilon}$. And once again, because the envelope frequency ε is much lower than the frequency f of the original cosine signal $g(x)$ being sampled, this sampling-induced artifact may become quite conspicuous and distort our perception of the true nature of the original signal. Note, however, that this artifact becomes less prominent for higher values of m and n (see Appendix A, soon after Theorem A.1).

This result, which is expressed more formally by Theorem B.1 in Appendix B, gives us the spectral-domain interpretation of the beating effect (the modulation envelopes) that appear in the sampled signal $g(x_k) = \cos(2\pi f x_k)$ when $f = \frac{m}{n} f_s - \varepsilon$. As we can see, the spectral-domain approach offers a new insight into this phenomenon, and establishes an interesting connection with a similar beating modulation effect that occurs in the continuous world, in the sum of two cosinusoidal functions whose frequencies are related by $f_2 = \frac{k}{j} f_1 + \delta$.

4. Extension of the spectral-domain approach to general periodic functions

So far we have only considered the simplest setting, in which the continuous-world function being sampled is $g(x) = \cos(2\pi f x)$. What happens in the case of a general periodic function $g(x)$? This question can be best answered by representing our general

Figure 5: The (2/5)-order sub-Nyquist artifact. This figure is similar to Figs. 1-4, except for the signal-frequency f being used in each row: (a) $f = \frac{2}{5} f_s$ (the singular state). (b) $f = \frac{2}{5} f_s - 1/32$. (c) $f = \frac{2}{5} f_s - 1/16$. (d) $f = \frac{2}{5} f_s - 1/8$. (e) $f = \frac{2}{5} f_s - 1/4$. The highly visible (2/5)-order sub-Nyquist artifact is generated because consecutive points $g(x_k)$ of the sampled signal alternately jump between the $n = 5$ modulating envelopes (each of these modulating envelopes being simply a stretched and shifted version of $g(x)$). These 5 interlaced modulating envelopes are highlighted in the figure in different colours or line styles. Since we have in this case $m = 2$, successive envelopes are shifted by *twice* one fifth of their period. Note that their new low frequency is not visible in the DFT of the sampled signal.

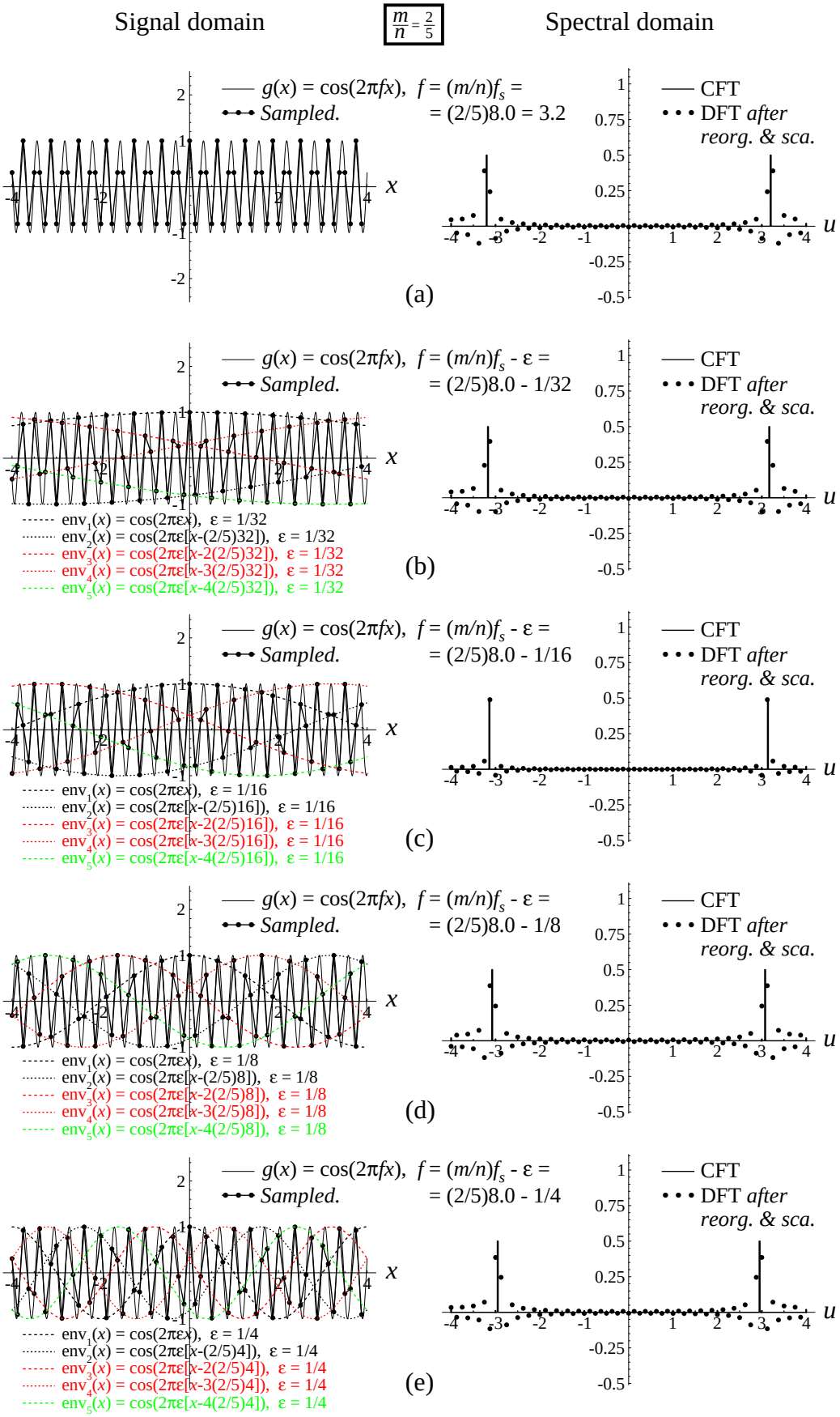
Signal domain
m/n = 2/5
Spectral domain
g(x) = cos(2πfx), f = (m/n)f_s = = (2/5)8.0 = 3.2
Sampled.
CFT
DFT after reorg. & sca.
x
u
(a)
g(x) = cos(2πfx), f = (m/n)f_s - ε = = (2/5)8.0 - 1/32
env1(x) = cos(2πεx), ε = 1/32
env2(x) = cos(2πε[x-(2/5)32]), ε = 1/32
env3(x) = cos(2πε[x-2(2/5)32]), ε = 1/32
env4(x) = cos(2πε[x-3(2/5)32]), ε = 1/32
env5(x) = cos(2πε[x-4(2/5)32]), ε = 1/32
(b)
g(x) = cos(2πfx), f = (m/n)f_s - ε = = (2/5)8.0 - 1/16
env1(x) = cos(2πεx), ε = 1/16
env2(x) = cos(2πε[x-(2/5)16]), ε = 1/16
env3(x) = cos(2πε[x-2(2/5)16]), ε = 1/16
env4(x) = cos(2πε[x-3(2/5)16]), ε = 1/16
env5(x) = cos(2πε[x-4(2/5)16]), ε = 1/16
(c)
g(x) = cos(2πfx), f = (m/n)f_s - ε = = (2/5)8.0 - 1/8
env1(x) = cos(2πεx), ε = 1/8
env2(x) = cos(2πε[x-(2/5)8]), ε = 1/8
env3(x) = cos(2πε[x-2(2/5)8]), ε = 1/8
env4(x) = cos(2πε[x-3(2/5)8]), ε = 1/8
env5(x) = cos(2πε[x-4(2/5)8]), ε = 1/8
(d)
g(x) = cos(2πfx), f = (m/n)f_s - ε = = (2/5)8.0 - 1/4
env1(x) = cos(2πεx), ε = 1/4
env2(x) = cos(2πε[x-(2/5)4]), ε = 1/4
env3(x) = cos(2πε[x-2(2/5)4]), ε = 1/4
env4(x) = cos(2πε[x-3(2/5)4]), ε = 1/4
env5(x) = cos(2πε[x-4(2/5)4]), ε = 1/4
(e)

periodic function $g(x)$ as a Fourier series, i.e. as a sum of cosines and sines of various harmonics having coefficients a_l and b_l [7, p. 236]:

$$g(x) = a_0 + 2\sum_{l=1}^{\infty}\left[a_l\cos(2\pi lx/p) + b_l\sin(2\pi lx/p)\right] \tag{12}$$

where p is the period of our function $g(x)$, and the l-th Fourier series coefficients a_l and b_l are given by Eq. (A.14) in Appendix A.

4.1 The case of the sine function

In order to extend our discussion to any general periodic signal, we need to consider sine signals, too. And indeed, since the sine signal is a shifted version of the cosine, it is not surprising that very similar artifacts also occur when sampling sinusoidal signals. This can be explained using practically the same considerations as in the cosine case. Note however that because the sine signal and its sampled version are odd (antisymmetric), the corresponding spectra are purely imaginary-valued [7 pp. 14-15]. As an illustration, the case of $(m/n) = (1/2)$ is explained in the two last rows of Fig. 6: Consider a continuous-world sine $g(x) = \sin(2\pi fx)$ whose frequency f is slightly below $\frac{1}{2}f_s$, $f = \frac{1}{2}f_s - \varepsilon$. Its spectrum $G(u) = i[\frac{1}{2}\delta(u+f) - \frac{1}{2}\delta(u-f)]$ is shown in Fig. 6(c), and the spectrum of its sampled version is shown in Fig. 6(d). As we can see, in this case, too, the new sampling-induced replicas add to the continuous-world spectrum a new impulse pair that is located just slightly beyond the impulse pair of the original continuous sine. This new impulse pair corresponds to a newly added *minus* sine in the signal domain, whose frequency is $f' = \frac{1}{2}f_s + \varepsilon$. We denote the sum of the positive and negative sines in question (again, with halved amplitudes) by:

$$g_{\mathrm{A}}(x) = \tfrac{1}{2}\sin(2\pi fx) - \tfrac{1}{2}\sin(2\pi f'x) \tag{13}$$

Figure 6: Explanation in the continuous-world spectrum of the (1/2)-order sub-Nyquist artifact that occurs when sampling a continuous cosine function $g(x) = \cos(2\pi fx)$ whose frequency f is just slightly below half of the sampling frequency ($\frac{1}{2}f_s$). (a) The continuous-world spectrum $G(u) = \frac{1}{2}\delta(u-f) + \frac{1}{2}\delta(u+f)$ of our original cosine. (b) The continuous-world spectrum of the sampled cosine. As a result of the sampling, spectrum (b) is an infinite replication of the original spectrum $G(u)$, where the replicas are centered about all the integer multiples of the sampling frequency f_s. Thanks to the first two impulse-pairs centered about its origin, the spectrum (b) of the sampled cosine basically corresponds to a sum of two cosines: our original continuous cosine, whose frequency is slightly below $\frac{1}{2}f_s$, and a new continuous cosine, whose frequency is slightly above $\frac{1}{2}f_s$. We denote the sum of these two cosines (with halved amplitudes) by $g_{\mathrm{A}}(x) = \frac{1}{2}\cos(2\pi[\frac{1}{2}f_s-\varepsilon]x) + \frac{1}{2}\cos(2\pi[\frac{1}{2}f_s+\varepsilon]x)$. The spectrum $G_{\mathrm{A}}(u)$ of this sum of cosines is shown in the figure in a separate panel (a′). Now, as explained in detail in the text, the continuous-world spectrum (b) is also the spectrum of the sampled version of $g_{\mathrm{A}}(x)$, using the same sampling frequency f_s. This means, in turn, that the *sampled* version of our given cosine $g(x)$ is identical to the *sampled* version of the cosine sum $g_{\mathrm{A}}(x)$ (although obviously $g(x)$ and $g_{\mathrm{A}}(x)$ themselves are

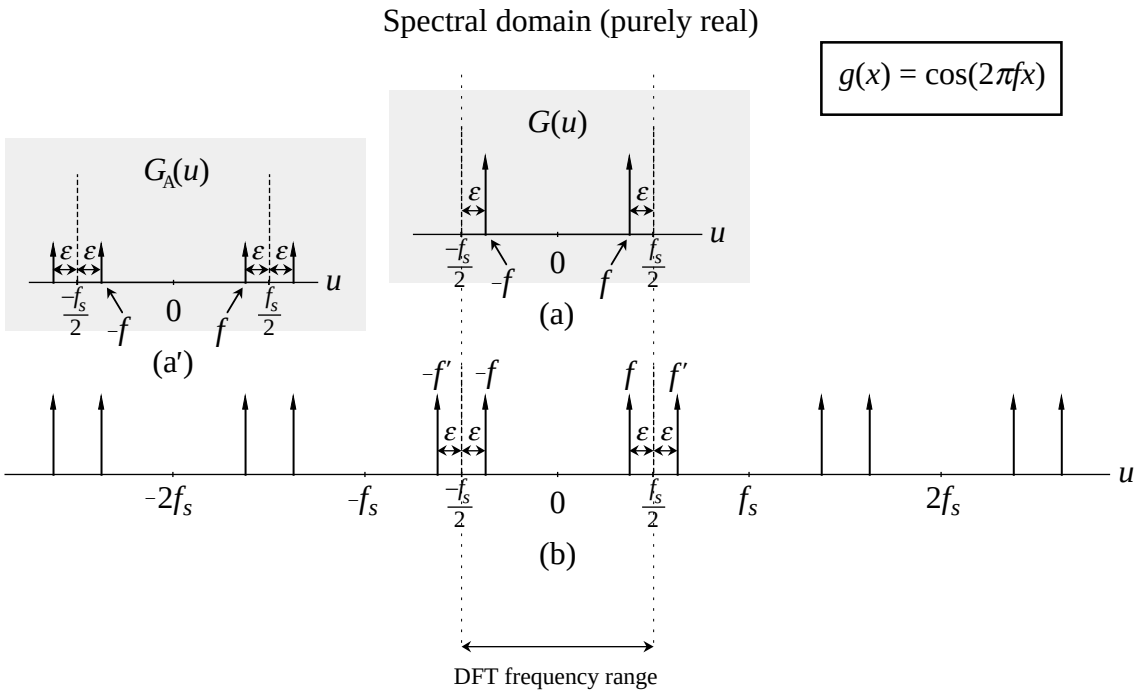

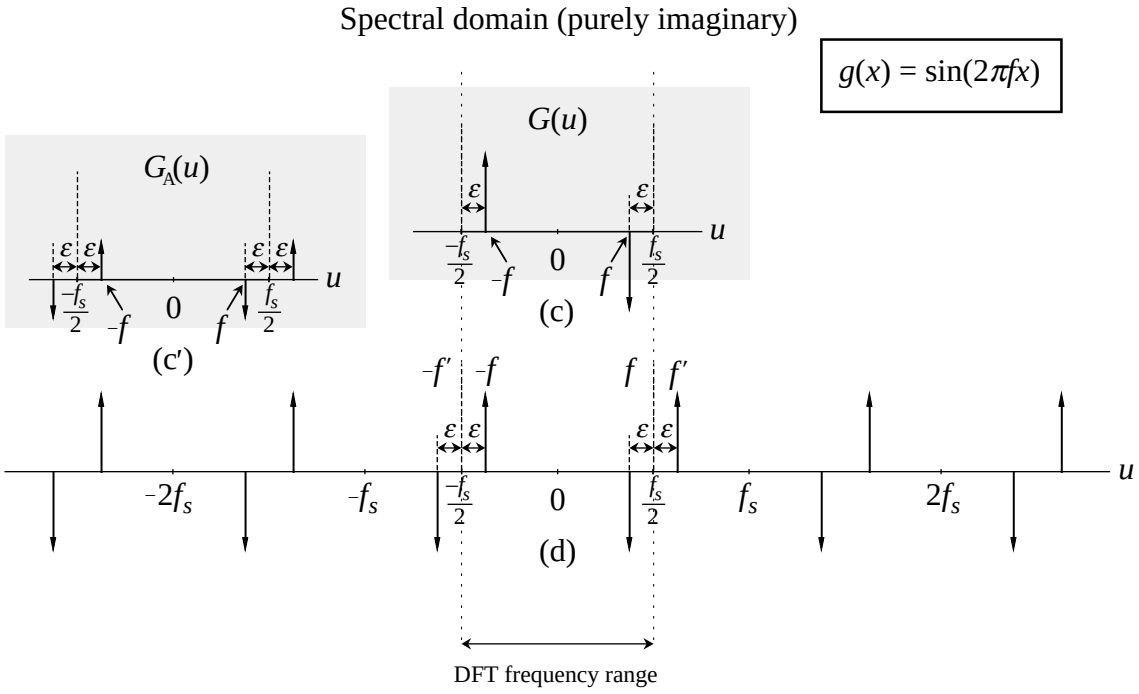

different). Now, as shown in Appendix A, the sum of two continuous cosines with slightly different frequencies gives a beating modulation effect. Thus, the (1/2)-order sub-Nyquist artifact that appears when our original cosine $g(x)$ is being sampled (see Fig. 3) is simply the sampled version of the beating modulation effect that occurs in the continuous cosine sum $g_A(x)$. Rows (c), (d) and the separate panel (c′) show the respective considerations for the case of the sine function $g(x) = \sin(2\pi fx)$. Here, too, the explanation is very similar, but the spectra are imaginary-valued since $g(x)$, $g_A(x)$ and their sampled versions are odd (antisymmetric).

The spectrum $G_A(u)$ of this continuous-world sine difference is shown in Fig. 6 in a separate panel (c′). Now, just as in the case of the cosine, it is easy to see that the continuous-world spectrum of the sampled sine $g(x_k) = \sin(2\pi f x_k)$, shown in Fig. 6(d), is also the spectrum of the sampled version of $g_A(x)$, using the same sampling frequency f_s: The replication of $G_A(u)$ about all the integer multiples of f_s gives again exactly Fig. 6(d). This also remains true in the general (m/n) case, where $f = \frac{m}{n} f_s - \varepsilon$ and $f' = \frac{n-m}{m} f + \frac{n}{m}\varepsilon$. Thus, the beating effect we get when sampling the original continuous signal $g(x) = \sin(2\pi f x)$ whose frequency is $f = \frac{m}{n} f_s - \varepsilon$ is simply the sampled version of the continuous-world beating modulation effect that is generated in the continuous sine difference $g_A(x)$ (see Theorem A.2 in Appendix A). This modulation effect gives n interlaced low-frequency envelopes similar to those obtained in the case of the cosine (Eq. (11)), but with sines instead of cosines. This result is expressed more formally by Theorem B.2 in Appendix B (the sine counterpart of the cosine-based Theorem B.1).

4.2 Cases with higher harmonics

What happens now if the given periodic continuous function $g(x)$ contains also higher harmonics of its frequency f? For the sake of simplicity we will consider here the higher cosine harmonics, but similar results can be also obtained *mutatis mutandis* for the sine harmonics. We first concentrate on the simple case of the (1/2)-order sub-Nyquist artifact, and only then we generalize our discussion to the general (m/n) case.

Figure 7: Explanation in the continuous-world spectrum of some typical sub-Nyquist artifacts that occur when sampling a continuous cosine function $g(x) = \cos(2\pi f x)$ with various frequencies f. Each row shows the continuous-world spectrum of the corresponding sampled cosine. Due to the sampling, each of these spectra is an infinite replication of the original continuous-world spectrum $G(u) = \frac{1}{2}\delta(u-f) + \frac{1}{2}\delta(u+f)$, where the replicas are centered about all integer multiples of the sampling frequency f_s. The replica centered about the origin, which corresponds to the original continuous-world spectrum $G(u)$ itself, is highlighted in red; replicas 1 and -1 are highlighted in green. Whenever the replication generates new lower-frequency impulses that are located close to the spectrum origin, and which correspond therefore to a true sampling moiré effect, the corresponding moiré is indicated by blue arrows. (a) The artifact that occurs when $f \approx (1/1)f_s$, which is a true (1,-1)-sampling moiré effect, as shown in Fig. 1. (b) The artifact that occurs when $f \approx (2/1)f_s$, which is a true (2,-1)-sampling moiré effect, as shown in Fig. 2. (c) A (1/2)-order sub-Nyquist artifact, as shown in Fig. 3. (d) A (1/3)-order sub-Nyquist artifact, as shown in Fig. 4. (e) A (2/5)-order sub-Nyquist artifact, as shown in Fig. 5. We use this last case as a prototype for illustrating the general (m/n)-sub-Nyquist artifact. In rows (a) and (b), the impulses $\pm f_M$ near the spectrum origin, which originate from the replicas 1 and -1 (or 2 and -2, respectively), give in the signal domain a new low-frequency cosinusoidal moiré effect. On the other hand, in rows (c)-(e), the impulses $\pm f$ and $\pm f'$ give in the signal domain a sum of two cosines with frequencies f and f', which generates a beating (modulation) effect.

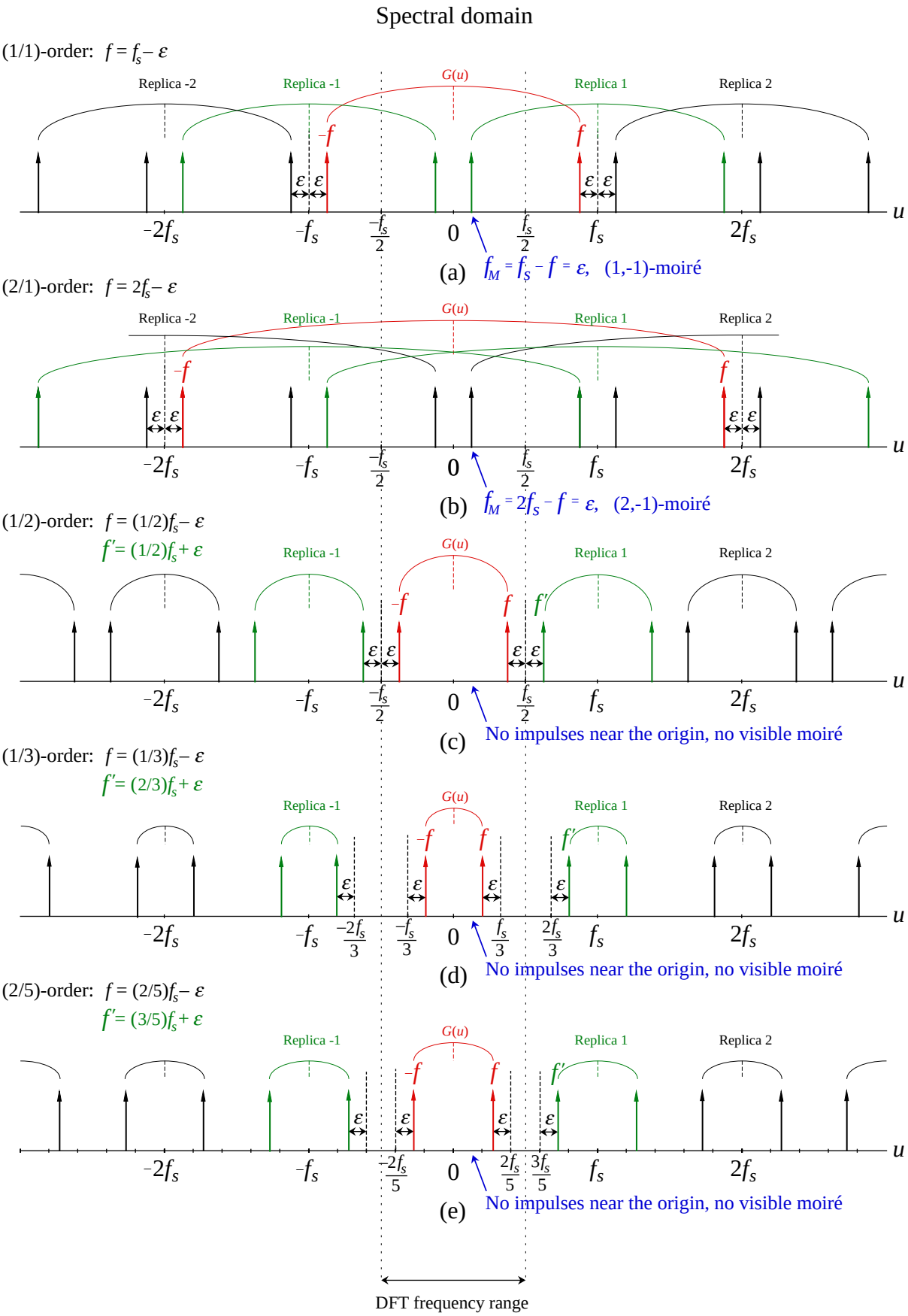
Spectral domain
(1/1)-order: $f = f_s - \varepsilon$
Replica -2
Replica -1
G(u)
Replica 1
Replica 2
$-f$
f
ε ε
u
$-2f_s$
$-f_s$
$\frac{-f_s}{2}$
0
$\frac{f_s}{2}$
f_s
$2f_s$
(a) $f_M = f_s - f = \varepsilon$, (1,-1)-moiré
(2/1)-order: $f = 2f_s - \varepsilon$
(b) $f_M = 2f_s - f = \varepsilon$, (2,-1)-moiré
(1/2)-order: $f = (1/2)f_s - \varepsilon$
$f' = (1/2)f_s + \varepsilon$
f'
(c) No impulses near the origin, no visible moiré
(1/3)-order: $f = (1/3)f_s - \varepsilon$
$f' = (2/3)f_s + \varepsilon$
$\frac{-2f_s}{3}$
$\frac{-f_s}{3}$
$\frac{f_s}{3}$
$\frac{2f_s}{3}$
(d) No impulses near the origin, no visible moiré
(2/5)-order: $f = (2/5)f_s - \varepsilon$
$f' = (3/5)f_s + \varepsilon$
$\frac{-2f_s}{5}$
$\frac{2f_s}{5}$
$\frac{3f_s}{5}$
(e) No impulses near the origin, no visible moiré
DFT frequency range

Let us consider Fig. 8. This figure shows the CFT (continuous-world spectrum) of a typical (1/2)-order sub-Nyquist artifact that is generated when a continuous signal $g(x)$ having frequency $f = \frac{1}{2}f_s - \varepsilon$ is being sampled at the rate of f_s. Row (a) shows the continuous-world spectrum of the sampled signal when $g(x)$ contains only a cosine with the fundamental frequency f, and row (b) shows the continuous-world spectrum of the sampled signal when $g(x)$ also contains a cosine with the frequency $2f$, i.e. a second harmonic. As we can see, each replica in the spectrum (due to the sampling) is simply a shifted copy of the entire original spectrum $G(u)$, including all its higher-order impulses.

So what does the existence of higher harmonics in each of the replicas contribute to the spectral explanation of the sub-Nyquist artifact? Consider row (b) of Fig. 8. In this case the original periodic function $g(x)$ contains two harmonics, so that each of the replicas of $G(u)$ consists of two concentric impulse pairs. Just like in row (a), a (1/2)-order sub-Nyquist artifact is generated in row (b), too, since the impulse of the fundamental frequency f is close to $\frac{1}{2}f_s$ (see Sec. 3.1). But unlike in row (a), we have in row (b) an additional phenomenon: A new higher-harmonic impulse belonging to one of the neighbouring replicas (the -2 harmonic of replica 1) happens to fall close to the spectrum origin, at the point $f_M = f_s - 2f = f_s - 2(\frac{1}{2}f_s - \varepsilon) = 2\varepsilon$. This new impulse (together with its symmetric twin at $-f_M$) corresponds to a new cosine having the low frequency $f_M = 2\varepsilon$ that is generated in the sampled signal. This new low-frequency cosine is a true second-order (1,-2) sampling moiré effect, since it is represented in the spectrum by a corresponding low-frequency impulse pair with $f_M = f_s - 2f$.[6] This means that in row (b) the sampled signal suffers simultaneously from two sampling-induced artifacts: The (1/2)-order sub-Nyquist artifact that is generated here just as in row (a), and a new true (1,-2) sampling moiré effect. How is this reflected in the signal domain, in the sampled signal itself?

The case shown in Fig. 8(a) is illustrated by Fig. 3, in which the continuous-world function being sampled is $g(x) = \cos(2\pi fx)$. To illustrate the case shown in Fig. 8(b), consider Fig. 9, in which the continuous-world function being sampled is $g(x) = \cos(2\pi fx) + 0.8\cos(2\pi[2f]x)$.[7] As we can see, in Fig. 9 too, the sampled signal $g(x_k)$ is modulated by two interlaced envelopes, that are highlighted in the figure by red and green curves, each of which being a stretched and shifted version of $g(x)$:

$$\begin{aligned} \mathrm{env}_1(x) &= \cos(2\pi\varepsilon x) + 0.8\cos(2\pi[2\varepsilon]x) \\ \mathrm{env}_2(x) &= \cos(2\pi\varepsilon[x + a]) + 0.8\cos(2\pi[2\varepsilon][x + a]) \end{aligned} \tag{14}$$

where the envelope frequency is $\varepsilon = \frac{1}{2}f_s - f$, and the shift a equals half of the envelope's period $1/\varepsilon$, i.e. $a = 1/(2\varepsilon)$. This is ascertained by Theorem A.3 in Appendix A, which

---

[6] Note that the (1,-2) sampling moiré is not the same as the (2,-1) sampling moiré shown in Fig. 2: Our (1,-2)-moiré here is generated between f_S and the second harmonic of $g(x)$, $2f$, and its frequency is $f_M = f_S - 2f$; while the (2,-1)-moiré is generated between $2f_S$ and f and its frequency is $f_M = 2f_S - f$. As we can see in Fig. 2, the generation of the (2,-1)-moiré does not require the presence of a second harmonic component in $g(x)$. See also Remark 7 in Appendix C.

[7] We have scaled the second-harmonic cosine by 0.8 in order to be able to easily distinguish between the first and second harmonic impulses in the spectral domain according to their height.

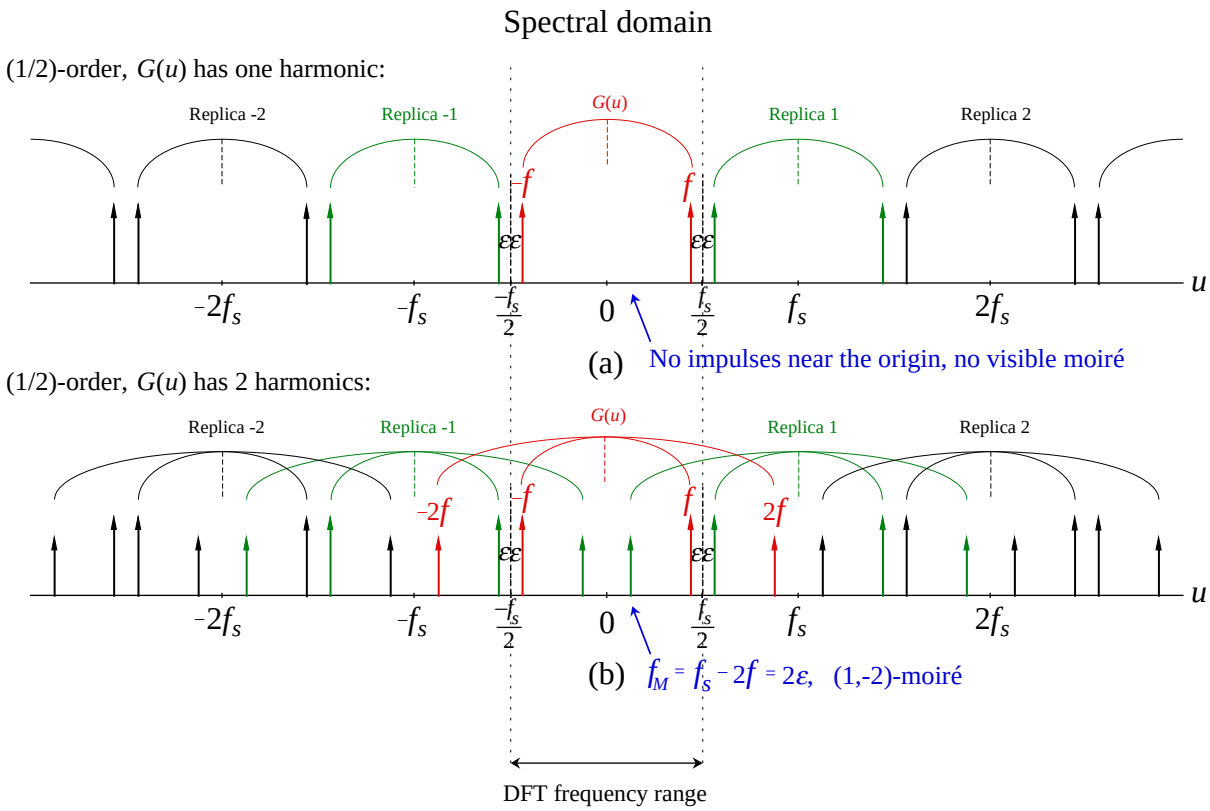

Figure 8: Explanation in the continuous-world spectrum of the (1/2)-order sub-Nyquist artifact: (a) When the original continuous-world spectrum $G(u)$ only contains one impulse pair; and (b) when $G(u)$ also contains second-order harmonics. The original continuous functions being sampled are: (a) $g(x) = \cos(2\pi fx)$; (b) $g(x) = \cos(2\pi fx) + 0.8\cos(2\pi[2f]x)$. Each row shows the continuous-world spectrum of the corresponding sampled function $g(x_k)$. Due to the sampling, each of these spectra is an infinite replication of the original continuous-world spectrum $G(u)$, where the replicas are centered about all integer multiples of the sampling frequency f_s. The replica centered about the origin, which corresponds to the original continuous-world spectrum $G(u)$ itself, is highlighted in red; replicas 1 and -1 are highlighted in green. In (a) $G(u)$ contains only the fundamental impulse pair (at the frequencies $\pm f$), while in (b) $G(u)$ contains two harmonics (at the frequencies $\pm f$ and $\pm 2f$, respectively). Note that in (b) a new lower-frequency impulse is generated close to the origin, at the low frequency $f_M = f_s - 2f = f_s - 2(\frac{1}{2}f_s - \varepsilon) = 2\varepsilon$. In terms of sampling theory, this is a false folded-over low frequency due to aliasing; in terms of the moiré theory, this low-frequency second-harmonic impulse corresponds to a (1,-2)-sampling moiré effect in the sampled signal, as indicated in blue. Thus, in row (b) the sampled signal suffers simultaneously from two sampling-induced artifacts: The (1/2)-order sub-Nyquist artifact that is generated here just as in row (a), and a new true (1,-2) sampling moiré effect.

extends the cosine-based Theorem A.1 to the case of a general periodic function $g(x)$ having any number of harmonics.

However, the resulting effect in Fig. 9 is no longer a pure sub-Nyquist artifact like its single-harmonic counterpart of Fig. 3: On the one hand, as we can see in the DFT spectra of Fig. 9, we *do* have here a new folded-over low-frequency impulse pair close to the origin, at $f_M = 2\varepsilon$, that corresponds to a new (1,-2)-moiré effect. But on the other hand, the phenomenon we see in the signal domain of Fig. 9 is not a pure moiré effect, either: Our sampled signal $g(x_k)$ is not a pure cosine with the low frequency of $f_M = 2\varepsilon$; rather, it rapidly oscillates between the two interlaced envelopes $\text{env}_1(x)$ and $\text{env}_2(x)$, much like a sub-Nyquist artifact. As we can see, this is a hybrid case between a true moiré effect and a pure sub-Nyquist artifact, having an intermediate behaviour between the two. Let us study this behaviour in more detail.

Comparing the sampled signal in each row of Fig. 9 with its counterpart in Fig. 3, we notice an interesting difference: Suppose we apply to each of our sampled signals $g(x_k)$ (in the left-hand column of Figs. 3 or 9) a smoothing filter such as a moving average [6, pp. 277-280]. This smoothing will give us the centreline curve of each sampled signal. In Fig. 3 these centrelines are identically zero and coincide with the x axis, but in Fig. 9 the resulting centrelines are cosinusoidal curves having the frequency $f_M = 2\varepsilon$. More precisely, while the sampled signal in each row of Fig. 3 oscillates about (i.e. above and below) the x axis, in Fig. 9 the sampled signal oscillates about the curve $c(x) = 0.8\cos(2\pi[2\varepsilon]x)$. This confirms the presence of a true low-frequency component in the sampled signal $g(x_k)$ of Fig. 9, as we already noticed in the corresponding DFT spectra of Fig. 9 (and in the CFT of $g(x_k)$, shown in Fig. 8(b)).

This can be readily understood by comparing Eq. (14) with Eq. (4): Note that the cosine $0.8\cos(2\pi[2\varepsilon]x)$ in Eq. (14) has the frequency 2ε, i.e. a period of $1/(2\varepsilon)$; therefore the shift of $a = 1/(2\varepsilon)$ that is applied to $\text{env}_2(x)$ has no effect on its second term. In other words, the second term of $\text{env}_2(x)$ remains identical to the second term in $\text{env}_1(x)$, so that the two envelopes of Eq. (14) are simply raised by the same curve $0.8\cos(2\pi[2\varepsilon]x)$ with respect to the envelopes of Eq. (4). And indeed, we see that in Fig. 9 the rapidly oscillating points $g(x_k)$ are raised by $c(x) = 0.8\cos(2\pi[2\varepsilon]x)$ with respect to Fig. 3.

Figure 9: The (1/2)-order sub-Nyquist artifact, where the periodic signal being sampled contains two harmonics: $g(x) = \cos(2\pi fx) + 0.8\cos(2\pi[2f]x)$. The only difference between the 5 rows is in the frequency f of the original signal $g(x)$: (a) $f = \frac{1}{2}f_S$ (the singular state). (b) $f = \frac{1}{2}f_S - 1/32$. (c) $f = \frac{1}{2}f_S - 1/16$. (d) $f = \frac{1}{2}f_S - 1/8$. (e) $f = \frac{1}{2}f_S - 1/4$. The highly visible (1/2)-order sub-Nyquist artifact is generated because consecutive points $g(x_k)$ of the sampled signal alternately jump between the $n = 2$ modulating envelopes (each of the two modulating envelopes being a stretched and shifted version of $g(x)$). These two interlaced modulating envelopes are highlighted in the figure in different colours. As explained in the text, this example is a hybrid case in which the (1/2)-order sub-Nyquist artifact is also accompanied by a true (1,-2)-sampling moiré having the frequency $f_M = 2\varepsilon$.

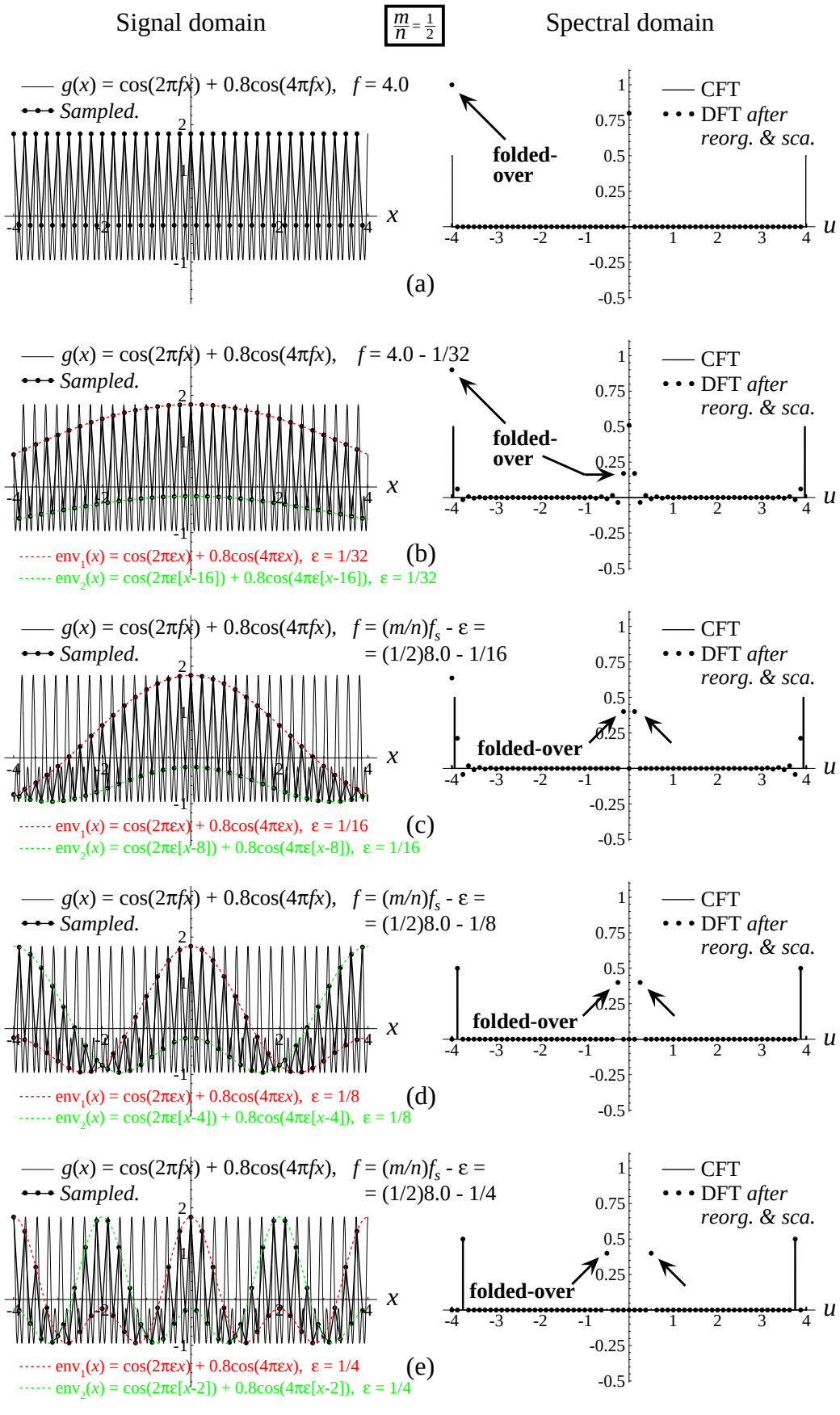
Signal domain
m/n = 1/2
Spectral domain
g(x) = cos(2πfx) + 0.8cos(4πfx), f = 4.0
Sampled.
folded-over
CFT
DFT after reorg. & sca.
x
u
(a)
g(x) = cos(2πfx) + 0.8cos(4πfx), f = 4.0 - 1/32
Sampled.
folded-over
CFT
DFT after reorg. & sca.
x
u
env1(x) = cos(2πεx) + 0.8cos(4πεx), ε = 1/32
env2(x) = cos(2πε[x-16]) + 0.8cos(4πε[x-16]), ε = 1/32
(b)
g(x) = cos(2πfx) + 0.8cos(4πfx), f = (m/n)fs - ε =
= (1/2)8.0 - 1/16
Sampled.
folded-over
CFT
DFT after reorg. & sca.
x
u
env1(x) = cos(2πεx) + 0.8cos(4πεx), ε = 1/16
env2(x) = cos(2πε[x-8]) + 0.8cos(4πε[x-8]), ε = 1/16
(c)
g(x) = cos(2πfx) + 0.8cos(4πfx), f = (m/n)fs - ε =
= (1/2)8.0 - 1/8
Sampled.
folded-over
CFT
DFT after reorg. & sca.
x
u
env1(x) = cos(2πεx) + 0.8cos(4πεx), ε = 1/8
env2(x) = cos(2πε[x-4]) + 0.8cos(4πε[x-4]), ε = 1/8
(d)
g(x) = cos(2πfx) + 0.8cos(4πfx), f = (m/n)fs - ε =
= (1/2)8.0 - 1/4
Sampled.
folded-over
CFT
DFT after reorg. & sca.
x
u
env1(x) = cos(2πεx) + 0.8cos(4πεx), ε = 1/4
env2(x) = cos(2πε[x-2]) + 0.8cos(4πε[x-2]), ε = 1/4
(e)

We can therefore say that the first term in $\text{env}_1(x)$ and $\text{env}_2(x)$ (see Eq. (14)) corresponds to the (1/2)-order sub-Nyquist artifact, while the remaining term corresponds to the true moiré effect, which is embodied by the above-mentioned centreline $c(x)$. This becomes clearer if we rewrite Eq. (14) as follows:

$$\begin{aligned} \text{env}_1(x) &= \cos(2\pi\varepsilon x) + c(x) \\ \text{env}_2(x) &= \cos(2\pi\varepsilon[x + a]) + c(x) \end{aligned} \tag{15}$$

where $c(x) = 0.8\cos(2\pi[2\varepsilon]x)$. Here, $c(x)$ is the true moiré effect (the centreline), having the frequency 2ε, while the first term, which is different in each envelope, corresponds to the vertical distance of $\text{env}_1(x)$ or $\text{env}_2(x)$ above or below the centreline $c(x)$. Because successive points of our sampled signal $g(x_k)$ fall intermittently on $\text{env}_1(x)$ or $\text{env}_2(x)$, as stipulated by Theorem B.3 in Appendix B, we see that the first term in both lines of Eq. (15) corresponds to the alternating jumps of the sampled points $g(x_k)$ above and below the centreline $c(x)$. The rapid oscillations of our sampled signal $g(x_k)$ between $\text{env}_1(x)$ and $\text{env}_2(x)$, above and below $c(x)$, correspond to the sub-Nyquist artifact.

It should be stressed here that the two interlaced envelopes (14) still behave as predicted by Theorems A.1 and B.1, even though $g(x)$ is no longer a pure cosine and contains a second harmonic, too. As we have seen, this happens thanks to Theorems A.3 and B.3, which extend the scope of theorems A.1 and B.1 to cases where $g(x)$ is a general periodic function having any number of harmonics. We can therefore freely use in the multiple-harmonics case Theorems A.3 and B.3 instead of their cosine counterparts A.1 and B.1.

So what happens if the Fourier series development of our given continuous-world function $g(x)$ contains more than two cosine harmonics? Note that the above considerations remain true for all further even-numbered cosine harmonics too, since any additional term of the form $a_{2k}\cos(2\pi[2k\varepsilon]x)$ in $\text{env}_1(x)$ and $\text{env}_2(x)$ of the (1/2)-order sub-Nyquist artifact has the frequency $2k\varepsilon$, i.e. a period of $1/(2k\varepsilon)$, and thus it remains invariant under shifts of $a = 1/(2\varepsilon)$:

$$a_{2k}\cos(2\pi[2k\varepsilon][x + 1/(2\varepsilon)]) = a_{2k}\cos(2\pi[2k\varepsilon]x) \tag{16}$$

This means that the splitting suggested by Eq. (15) can be generalized as follows:

$$\begin{aligned} \text{env}_1(x) &= n(x) + c(x) \\ \text{env}_2(x) &= n(x + a) + c(x) \end{aligned} \tag{17}$$

Here, $c(x)$ lumps together the constant a_0 of the Fourier series (12) and all the even cosine harmonics, all of which are invariant under the envelope shift $a = 1/(2\varepsilon)$. All the other cosine harmonics, which are not invariant under this shift, are lumped together into $n(x)$. Thus, $c(x)$ gives the centreline about which the (1/2)-order sub-Nyquist artifact oscillates, and $n(x)$ gives the alternating jumps of the sampled points $g(x_k)$ above and below the centreline $c(x)$, i.e. the rapid oscillations due to the sub-Nyquist artifact. Now, if the centreline $c(x)$ contains a low-frequency component, this component corresponds to a true moiré effect in the sampled signal. But if this centreline does not contain a low-

frequency component (see, for example, Fig. 3, where the centreline is identically zero), no true moiré effect is visible in the sampled signal.

Example (*(1/2)-order sub-Nyquist artifacts with multiple cosine harmonics*):

To illustrate the situation in a case having multiple cosine harmonics, consider Fig. 10. Here, $g(x)$ is a symmetric (even) continuous-world square wave, whose spectrum $G(u)$ consists of infinitely many cosine harmonics. As we can see in the figure, this is a hybrid case in which both a (1/2)-order sub-Nyquist artifact and a true (1,-2)-moiré effect are visible. Considering first the *spectral domain* point of view, we see that in rows (b)-(e) of Fig. 10 the discrete-world spectrum (DFT) of the sampled signal $g(x_k)$ *does* contain new low frequencies near the origin, that did not exist in the continuous-world spectrum (CFT) of the original continuous signal $g(x)$. These new low frequencies correspond, indeed, to a true (1,-2)-moiré effect as shown in Fig. 8(b), but this time they include *all the even-numbered harmonics* of f: Not only the (1,-2)-impulse itself (like in Fig.8(b)), which is located at $f_M = f_s - 2f = 2\varepsilon$ and corresponds to the fundamental frequency of the (1,-2)-moiré, but also the entire impulse-comb $(1,-2)k$, $k\in\mathbb{Z}$ that it spans, i.e. all the impulses located at $kf_M = kf_s - 2kf = 2k\varepsilon$. And yet, the fundamental frequency f of our original continuous-world square wave $g(x)$ is located just below half of the sampling frequency, $\frac{1}{2}f_s = 4$, as we clearly see both in the CFT and in the DFT in the spectral domain of Fig. 10. This indicates the existence of a (1/2)-order sub-Nyquist artifact that is also generated simultaneously in the same sampled signal.

From the *signal-domain* point of view, the (1,-2)-moiré effect corresponds to the periodic centreline curve $c(x)$, having the frequency 2ε, which consists of all the even-numbered cosine harmonics. This centreline is plotted in rows (b)-(e) of Fig. 10 by a blue curve; its slight undulations occur since it was only calculated there using a finite number of even harmonics. The (1/2)-order sub-Nyquist artifact, on its part, corresponds to the alternating jumps of the sampled points $g(x_k)$, $k = 0, 1, 2,...$ above and below this centreline, between the two envelopes $\mathrm{env}_1(x)$ and $\mathrm{env}_2(x)$. ■

So far we only discussed multiple harmonic cases for the (1/2)-order sub-Nyquist artifact, but similar considerations apply also to any (m/n)-order sub-Nyquist artifact. Consider, for example, a generalization of Fig. 7(d) (or Fig. 7(e)) in which $G(u)$ has two harmonics, like in Fig. 8(b), or even more than two harmonics. If in the spectrum of the sampled signal the $-n$-th impulse of the m-th sampling-induced replica of $G(u)$ exists (is non-zero) and falls close to the spectrum origin, the sub-Nyquist artifact of Fig. 7(d) (or Fig. 7(e)) will also be accompanied by a true $(m,-n)$ sampling moiré effect. In such "hybrid" cases the low frequency $f_M = mf_s - nf$ of the $(m,-n)$ moiré effect will clearly manifest itself both in the sampled signal $g(x_k)$ and in its spectrum; and yet, the highly oscillating nature of the sub-Nyquist artifact will still be preserved.

Note that the condition $f \approx \frac{m}{n}f_s$ for the generation of the (m/n)-order sub-Nyquist artifact (Sec. 3.3) and the condition $mf_s - nf \approx 0$ for the generation of the $(m,-n)$-moiré effect are equivalent: For any m,n, $f \approx \frac{m}{n}f_s$ occurs *if and only if* $mf_s - nf \approx 0$. However, $mf_s - nf \approx 0$ only gives a true moiré effect if $g(x)$ possesses in its Fourier decomposition a non-zero n-th harmonic nf of its frequency f. But this additional condition is not required for the generation of the (m/n)-order sub-Nyquist artifact. For example,

compare Figs. 9-10 with Fig. 3, in which $g(x)$ does not contain higher harmonics of its frequency f; the sub-Nyquist artifact is present in all of these figures, but in Figs. 9-10 it is also accompanied by a true moiré effect, which is not present in Fig. 3.

Interestingly, the frequency of the $(m,\text{-}n)$ moiré effect is $f_M = mf_s - nf$, while the frequency of the modulating envelopes of the (m/n)-order sub-Nyquist artifact is, as explained in Sec. 3.3, $\varepsilon = \frac{m}{n}f_s - f$. It follows, therefore, that $f_M = n\varepsilon$, meaning that the period $p_M = 1/f_M$ of the true moiré effect is n times smaller than the period $p_{\text{env}} = 1/\varepsilon$ of each modulating envelope. In fact, each of the n shifted envelopes of the sub-Nyquist artifact includes exactly one period of the moiré effect; Fig. 10(e) shows a (1/2)-order case, where $n = 2$. Note that cases with $n = 1$ are pure moiré effects (see Sec. 2).

In conclusion, the (m/n)-order sub-Nyquist artifact that is generated by the fundamental frequency f of the original signal $g(x)$ when $f \approx \frac{m}{n}f_s$ (see Figs. 7(c)-(e) and Fig. 8) may be also accompanied by a true $(m,\text{-}n)$ sampling moiré effect. If both a visible sub-Nyquist artifact and a moiré effect are generated simultaneously, a hybrid effect results (like in Figs. 9-10). If no new impulses fall near the spectrum origin, no visible moiré can be recognized in the sampled signal, and only the sub-Nyquist artifact is visible (as in Figs. 3-5). And finally, in cases like Figs. 7(a),(b) where some new impulses do fall close to the origin but the fundamental frequency f does not generate a sub-Nyquist artifact, only a pure moiré effect becomes visible in the sampled signal. This is the case, indeed, in Figs. 1 and 2, which correspond to the spectra of Figs. 7(a) and 7(b), respectively: In such cases only a pure moiré effect is visible in the sampled signal, but no oscillations due to a sub-Nyquist artifact are present.

We see, therefore, that all of the 4 combinations are possible: sub-Nyquist artifact together with moiré, sub-Nyquist artifact alone, moiré alone, or none of the two. This last case, which is, of course, the most desirable in signal processing applications, occurs if none of the corresponding conditions is satisfied, namely: If the fundamental frequency f of our original periodic function $g(x)$ is not close to $\frac{m}{n}f_s$ for any integers m,n (so that no sub-Nyquist artifact occurs); and if no higher-harmonic impulses $\pm mf_s \pm nf$ happen to fall close to the spectrum origin (so that no sampling moiré occurs). Practically, only small values of m,n should be considered, since for higher values the phenomena in question (sub-Nyquist artifacts or sampling moirés) become negligible.

Figure 10: This figure is similar to Fig. 9, except that the original continuous function being sampled is the periodic square wave $g(x) = \text{wave}(fx)$ (with frequency f and opening ratio of $\tau/p = 1/5$). The highly visible (1/2)-order sub-Nyquist artifact is generated because consecutive points $g(x_k)$ of the sampled signal alternately jump from one of the $n = 2$ modulating envelopes to the other (each of the two modulating envelopes being simply a stretched and shifted version of $g(x)$). These two interlaced modulating envelopes are highlighted in the figure in different colours. The centreline $c(x)$ is plotted in rows (b)-(e) by a blue curve; its undulations occur because it was only calculated there using a finite number of harmonics.

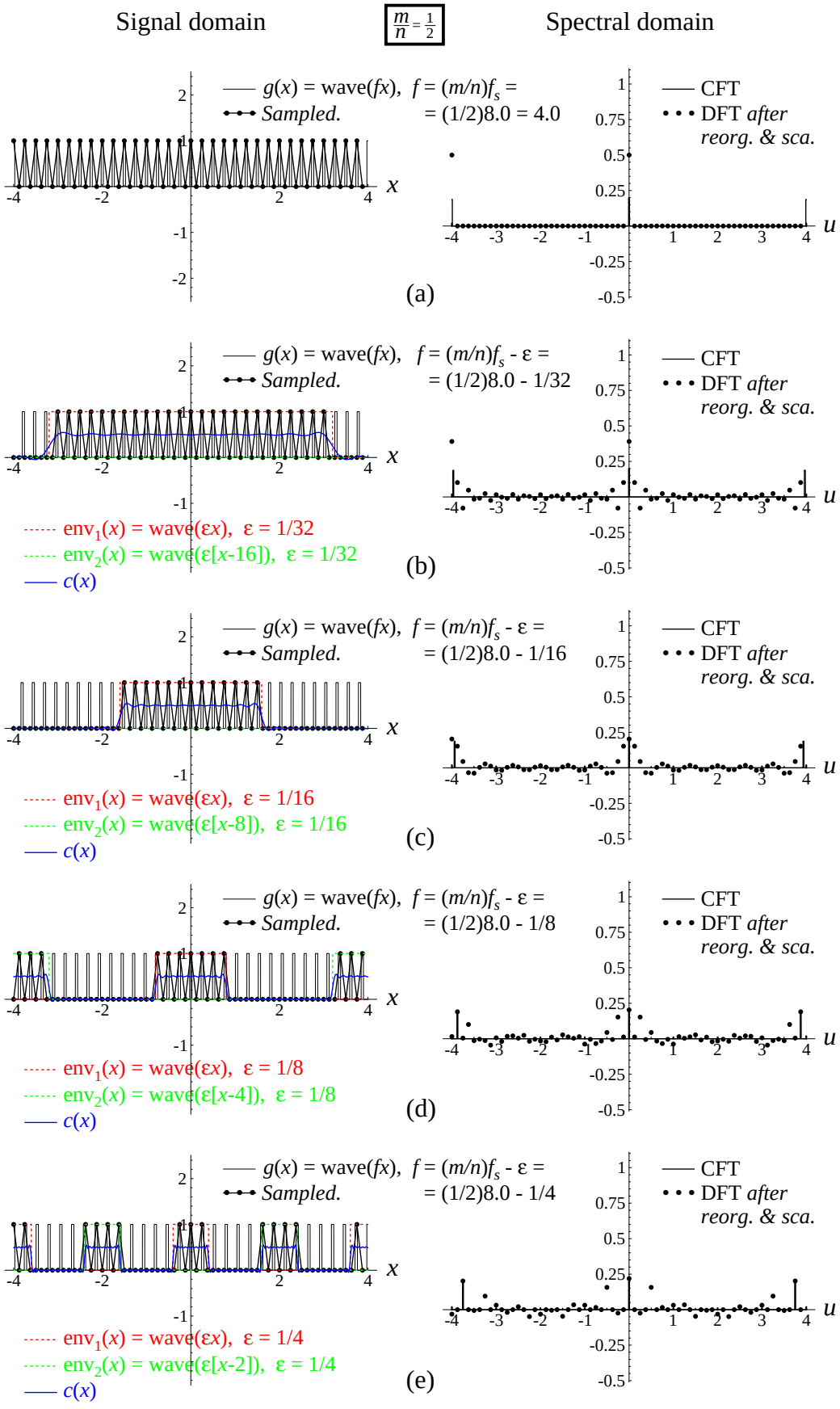
Signal domain
m/n = 1/2
Spectral domain
g(x) = wave(fx), f = (m/n)f_s =
Sampled.
= (1/2)8.0 = 4.0
CFT
DFT after reorg. & sca.
x
u
(a)
g(x) = wave(fx), f = (m/n)f_s - ε =
= (1/2)8.0 - 1/32
env1(x) = wave(εx), ε = 1/32
env2(x) = wave(ε[x-16]), ε = 1/32
c(x)
(b)
= (1/2)8.0 - 1/16
env1(x) = wave(εx), ε = 1/16
env2(x) = wave(ε[x-8]), ε = 1/16
(c)
= (1/2)8.0 - 1/8
env1(x) = wave(εx), ε = 1/8
env2(x) = wave(ε[x-4]), ε = 1/8
(d)
= (1/2)8.0 - 1/4
env1(x) = wave(εx), ε = 1/4
env2(x) = wave(ε[x-2]), ε = 1/4
(e)

4.3 Extension to general periodic functions

So far we have only discussed higher *cosine* harmonics, but the case of higher *sine* harmonics is obtained in a very similar way. The only difference is that for each of the sine harmonics we have to consider the difference (13) rather than the sum (9). This is the case whenever $g(x)$ is an odd (antisymmetric) periodic function, since the Fourier series decomposition of such functions contains only sine harmonics.

Finally, a combination of these results gives us the extension to any general periodic function $g(x)$, since such a function can always be considered as a sum of cosines and sines of various harmonics, as defined by the Fourier series decomposition of $g(x)$ (Eq. (12)). The most general case, which holds for any periodic function $g(x)$, is formally expressed by Theorem B.3 in Appendix B, and illustrated by Figs. B4-B6 there.

As we can see, we have now fully attained the goal set up in the introduction: In spite of the inherent difficulty in devising a spectral-domain explanation to phenomena which are not directly visible in the spectrum, we have succeeded to establish a general spectral-domain approach which is valid for any periodic function $g(x)$. This spectral-domain explanation covers all sub-Nyquist artifacts and sampling moiré effects which may occur when sampling a given continuous periodic function $g(x)$. Moreover, this spectral approach sheds new light on the connections between the classical true moiré effects and the sub-Nyquist artifacts, and on the precise nature of their hybrid combinations. This approach also provides new interesting links between the sampling-induced beating modulation effects in the discrete world, and the beating modulation effects which may occur in the continuous world between two mistuned instances of a continuous periodic function (see Appendices A and B for the full details).

As mentioned earlier in the introduction, we have already succeeded in [1] to explain the sub-Nyquist artifacts by using a purely signal-domain approach. However, the signal-domain approach does not explain as clearly as the spectral-domain approach the nature of the hybrid cases, and it does not provide the insightful connections with the continuous-world modulation effects. As is often the case in signal processing and in the moiré theory, both the signal- and spectral-domain approaches are useful, and none of them is redundant. On the contrary, they prove to be complementary, and each of them contributes a new interesting viewpoint of its own to the subject under discussion.

5. Reconstruction considerations

As already mentioned in [1], although sub-Nyquist artifacts are generated during the sampling process, they may be also considered as reconstruction artifacts. We can now illustrate this claim from the spectral-domain point of view, using Fig. 11. This spectral-domain figure shows a generic (m/n)-order sub-Nyquist artifact, that is generated when sampling a given continuous cosine $g(x) = \cos(2\pi fx)$ using a sampling frequency of f_s, where $f = \frac{m}{n} f_s - \varepsilon$. Let us denote the distance between f and $\frac{1}{2} f_s$ by Δ. As explained in Sec. 3.3, our (m/n)-order sub-Nyquist artifact is caused by the modulation effect that

occurs between the original cosine $g(x)$, whose frequency is $f = \frac{1}{2}f_s - \Delta$, and a new cosine with frequency $f' = \frac{1}{2}f_s + \Delta$ that is generated due to the impulse replication that the sampling process imposes on the spectrum (see row (b) of Fig. 11). Note that Fig. 11 is generic, and it may correspond to any of the different sub-Nyquist artifacts shown in Fig. 7(c)-(e), where only the distance Δ varies from case to case. Furthermore, although Fig. 11 shows the cosine case, the following discussion holds equally well for the sine case, too, using the reasoning shown in Fig. 6(c),(d), and by extension for any periodic functions having higher harmonics too.

Let us now consider rows (c)-(e) of Fig. 11. Because the frequency of our cosine function $g(x)$ is below $\frac{1}{2}f_s$, the sampling theorem guarantees that this function can be perfectly reconstructed from its sampled version $g(x_k)$. This perfect reconstruction is done, as stipulated by the sampling theorem, by multiplying the spectrum of Fig. 11(b) with a rect function extending from $-\frac{1}{2}f_s$ to $\frac{1}{2}f_s$ (see Figs. 11(c),(d)). Equivalently, in terms of the signal domain, perfect reconstruction is obtained by *sinc-function interpolation*, i.e. by convolving the sampled version of the cosine signal with the narrow sinc function that is the inverse Fourier transform of the above rect function; see [8, p. 83] or Fig. 8.11 in [5]. This ideal reconstruction removes the new impulse pair having the frequency $\pm f'$ from the spectrum, as shown in Fig. 11(d), and hence the corresponding new cosine disappears from the signal domain, so that no sub-Nyquist artifact can be generated.

However, in practice, the reconstruction of a sampled signal can never be done by a sinc interpolation as stipulated by the sampling theorem, because the sinc function extends *ad infinitum* to both directions. Instead, reconstruction is very often performed by means of a linear interpolation, meaning that successive sample points are simply connected by straight line segments, just as on the display of an oscilloscope. This is, indeed, what we are also doing in our figures here (see the sampled signals in Figs. 1-5). But since sinc-function interpolation is the only perfect reconstruction method, as stipulated by the sampling theorem, this alternative interpolation method cannot perfectly reconstruct the original signal $g(x)$ from its sampled version $g(x_k)$. Viewed from the spectral domain point of view, any alternative reconstruction method is equivalent to multiplying the spectrum of Fig. 11(b) with a non-ideal substitute of the ideal rect function. But when doing such a multiplication, the new replicas that appeared in row (b) due to the sampling will not be completely removed, and some debris thereof may still subsist in the spectrum, as shown in Fig. 11(e). In such cases, a low-frequency sub-Nyquist artifact may indeed become visible in the sampled signal (see Figs. 3-5); this is simply the beating modulation effect that occurs in the sum of the newly generated cosine (due to the new impulses in the spectrum) and the original cosine function.

These reconstruction considerations remain valid even when $g(x)$ contains higher harmonics, since only the fundamental frequency f of $g(x)$ is involved in the generation of sub-Nyquist artifacts. However, when higher harmonics exist, they may give rise to a true sampling moiré effect if any impulse of the form $\pm mf_s \pm nf$ happens to fall close to the spectrum origin. Obviously, such impulses cannot be removed during the reconstruction process even when using ideal reconstruction, since they are located near the spectrum origin, inside the interval $-\frac{1}{2}f_s \ldots \frac{1}{2}f_s$.

As we can see, the surprising fact that low-frequency artifacts may exist in a sampled signal even when the sampling rate is located *within* the frequency range that is supposed to be safe by virtue of the sampling theorem, is based, in fact, on a misconception. "Safe" in terms of the sampling theorem does not mean that under the specified conditions (i.e. when the sampling rate is at least twice the highest frequency present in the signal) the sampled signal is perfectly faithful to the original continuous-world signal, and does not show new parasite structures due to sampling. The sampling theorem only states that under the specified conditions there is no aliasing, and the original continuous signal can be perfectly reconstructed from its sampled version by convolution with a specified sinc function. But no guarantee is provided that a continuous signal reconstructed by any other method (such as linear interpolation, or the reconstruction method tacitly used by our eyes when looking at a sampled signal) will exactly follow the shape of the original signal $g(x)$, and have no new apparent artifacts.

6. Conclusions

Sub-Nyquist artifacts are parasite beating effects that may "creep in" when sampling a continuous periodic signal $g(x)$, even when the Nyquist condition is fully satisfied, like in Figs. 3-5. Although sub-Nyquist artifacts are clearly visible in the sampled signal $g(x_k)$, in the form of new periodic beats or modulation envelopes that did not exist in $g(x)$ itself, they are not directly represented in the spectral domain: No new impulses appear in the spectrum of the sampled signal at the frequency of this beating effect. This fact makes sub-Nyquist artifacts more difficult to analyze, since our main analysis tool, the Fourier approach, seems in this case to be unusable. And yet, we show in the present contribution that in spite of this difficulty, sub-Nyquist artifacts can be explained from the point of view of the spectral domain, too. It turns out that these beating effects are generated due to an interaction between the fundamental frequency f of the original periodic function $g(x)$ and a new slightly higher frequency f' that is generated in the

Figure 11: The (m/n)-order sub-Nyquist artifact explained using reconstruction considerations. (a) Schematic view of the continuous-world spectrum $G(u)$ of a continuous cosine function $g(x) = \cos(2\pi fx)$ whose frequency is lower than half of the sampling frequency $\frac{1}{2}f_s$: $f = \frac{1}{2}f_s - \Delta$. Note that the distance Δ equals ε in the (1/2)-order sub-Nyquist artifact (see Fig. 7(c)), but in other cases such as the (1/3)- or (2/5)-order sub-Nyquist artifact (see Figs. 7(d) and (e), respectively) the distance Δ may be bigger than ε. (b) The continuous-world spectrum of the sampled version of $g(x)$. As a result of the sampling, spectrum (b) is an infinite replication of the original spectrum $G(u)$, where the replicas are centered about all the integer multiples of the sampling frequency f_s. (c), (d) Because the frequency of our cosine function is below $\frac{1}{2}f_s$, it can be perfectly reconstructed from its sampled version as stipulated by the sampling theorem, by multiplying the spectrum (b) with a rect function (a 1-valued pulse) extending from $-\frac{1}{2}f_s$ to $\frac{1}{2}f_s$ (or, equivalently, by convolving the sampled version of the cosine

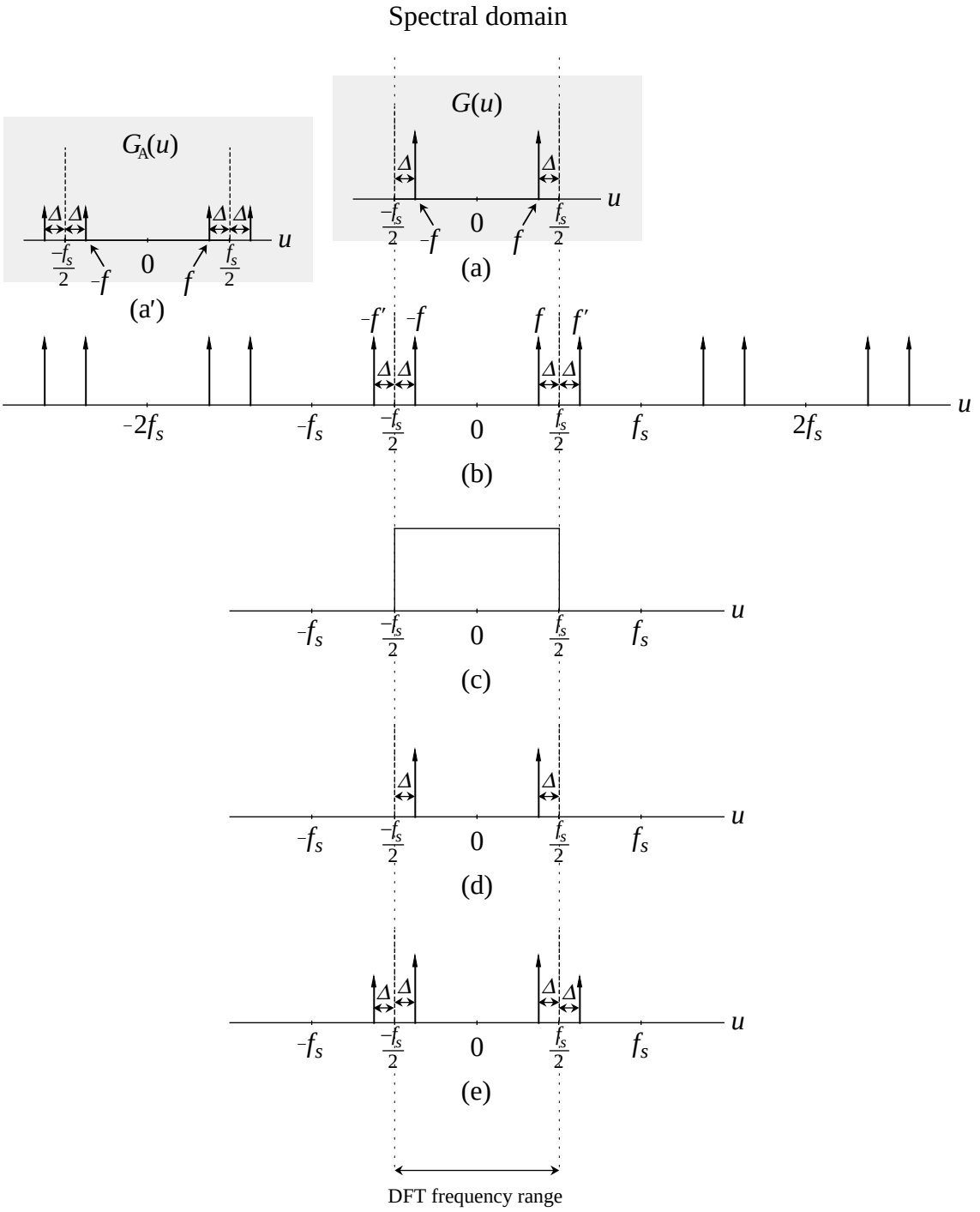

signal with the corresponding sinc function). (e) When reconstructed by multiplying the spectrum (b) with a non-ideal substitute of the ideal rect function, debris of the new replicas that appeared in (b) due to the sampling may still subsist in the spectrum, causing a visible sub-Nyquist artifact. As shown in (b), this beating effect is generated by the sampling operation; but as we can see in (e), it becomes actually visible due to the non-ideal reconstruction. Note that the low beating frequency itself is not present in the spectrum, meaning that it is not a true moiré effect. Panel (a′) is only used for demonstrating Theorem B.1. It shows the spectrum $G_A(u)$ of the cosine sum $g_A(x) = \frac{1}{2}\cos(2\pi[\frac{1}{2}f_S - \Delta]x) + \frac{1}{2}\cos(2\pi[\frac{1}{2}f_S + \Delta]x)$; see the detailed explanation given in Fig. 6 for the case of $(m/n) = (1/2)$.

spectrum due to the sampling process. More precisely, if f is close to an integer fraction of the sampling frequency f_s, namely if $f = \frac{m}{n} f_s - \varepsilon$ for some integers m,n, then a beating effect may be generated due to the interaction between the frequency f and the new frequency $f' = \frac{n-m}{n} f_s + \varepsilon$ that is contributed by the neighbouring replica in the spectrum of the sampled signal. We show that this beating effect is tightly related to another beating phenomenon, that occurs this time in the continuous world, in the sum of two periodic functions whose frequencies f_1 and f_2 are related by $f_2 = \frac{k}{j} f_1 + \delta$. This continuous-world beating phenomenon is widely known in the particular case of two sinusoidal (or cosinusoidal) functions with $k = j = 1$: This is simply the beating effect that occurs in the sum of two sines (or two cosines) with frequencies $f_2 \approx f_1$. But beating phenomena may also occur for any other integer ratios k/j. These continuous-world beats are known in the field of acoustics as "beats of mistuned consonances" [9]. We show that this phenomenon is not limited to the sum of sinusoidal or cosinusoidal functions, and it actually occurs in the sum of two mistuned instances of any periodic function, having any number of harmonics in its Fourier series representation. This explains indeed the sub-Nyquist artifacts that occur back in the discrete case when sampling a general periodic function having any number of harmonics.

We thus extend the scope of the moiré theory (and of the sampling theory) to include pseudo-moiré cases, which were so far hard-to-explain "stepsons", because they defied the standard Fourier analysis tools being used for their investigation.

The present contribution also illustrates another interesting point: The "Fourier paradigm" saying that every periodicity in the signal domain must be represented by corresponding spikes (impulse or impulse pair) in the Fourier frequency domain is based in fact on a misconception. Various periodic modulation phenomena, such as sub-Nyquist artifacts in the sampling process or beating effects in the sum of mistuned periodic functions, may be present in the signal domain, without being directly represented by corresponding spikes of their own in the spectrum.

Finally, it should be noted that although only the one-dimensional case has been considered here, our results can be also extended to two or higher dimensional settings. A first step in this direction, concerning the (1/2)-order sub-Nyquist artifact in the two dimensional setting, can be found in [5, Sec. 8.6].

Appendix A: The beating effect between two mistuned instances of a periodic function

In this appendix we review the beating modulation effects which may occur in the *continuous world* between two mistuned cosines or between two mistuned sines. We then extend our discussion to the case of general periodic functions, that may have any number of cosine and/or sine harmonics in their Fourier series representation.

A.1 The beating effect in the sum of two mistuned continuous cosines

Consider the sum of two continuous-world cosines having frequencies f_1 and f_2:

$$s(x) = \cos(2\pi f_1 x) + \cos(2\pi f_2 x) \tag{A.1}$$

When $f_2 = f_1$, the sum $s(x)$ is simply a cosine having the same frequency and twice the amplitude. But how does the sum look like when $f_2 \neq f_1$? Let us proceed step by step as follows:

(1) Consider first the case where $f_2 \approx f_1$ (or in other words $f_2 = f_1 + \delta$ for some small value δ).

Using the well-known trigonometric identity [10, p. 284]:

$$\cos\alpha + \cos\beta = 2\cos\frac{\alpha+\beta}{2}\cos\frac{\alpha-\beta}{2} \tag{A.2}$$

we can reformulate the sum (A.1) as follows:

$$s(x) = \cos(2\pi f_1 x) + \cos(2\pi f_2 x) = 2\cos(2\pi\frac{f_1+f_2}{2}x)\cos(2\pi\frac{f_1-f_2}{2}x) \tag{A.3}$$

In our present case, where $f_2 \approx f_1$, the cosine product in the right hand side of (A.3) corresponds to a modulation effect, where the cosine with the higher frequency $\frac{f_1+f_2}{2}$ represents the carrier and the cosine with the low frequency $\frac{f_1-f_2}{2}$ represents the modulating envelope (see Fig. A1). More precisely, this modulating envelope consists of *two* cosinusoidal curves with the same frequency $f_{env} = (f_2 - f_1)/2 = \delta/2$ and the same period $p_{env} = 1/f_{env} = 2/\delta$, one of these two curves being shifted by half a period, i.e. by $a = 1/\delta$:[8]

$$\begin{aligned} env_1(x) &= 2\cos(2\pi(\delta/2)x) \\ env_2(x) &= 2\cos(2\pi(\delta/2)[x+a]) \end{aligned} \tag{A.4}$$

Thanks to this modulation, the sum $s(x)$ of two cosines with close frequencies f_1 and $f_2 = f_1 + \delta$ gives rise to a low-frequency beating effect (pseudo moiré). This beating is not a true moiré effect, since the spectrum of $s(x)$ does not contain impulses having the corresponding new low frequency: Based on the addition rule for the Fourier transform, the spectrum of the cosine sum $s(x) = \cos(2\pi f_1 x) + \cos(2\pi f_2 x)$ only contains the frequencies that are contributed by the two original cosines

[8] If $f_2 > f_1$, we may prefer to consider the difference $f_2 - f_1$ rather than $f_1 - f_2$. This makes no difference here, since the cosine function is insensitive to the sign of δ.

themselves, namely, $\pm f_1$ and $\pm f_2$, but no new lower frequencies such as $(f_2 - f_1)/2$ are present in the spectrum of $s(x)$.

(2) Let us now consider the other extreme case, where the frequencies f_1, f_2 of the two given cosines are very far apart, say $f_2 >> f_1$. Although identity (A.3) obviously still holds here, in the present case the cosine sum $s(x)$ no longer resembles a modulation. Instead, it takes the more intuitively expected form of a cosine sum (see Fig. A2): A high-frequency cosine wave of frequency f_2 that is added to (or "rides" on) a low-frequency cosine wave of frequency f_1. The fact that the modulation due to identity (A.3) is no longer prominent here is easily understood: Since $f_2 >> f_1$ implies $(f_2 + f_1)/2 \approx (f_2 - f_1)/2$, the carrier and the modulating wave have almost the same frequency, and the modulation effect is no longer visible.[9]

(3) So far we have seen how the cosine sum $s(x)$ behaves in the two extreme cases, where $f_2 \approx f_1$ and where $f_2 >> f_1$. What happens to $s(x)$ between these two cases?

It turns out that whenever $f_2 \approx kf_1$ with an integer k (namely $f_2 = kf_1 + \delta$), a new modulation phenomenon appears in the sum $s(x)$. This is a simple generalization of case (1) above, and we call it a *k-th order modulation*. Fig. A3 shows a modulation effect that occurs in the cosine sum $s(x)$ when $k = 2$. As we can see by comparing Figs. A3 and A1, the second-order modulation with $k = 2$ looks more complex and intricate than the first-order modulation with $k = 1$.[10]

However, this is not yet all: it turns out that a similar phenomenon may also occur whenever $f_2 \approx (k/j)f_1$ (namely $f_2 = (k/j)f_1 + \delta$), where k/j is considered as a reduced integer ratio. We call such cases (k/j)-*order modulation* effects. For example, Fig. A4 shows the (3/2)-order modulation that occurs in the cosine sum $s(x)$ when $(k/j) = (3/2)$. More formally, we have the following theorem:

Figure A1: (a) The sum $s(x)$ of two continuous cosinusoidal waves with similar frequencies $f_1 = 3$ and $f_2 = f_1 + \delta$, where $\delta = 0.1$. (b) The two interlaced envelopes of the modulation effect that occurs in the sum (a) are given by Eq. (A.4). Their frequency is $f_{\text{env}} = \delta/2 = 0.05$ and their period is $p_{\text{env}} = 2/\delta = 20$. (c) The carrier of the modulation effect in the sum (a) is given by the cosine $\cos(2\pi \frac{f_1 + f_2}{2} x)$. For the sake of completeness, we show in (d) the two original cosines themselves: The cosine $\cos(2\pi f_1 x)$ is plotted with a continuous line (left), while the cosine $\cos(2\pi f_2 x)$ is dashed (right); both curves are overprinted in the central part of (d) to allow a better understanding of their sum in (a).

[9] Nevertheless, because identity (A.3) is *always* true, the modulating envelopes given by Eq. (A.4) still remain valid in this case, too. This can be seen by looking carefully at row (b) of Fig. A2: Although the modulation effect of type (1) is no longer prominent here in the cosine sum $s(x)$, the two curves $\text{env}_1(x)$ and $\text{env}_2(x)$ still "envelop" the signal $s(x)$ correctly. Indeed, this modulation or beating effect is only conspicuous in the sum $s(x)$ when $f_2 \approx f_1$, but formally the curves (A.4) remain envelopes of $s(x)$ in *all* cases, whether or not a modulation effect is visible in the sum $s(x)$.

[10] Situations with $k >> 1$ (so that $f_2 >> f_1$) already belong to case (2). On the gradual transition between cases of types (3) and (2), see the paragraph soon after Theorem A.1 as well as Remark 1.

The (1/1)-order modulation effect in $s(x) = \cos(2\pi f_1 x) + \cos(2\pi f_2 x)$ with:

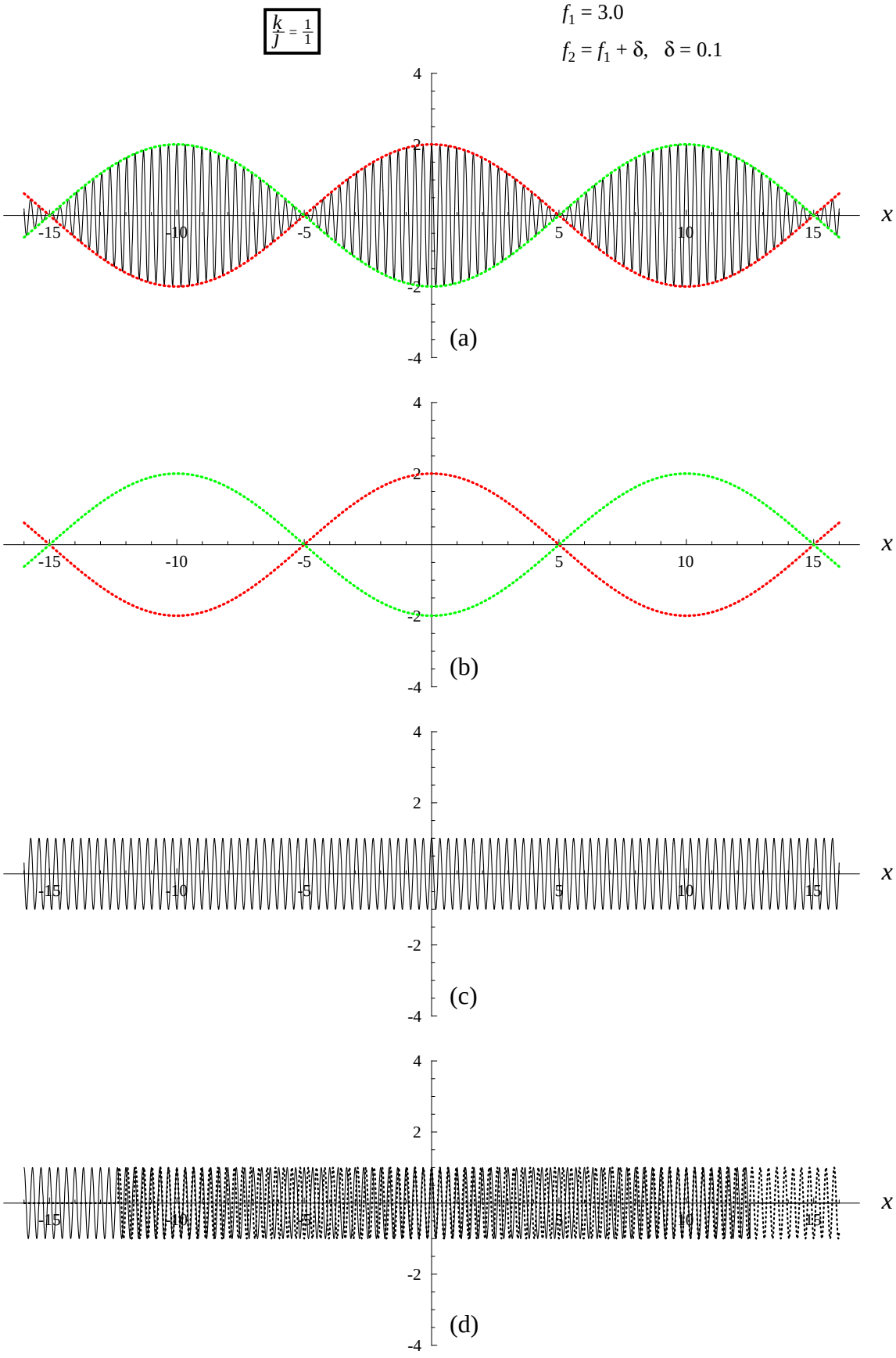

The "riding" effect in $s(x) = \cos(2\pi f_1 x) + \cos(2\pi f_2 x)$ where $f_2 >> f_1$:

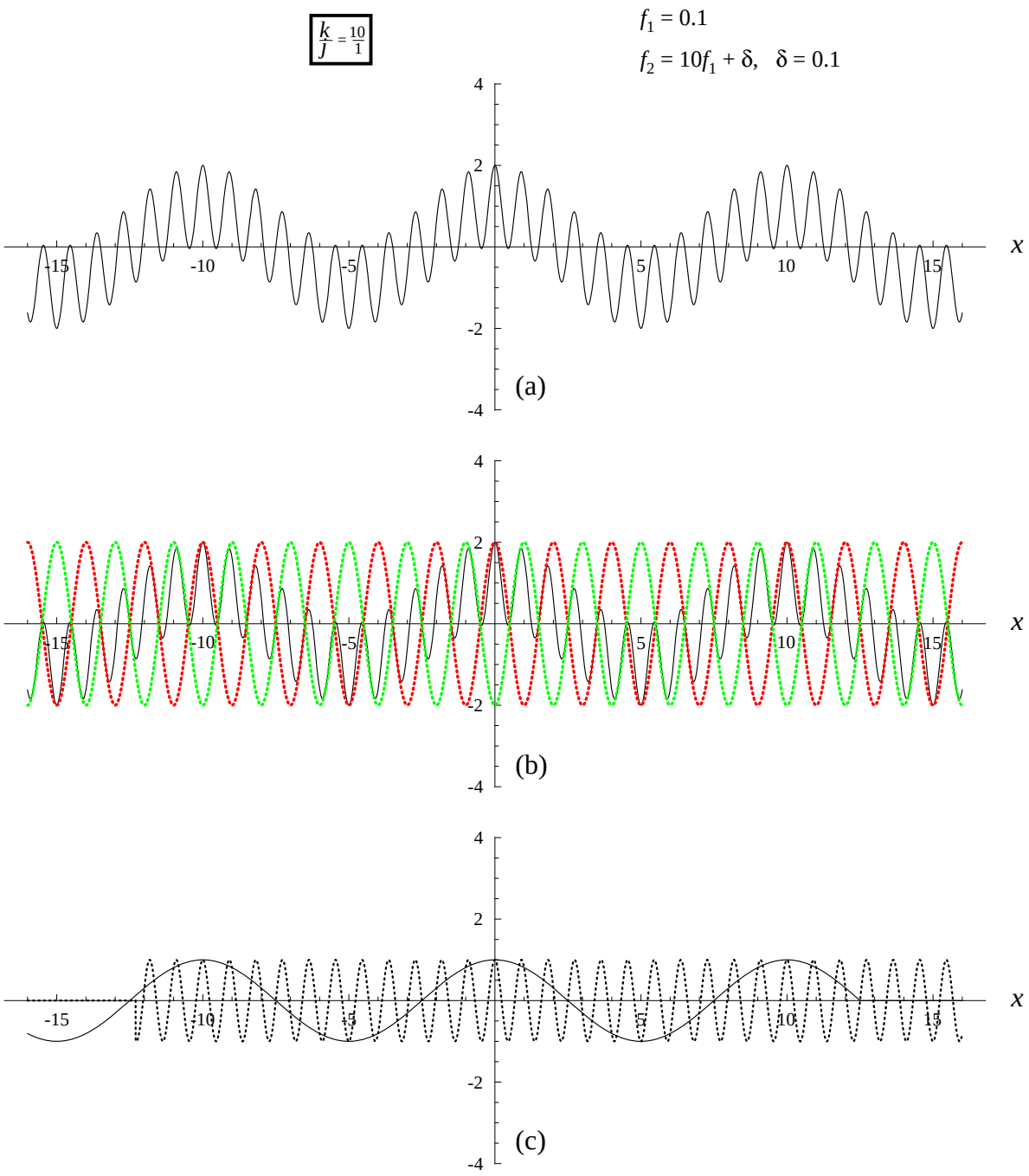

Figure A2: (a) The sum $s(x)$ of two continuous cosinusoidal waves with very different frequencies $f_1 = 0.1$ and $f_2 = 10f_1 + \delta$, where $\delta = 0.1$, looks as a cosine wave of frequency $10f_1$ that "rides" on a lower-frequency cosine wave of frequency f_1. (b) The two interlaced cosines of Eq. (A.4) still "envelop" the sum $s(x)$ correctly, although the modulation effect is no longer prominent. For the sake of completeness, we show in (c) the two original cosines themselves: The cosine $\cos(2\pi f_1 x)$ is plotted with a continuous line (left), while the cosine $\cos(2\pi f_2 x)$ is dashed (right); both curves are overprinted in the central part of (c) to allow a better understanding of their sum in (a).

The (2/1)-order modulation effect in $s(x) = \cos(2\pi f_1 x) + \cos(2\pi f_2 x)$ with:

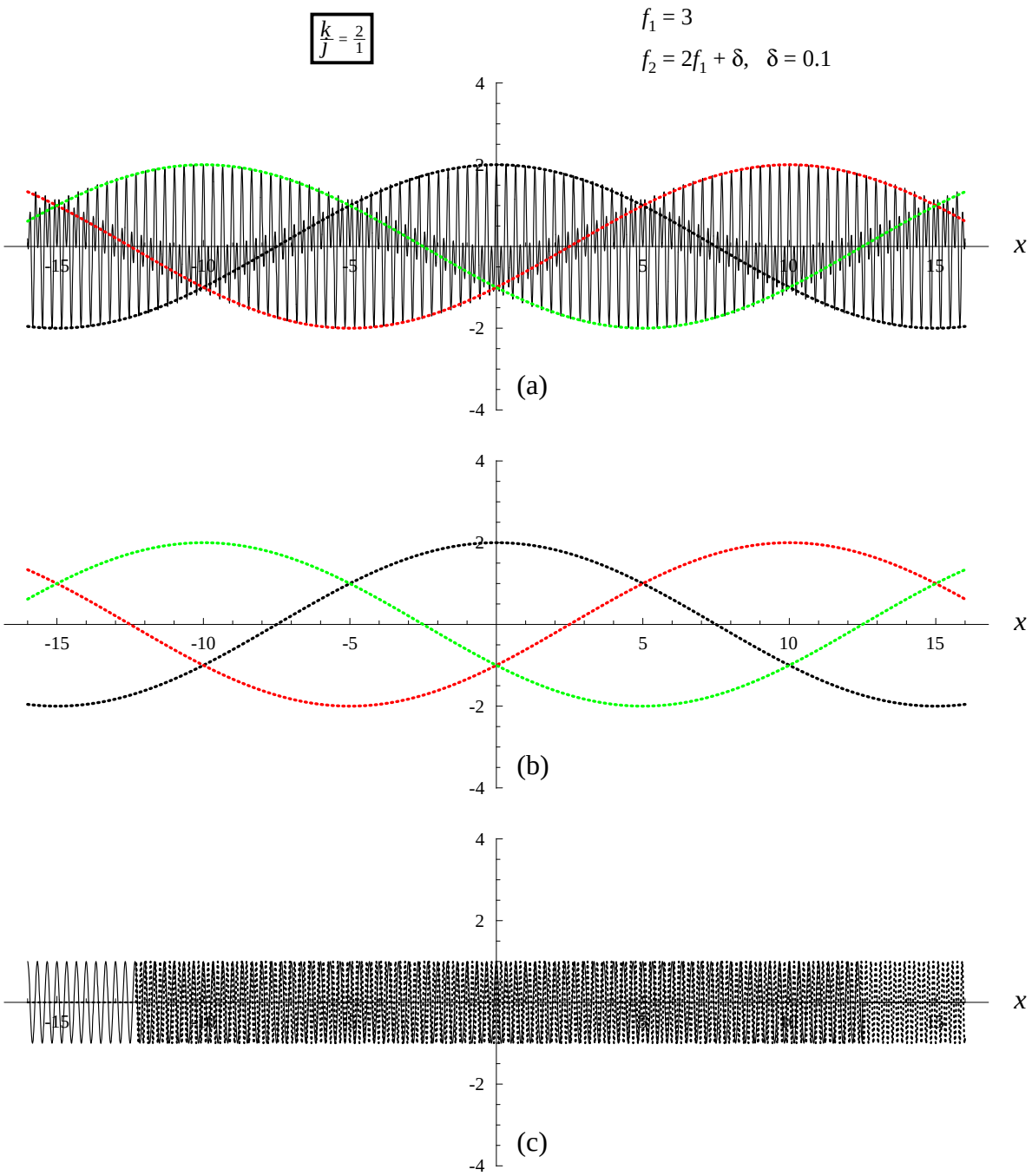

Figure A3: (a) The sum $s(x)$ of two continuous cosinusoidal waves with frequencies $f_1 = 3$ and $f_2 = 2f_1 + \delta$, where $\delta = 0.1$. (b) The 3 interlaced envelopes of the modulation effect that occurs in the sum (a) are given by Eqs. (A.6) with $k = 2$, $j = 1$. Their frequency is $f_{env} = \delta/3 = 0.0333$ and their period is $p_{env} = 3/\delta = 30$. For the sake of completeness, we show in (c) the two original cosines themselves.

The (3/2)-order modulation effect in $s(x) = \cos(2\pi f_1 x) + \cos(2\pi f_2 x)$ with:

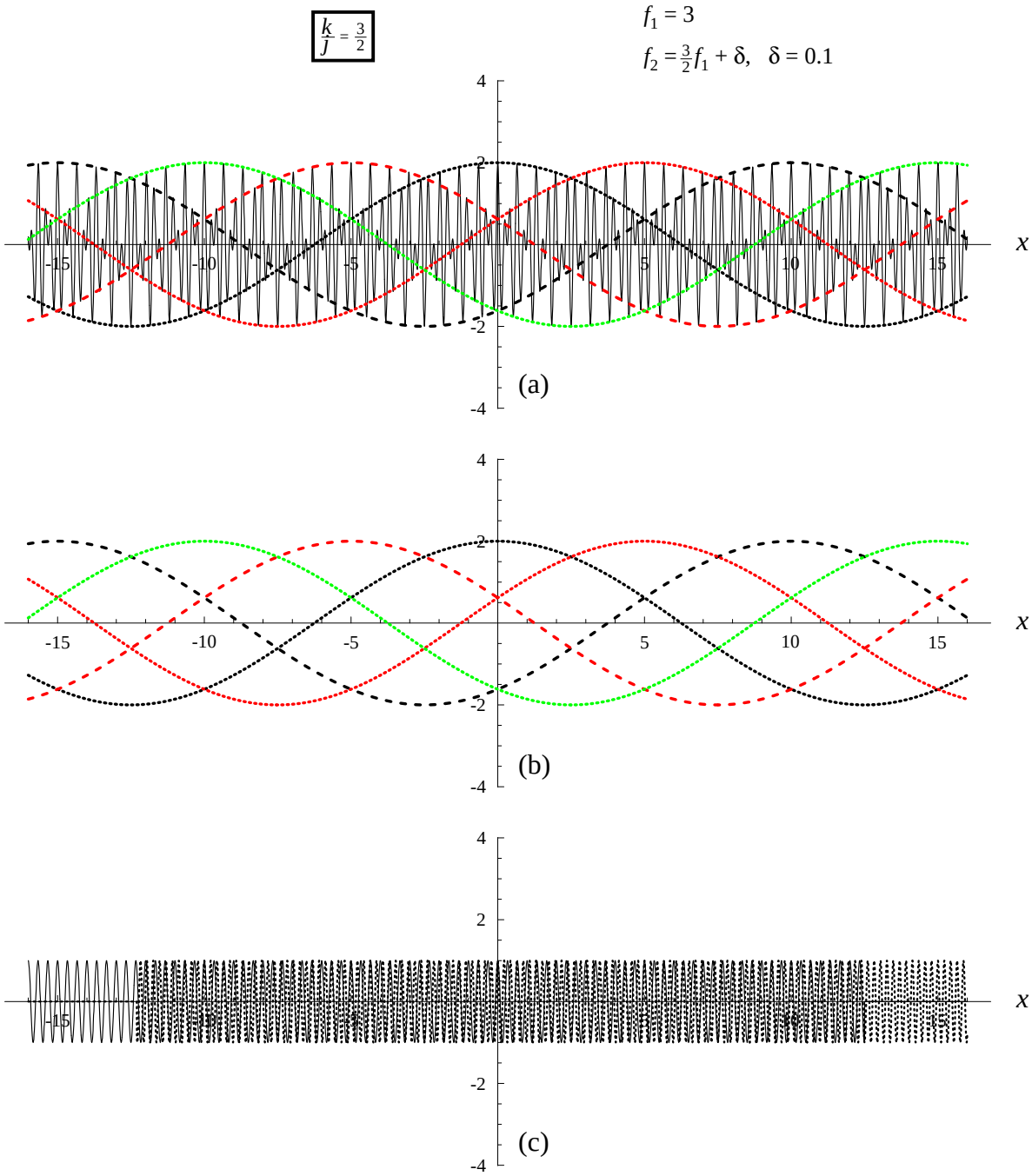

Figure A4: (a) The sum $s(x)$ of two continuous cosinusoidal waves with frequencies $f_1 = 3$ and $f_2 = \frac{3}{2}f_1 + \delta$, where $\delta = 0.1$. (b) The 5 interlaced envelopes of the modulation effect that occurs in the sum (a) are given by Eqs. (A.6) with $k = 3$, $j = 2$. Their frequency is $f_{\text{env}} = \frac{2}{5}\delta = 0.04$ and their period is $p_{\text{env}} = \frac{5}{2}/\delta = 25$. For the sake of completeness, we show in (c) the two original cosines themselves.

Theorem A.1 (*the sum of two mistuned cosine functions*):

Suppose we are given two continuous cosine functions with frequencies f_1 and f_2, respectively:

$$g_1(x) = \cos(2\pi f_1 x) \qquad \text{and} \qquad g_2(x) = \cos(2\pi f_2 x),$$

where:

$$f_2 = \tfrac{k}{j} f_1 + \delta \tag{A.5}$$

(δ being positive or negative, and k/j being a reduced integer ratio). Then the sum of the two given cosines, $s(x) = g_1(x) + g_2(x)$, is modulated by $k+j$ interlaced periodic curves (called envelopes), each of which being a stretched and shifted cosine. These envelopes have all the same frequency

$$f_{\text{env}} = \tfrac{j}{k+j}\delta$$

and the same period $p_{\text{env}} = \tfrac{k+j}{j}/\delta$, and they only differ from each other in their phase. Any two successive envelopes are simply displaced from each other by a fraction $\frac{j}{k+j}$ of their period p_{env}, i.e. by a shift of $a = 1/\delta$:

$$\begin{aligned}
&\text{env}_1(x) = 2\cos(2\pi \tfrac{j}{k+j}\delta x)\\
&\text{env}_2(x) = 2\cos(2\pi \tfrac{j}{k+j}\delta [x+a])\\
&\text{env}_3(x) = 2\cos(2\pi \tfrac{j}{k+j}\delta [x+2a])\\
&\qquad\qquad . \;.\;.\\
&\text{env}_{k+j}(x) = 2\cos(2\pi \tfrac{j}{k+j}\delta [x+(k+j-1)a])
\end{aligned} \tag{A.6}$$

■

This result is indeed a generalization of case (1) above, in which we had $(k/j) = (1/1)$ (see Eq. (A.4)). Figs. A1, A3 and A4 illustrate this generalized result for the cases of $(k/j) = (1/1)$, (2/1) and (3/2), respectively. However, as the integers k or j become bigger, this beating modulation effect becomes less prominent, until it finally disappears. This can be seen for example in Fig. A2 for the case of $(k/j) = (10/1)$, in which the 11 interlaced envelopes of the (10/1)-order modulation are no longer visible.[11]

Interestingly, this result has been known in the field of acoustics at least since the 19th century, although in a slightly different form: When two pure tones of $f_1 = jf$ and $f_2 = kf + \delta$ cycles per second (i.e. f_1 and $f_2 = \tfrac{k}{j} f_1 + \delta$) are sounded together, they give rise to $f_b = j\delta$ beats per second [11, pp. 167-168], [12, pp. 46-49]. This result agrees with our theorem since within any one-period span p_{env}, each of the $k+j$ interlaced cosinusoidal envelopes contributes exactly one shifted beat (i.e. exactly one envelope-maximum), so that within each one-period span of the envelope we have $k+j$ beats (see Figs. A1, A3,

[11] When both k and j are increased, (k/j)-order cases can be often assimilated with a close-by (k/j)-order case having smaller integers k and j, that gives a stronger beating effect. For example, a (11/10)-order case would rather look like a (1/1) case with a slightly different δ: Since $(11/10) \approx (1/1)$, we have for the same frequencies f_1 and f_2 both $f_2 = (11/10)f_1 + \delta_1$ and $f_2 = (1/1)f_1 + \delta_2$; but because the beating effect of the latter is much stronger, it will take the upper hand and completely obscure the former (even if theoretically the curves belonging to the former still "envelop" the signal $s(x)$ correctly, too).

A4). This means that the beat frequency is $k+j$ times the envelope frequency: $f_b = (k+j)f_{env} = j\delta$. A historical account on this result and its various demonstrations and interpretations in the field of acoustics, as well as an extended bibliography, can be found in [9]. These beats are known in acoustics as "beats of mistuned consonances" or "second-order beats". Nice pictures of such beats are plotted in [13, pp. 484-487]; other pictures, that have been photographed on an oscilloscope, can be found in [14].

Remark 1 (*on the smooth transition between cases of types* (*3*) *and* (*2*)):

Note that Theorem A.1 does not contradict case (2) above, and it remains valid even when $f_2 >> f_1$ (see for example Fig. A2, in which $\frac{k}{j} = 10$ so that $f_2 \approx 10\, f_1$). In such cases the modulation described by this theorem is already too weak to be noticed, but formally our theorem still holds, meaning that the $k+j$ curves $\text{env}_1(x)$ … $\text{env}_{k+j}(x)$ still "envelop" the signal $s(x)$ correctly (see Fig. C1(c)). This is a generalization of the footnote in case (2) above. Note also that the transition between "*modulation-shaped*" cases of type (1) or (3) and "*riding-shaped*" cases of type (2) is not abrupt, but rather smooth. This can be observed by plotting a series of cases, gradually varying between $\frac{k}{j} = 2$ (i.e. $f_2 \approx 2f_1$, as in Fig. A3) and $\frac{k}{j} = 10$ (i.e. $f_2 \approx 10\, f_1$, as in Fig. A2); see also Fig. C1(a)-(c). ■

Remark 2 (*envelopes vs. beats*):

Note that talking in terms of *envelopes* (as in our theorem) is more judicious than talking in terms of *beats* (as in the classical results), since in cases with odd ripple effects such as in Figs. A3 or A4 the maxima of the beats do not occur at the same points along the x axis as the minima, and the notion of a "beat" is not quite clear. It should be noted, however, that except in the case of $(k/j) = (1/1)$ our envelopes do not necessarily follow all the local peaks of the sum $s(x)$. As we can see for example in Fig. A3(a), our envelopes provide a correct contour of the beat's maxima and minima, but in intermediate zones they simply pass through the local oscillations of $s(x)$. ■

Remark 3 (*the dynamic behaviour of this modulation effect when* δ *is being varied*):

Consider the (k/j)-order modulation effect that is generated in the sum $s(x) = \cos(2\pi f_1 x) + \cos(2\pi f_2 x)$ when $f_2 = (k/j)f_1 + \delta$. As $\delta \to 0$, the resulting modulation period gradually increases, until when $\delta = 0$ it becomes infinitely big and disappears. This is, indeed, the *singular point* of the (k/j)-order modulation. Then, when δ pursues its way beyond 0 and becomes negative, the modulation effect "comes back from infinity" and reappears once again with a very large period. But as δ moves away from the singular point 0 (to either direction), the modulation period becomes smaller and less prominent, until the effect finally fades out and disappears. This may remind us of the behaviour of sampling moiré effects or sub-Nyquist artifacts that occur when sampling a continuous periodic signal, as described in [1]. And indeed, as shown in Appendix B, this similarity is not just a coincidence, and it results from a true connection that exists between these two phenomena. ■

Remark 4 (*sums of cosines never give true moiré effects*):

Note that unlike in the discrete-world configuration (effects that occur due to sampling), in our present continuous-world configuration (effects that occur in the sum of two

continuous cosine functions having frequencies f_1 and $f_2 = \frac{k}{j} f_1 + \delta$) no new frequencies can be generated in the spectrum, and hence no true moiré effects may appear in the cosine sum.[12] Therefore, all the beating artifacts that may occur in this configuration, as shown in Figs. A1, A3 and A4, are only *pseudo* moiré effects (see also [15] or [16, pp. 17-18, 53-55]). ■

Remark 5 (*on the various envelope definitions*):

It is interesting to note that the term "envelope" is not uniquely defined, and it may have different meanings in different contexts. This is not really surprising, since the envelope curve only touches the "enveloped objects" at certain points, but elsewhere the envelope may behave in various ways [7, p. 363].

In differential geometry, the envelope of a family of curves $F(x,y,c) = 0$ with a single parameter c is defined as a curve that is tangent to each member of the family at some point [17, p. 559]. This envelope curve is obtained by eliminating the parameter c from the two equations:

$$F(x,y,c) = 0, \qquad \frac{\partial F(x,y,c)}{\partial \mathrm{c}} = 0$$

In the context of amplitude modulation, however, the envelope of a rapidly oscillating signal $h(x)$ is understood as a tangent curve that follows $h(x)$ along the extrema of its oscillations, thus outlining its maxima and minima. It is usually defined as the instantaneous amplitude of $h(x)$, and obtained using the Hilbert transform. A detailed explanation can be found, for example, in Chapter 18 of [18]. According to this classical definition, the envelope of $s(x) = \cos(2\pi f_1 x) + \cos(2\pi f_2 x)$ turns out to be:

$$E(x) = \pm\sqrt{2 + 2\cos(2\pi[f_2 - f_1]x)}$$

which can be reduced using the trigonometric identity $\cos(\alpha/2) = \pm\sqrt{\frac{1}{2} + \frac{1}{2}\cos\alpha}$ into:

$$E(x) = \pm 2\left|\cos(2\pi[(f_2 - f_1)/2]x)\right|$$

In the case of the first-order modulation (i.e. when $\frac{k}{j} = 1$; see, for example, Fig. A1) this classical envelope definition gives indeed the same curves as our envelopes $\mathrm{env}_1(x)$ and $\mathrm{env}_2(x)$ in Eq. (A.4), although expressed in a different way. However, the classical envelope definition only gives the envelopes of the first-order modulation, which become irrelevant and useless in cases like Fig. A3, where the prominent beating effect belongs to a higher-order modulation. Note, in particular, that the classical envelope definition always gives *two* envelope curves (as specified by the ± sign), while in a (k/j)-order modulation the number of envelope curves, as determined by Theorem A.1, is $k+j$. In particular, the classical envelope definition cannot handle cases with odd beat types (where the beat's global maxima and minima do not occur simultaneously): For example, in Fig. A3 it clearly fails to capture the true nature of the signal $s(x)$, that is described by our three envelopes $\mathrm{env}_1(x)$, $\mathrm{env}_2(x)$ and $\mathrm{env}_3(x)$ (see Eq. (7) in Sec. 3.2).

As we can see, the envelope definition being used in our theorems is a *generalization* of the above classical definition which is adapted to higher-order modulations, too. ■

[12] This follows, again, from the addition rule for the Fourier transform, as we have seen after Eq. (A.4).

A.2 The beating effect in the difference of two mistuned continuous sines

Because the sine function is simply a shifted version of the cosine, it is not surprising that very similar results also prevail for the sine function. Consider the difference of two continuous-world sines having frequencies f_1 and f_2:

$$s(x) = \sin(2\pi f_1 x) - \sin(2\pi f_2 x)$$

(the reason we need here the *difference* rather than the sum is explained in Sec. 5).[13]

Using the sine counterpart of identity (A.2) [10, p. 284]:

$$\sin\alpha - \sin\beta = 2\cos\frac{\alpha+\beta}{2}\sin\frac{\alpha-\beta}{2} \tag{A.7}$$

we can reformulate our sine difference $s(x)$ as follows:

$$s(x) = \sin(2\pi f_1 x) - \sin(2\pi f_2 x) = 2\cos(2\pi\tfrac{f_1+f_2}{2}x)\sin(2\pi\tfrac{f_1-f_2}{2}x) \tag{A.8}$$

This implies that when $f_2 \approx f_1$ (or in other words $f_2 = f_1 + \delta$), the product in the right hand side of (A.8) corresponds to a modulation effect, where the cosine with the higher frequency $\frac{f_1+f_2}{2}$ represents the carrier and the sine with the low frequency $\frac{f_1-f_2}{2}$ represents the modulating envelope. More precisely, this modulating envelope consists of *two* sinusoidal curves with the same frequency $f_{\text{env}} = (f_2 - f_1)/2 = \delta/2$ and the same period $p_{\text{env}} = 1/f_{\text{env}} = 2/\delta$, one of these two curves being shifted by half a period, i.e. by $a = 1/\delta$:[14]

$$\begin{aligned} \text{env}_1(x) &= 2\sin(2\pi(\delta/2)x) \\ \text{env}_2(x) &= 2\sin(2\pi(\delta/2)[x+a]) \end{aligned} \tag{A.9}$$

Proceeding to the general case of $f_2 = \frac{k}{j}f_1 + \delta$, we can formulate here in a similar way the sine counterpart of Theorem A.1, in which the cosines in the envelopes (A.6) are simply replaced by sines:

Theorem A.2 (*the difference of two mistuned sine functions*):

Suppose we are given two continuous sine functions with frequencies f_1 and f_2, respectively:

$$g_1(x) = \sin(2\pi f_1 x) \qquad \text{and} \qquad g_2(x) = \sin(2\pi f_2 x),$$

where:

$$f_2 = \frac{k}{j}f_1 + \delta$$

(δ being positive or negative, and k/j being a reduced integer ratio). Then the difference of the two given sines, $s(x) = g_1(x) - g_2(x)$, is modulated by $k+j$ interlaced periodic curves (called envelopes), each of which being a stretched and shifted sine. These envelopes have all the same frequency

---

[13] Note also that if we *do* take here the sum, the resulting envelopes will consist of *cosines* rather than sines, so the envelopes will no longer be "stretched and shifted sines" as claimed by Theorem A.2 below (see Eqs. (A.10)).

[14] Here, too, we may prefer to use the difference $f_2 - f_1$ rather than $f_1 - f_2$ if we assume that $f_2 > f_1$. But unlike in the cosine case (Eq. (A.4)), in the sine case this will cause a sign inversion in the envelopes, since $\sin(2\pi(-\delta/2)x) = \sin(2\pi(\delta/2)(-x)) = -\sin(2\pi(\delta/2)x)$.

$$f_{\text{env}} = \frac{j}{k+j}\delta$$

and the same period $p_{\text{env}} = \frac{k+j}{j}/\delta$, and they only differ from each other in their phase. Any two successive envelopes are simply displaced from each other by a fraction $\frac{j}{k+j}$ of their period p_{env}, i.e. by a shift of $a = 1/\delta$:

$$\begin{aligned}
&\text{env}_1(x) = 2\sin(2\pi\tfrac{j}{k+j}\delta x)\\
&\text{env}_2(x) = 2\sin(2\pi\tfrac{j}{k+j}\delta[x+a])\\
&\text{env}_3(x) = 2\sin(2\pi\tfrac{j}{k+j}\delta[x+2a])\\
&\qquad\qquad . \ . \ .\\
&\text{env}_{k+j}(x) = 2\sin(2\pi\tfrac{j}{k+j}\delta[x+(k+j-1)a])
\end{aligned} \qquad \text{(A.10)} \quad \blacksquare$$

A.3 Extension to the case of two mistuned instances of a general periodic function

An extended version of Theorems A.1 and A.2 also holds for any periodic continuous signal $g(x)$. Before we formulate our generalized theorem, we recall here the fact that any function $g(x)$ can be uniquely split into odd and even parts [7, pp. 11-13]:

$$\begin{aligned}
\text{even}[g(x)] &= \tfrac{1}{2}g(x) + \tfrac{1}{2}g(-x)\\
\text{odd}[g(x)] &= \tfrac{1}{2}g(x) - \tfrac{1}{2}g(-x)
\end{aligned}$$

so that $g(x) = \text{even}[g(x)] + \text{odd}[g(x)]$ and $g(-x) = \text{even}[g(x)] - \text{odd}[g(x)]$. The even part contains all the cosine harmonics of the Fourier series decomposition of $g(x)$, and the odd part contains all the sine harmonics. We now define the "signed sum" of two mistuned instances of $g(x)$, $g(f_1x)$ and $g(f_2x)$ as follows:

$$\begin{aligned}
s(x) &= (\text{even}[g(f_1x)] + \text{odd}[g(f_1x)]) + (\text{even}[g(f_2x)] - \text{odd}[g(f_2x)])\\
&= g(f_1x) + g(-f_2x)
\end{aligned}$$

Using these notations, our generalized result can be formulated as follows:

Theorem A.3 (*the case of two mistuned instances of a general periodic function*):

Let $g(x)$ be a continuous periodic function of frequency 1 and period 1. Suppose we are given two mistuned versions of $g(x)$ having frequencies f_1 and f_2, respectively: $g(f_1x) = \text{even}[g(f_1x)] + \text{odd}[g(f_1x)]$ and $g(f_2x) = \text{even}[g(f_2x)] + \text{odd}[g(f_2x)]$, where:

$$f_2 = \tfrac{k}{j}f_1 + \delta \qquad (11)$$

(δ being positive or negative, and k/j being a reduced integer ratio). Then the "signed sum" of the two mistuned functions, $s(x) = g(f_1x) + g(-f_2x)$, is modulated by $k+j$ interlaced periodic curves (called envelopes), each of which being a stretched and shifted version of $g(x)$.[15] These envelopes have all the same frequency

[15] The reason we have to use here the "signed sum" rather than the simple sum $s(x) = g(f_1x) + g(f_2x)$ is that for the odd part of $g(x)$, which is composed of sine harmonics, we need to take here the *difference* rather than the sum. The signed sum may be also called "conjugate sum", in analogy to its counterpart in complex-valued functions.

$$f_{\text{env}} = \frac{j}{k+j}\delta$$

and the same period $p_{\text{env}} = \frac{k+j}{j}/\delta$, and they only differ from each other in their phase. Any two successive envelopes are simply displaced from each other by a fraction $\frac{j}{k+j}$ of their period p_{env}, i.e. by a shift of $a = 1/\delta$:

$$\begin{aligned}
&\text{env}_1(x) = 2\,g(\tfrac{j}{k+j}\delta x)\\
&\text{env}_2(x) = 2\,g(\tfrac{j}{k+j}\delta[x+a])\\
&\text{env}_3(x) = 2\,g(\tfrac{j}{k+j}\delta[x+2a])\\
&\qquad\qquad . \;.\;.\\
&\text{env}_{k+j}(x) = 2\,g(\tfrac{j}{k+j}\delta[x+(k+j-1)a]) \quad \blacksquare
\end{aligned} \tag{A.12}$$

This generalized result is obtained by considering our general periodic function $g(x)$ as a Fourier series, i.e. as a sum of cosines and sines of various harmonics having coefficients a_l and b_l [7 p. 236]:

$$g(fx) = a_0 + 2\Sigma_{l=1}^{\infty}\left[a_l\cos(2\pi lfx) + b_l\sin(2\pi lfx)\right] \tag{A.13}$$

where $p = 1/f$ is the period of our function $g(fx)$, and the l-th Fourier series coefficients a_l and b_l are given by:

$$\begin{aligned}
a_l &= (1/p)\int_p g(fx)\cos(2\pi lfx)\,dx\\
b_l &= (1/p)\int_p g(fx)\sin(2\pi lfx)\,dx
\end{aligned} \tag{A.14}$$

This decomposition of $g(fx)$ allows us to apply Theorem A.1 (or its sine equivalent, Theorem A.2) to each of the cosine and sine terms of (A.13) individually. Every envelope $\text{env}_i(x)$ in Eq. (A.12) is then constructed as a sum of the individual cosinusoidal or sinusoidal envelopes we obtain by Theorem A.1 or A.2 for each of the terms of (A.13) separately. We thus obtain in each envelope $\text{env}_i(x)$ of (A.12) the very same Fourier series decomposition (A.13) of $g(fx)$, that is only stretched out, and shifted by $(i-1)a$. This means that every envelope $\text{env}_i(x)$ in (A.12) is indeed a stretched and shifted version of $g(fx)$ (multiplied by the constant 2, as in Theorems A.1 and A.2).

To illustrate our generalized Theorem A.3, consider Figs. A5-A7. Fig. A5 shows an example with an even periodic function (i.e. with cosine components only). It consists of two mistuned instances of the periodic square wave function $g(x) = \text{wave}(x)$, i.e. $g(f_1x)$ and $g(f_2x)$, with $(k/j) = (1/1), f_1 = 1, f_2 = f_1 + \delta$, and $\delta = -0.1$.

Fig. A6 shows an example with an odd periodic function (i.e. with sine components only). It consists of two mistuned instances of the periodic sawtooth function $g(x) = \text{saw}(x) = (x \bmod 1) - 0.5$, i.e. $g(f_1x)$ and $g(f_2x)$, again with $(k/j) = (1/1), f_1 = 1, f_2 = f_1 + \delta$, and $\delta = -0.1$. Note that the envelopes $\text{env}_1(x)$ and $\text{env}_2(x)$ in this case are mirror-imaged with respect to the original sawtooth function, due to the negative value of δ.

The (1/1)-order modulation effect in $s(x) = \text{wave}(f_1 x) + \text{wave}(f_2 x)$ with:

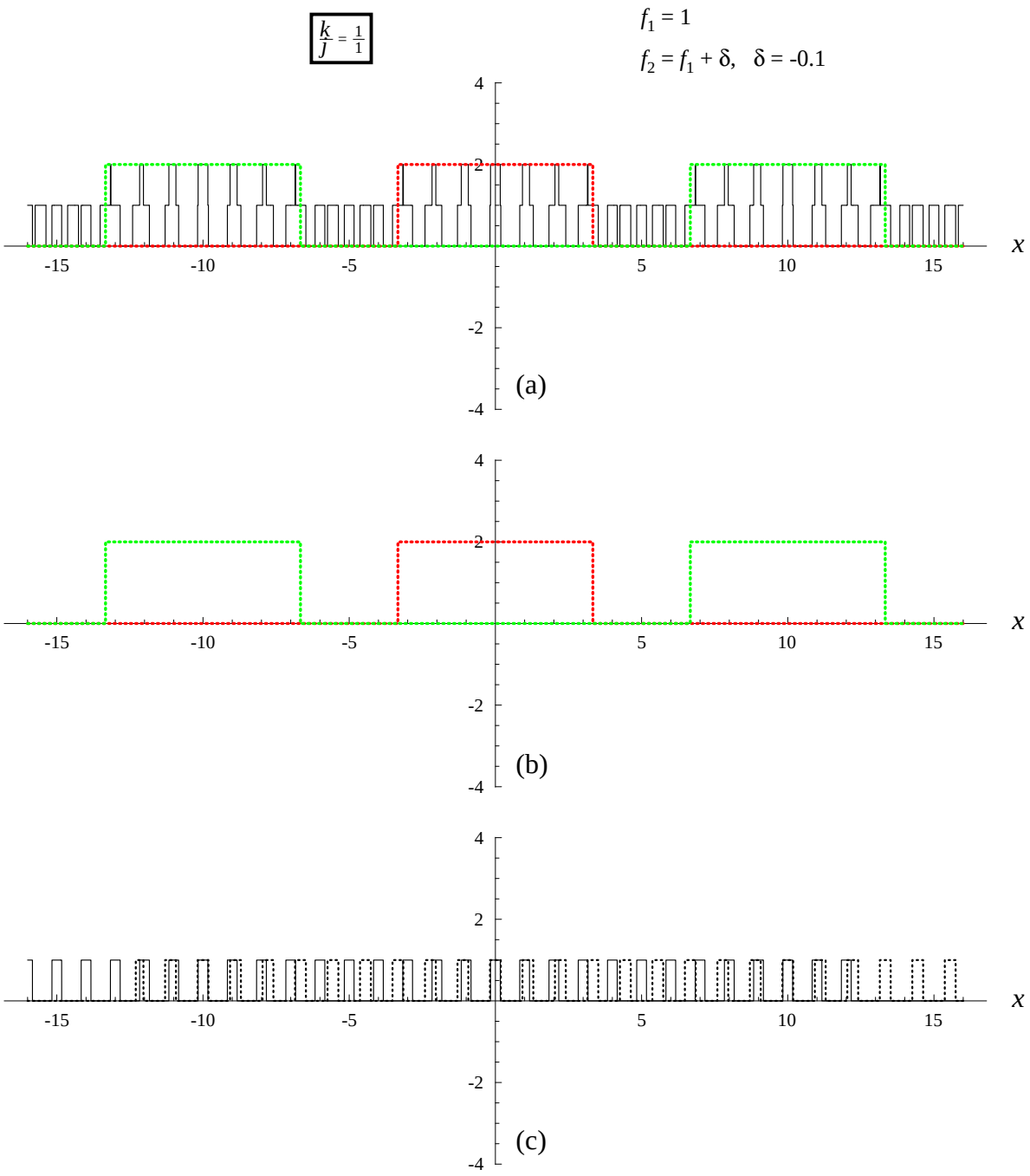

Figure A5: (a) The sum $s(x)$ of two mistuned instances of the square wave $g(x) = \text{wave}(x)$, namely $g(f_1 x) = \text{wave}(f_1 x)$ and $g(f_2 x) = \text{wave}(f_2 x)$, with frequencies $f_1 = 1$ and $f_2 = f_1 + \delta$, where $\delta = -0.1$. (b) The two interlaced envelopes of the modulation effect that occurs in the sum (a) are given by Eqs. (A.12) with $k = 1, j = 1$. Their frequency is $f_{\text{env}} = \delta = -0.1$ and their period is $p_{\text{env}} = 1/\delta = -10$. For the sake of completeness, we show in (c) the two original square waves $g(f_1 x)$ and $g(f_2 x)$ themselves. Just as in Fig. A1, the two interlaced envelopes follow the contour of the beat's maxima and minima (here: $y = 2$ and $y = 0$).

The (1/1)-order modulation effect in $s(x) = \text{saw}(f_1 x) - \text{saw}(f_2 x)$ with:

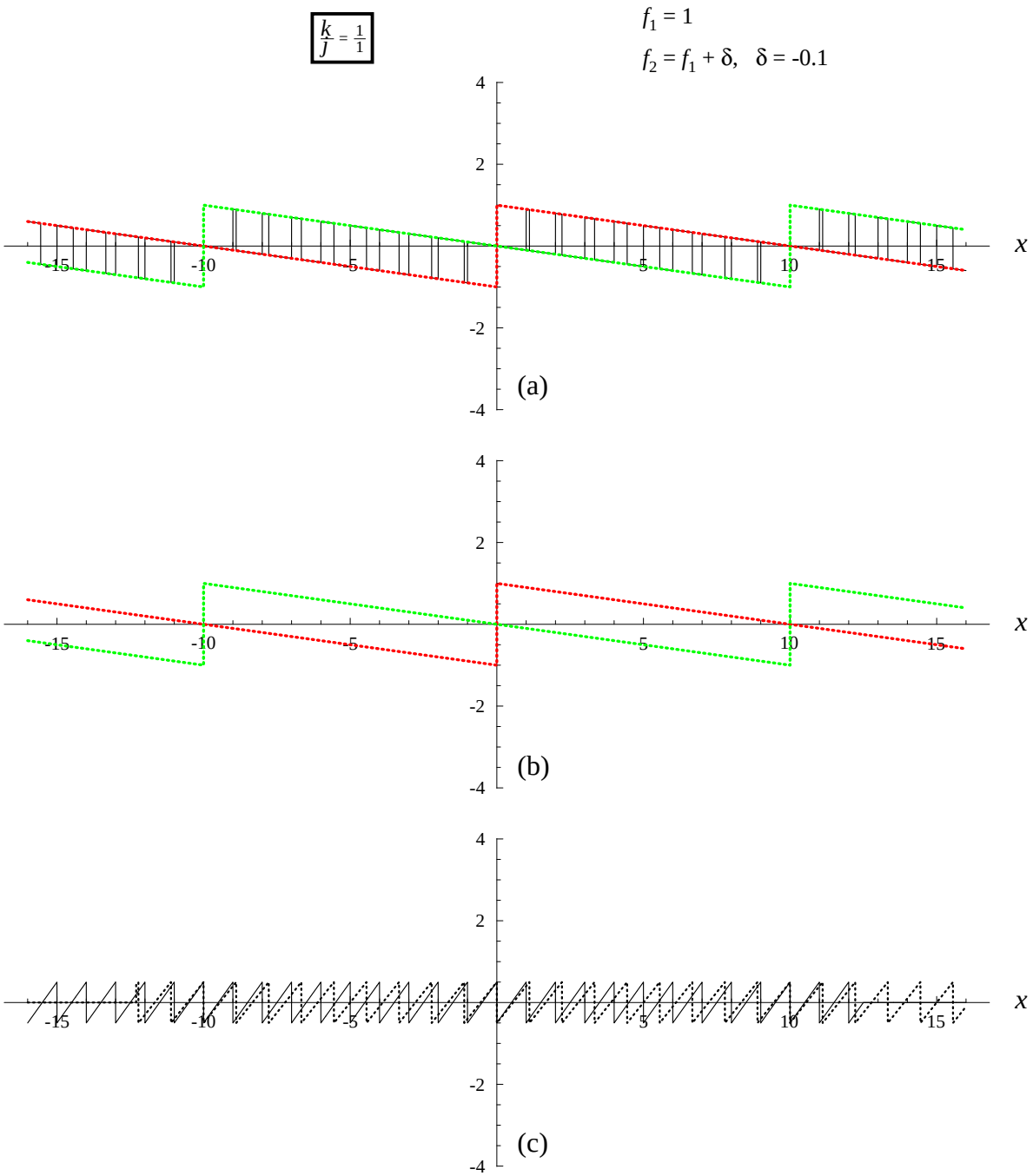

Figure A6: (a) The difference $s(x)$ of two mistuned instances of the sawtooth wave $g(x) = \text{saw}(x) = (x \bmod 1) - 0.5$, namely $g(f_1 x)$ and $g(f_2 x)$, with frequencies $f_1 = 1$ and $f_2 = f_1 + \delta$, where $\delta = -0.1$. (b) The two interlaced envelopes of the modulation effect that occurs in the difference (a) are given by Eqs. (A.12) with $k = 1$, $j = 1$. Their frequency is $f_{\text{env}} = \delta = -0.1$ and their period is $p_{\text{env}} = 1/\delta = -10$. Note that these envelopes are mirror-imaged with respect to the two original sawtooth waves $g(f_1 x)$ and $g(f_2 x)$ themselves, which are shown in (c). This happens due to the negative sign of δ.

The (1/1)-order modulation effect in $s(x) = [\text{wave}(f_1 x) + \text{saw1}(f_1 x)] + [\text{wave}(f_2 x) - \text{saw1}(f_2 x)]$ with:

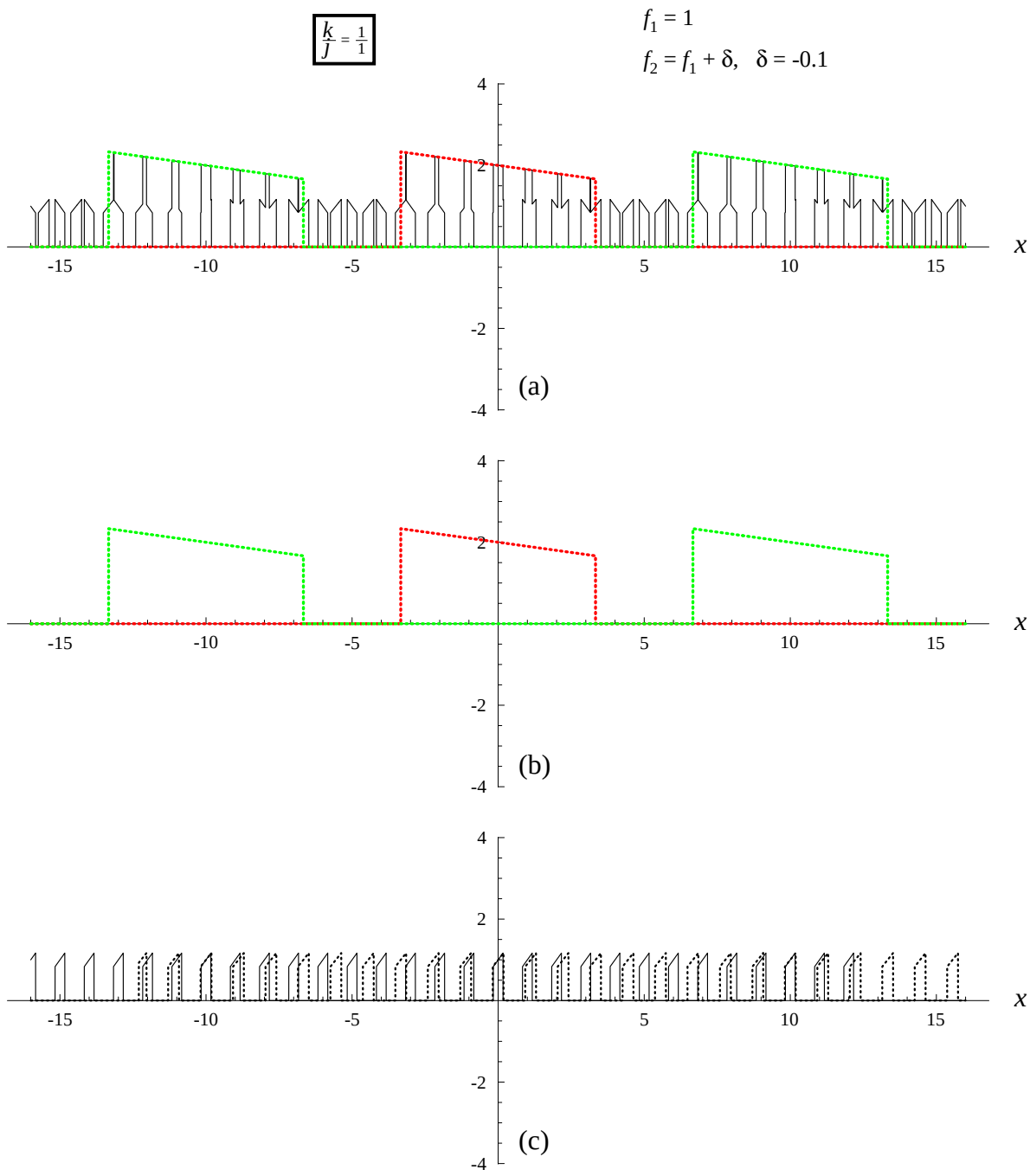

Figure A7: (a) The "signed sum" $s(x)$ of two mistuned instances of the general periodic function $g(x)$ = wave(x) + saw1(x), namely $g(f_1 x)$ and $g(f_2 x)$, with frequencies $f_1 = 1$ and $f_2 = f_1 + \delta$, where $\delta = -0.1$. The sawtooth wave saw1(x) is similar to saw(x) in Fig. A6, but it is shifted by half a period and truncated to the pulse-width of the square wave wave(x). (b) The two interlaced envelopes of the modulation effect that occurs in (a) are given by Eqs. (A.12) with $k = 1, j = 1$. Their frequency is $f_{\text{env}} = \delta = -0.1$ and their period is $p_{\text{env}} = 1/\delta = -10$. Note that these envelopes are mirror-imaged with respect to the two original waves $g(f_1 x)$ and $g(f_2 x)$ themselves, which are shown in (c). This happens due to the negative sign of δ.

Finally, Fig. A7 shows an example with a general periodic function (containing both sine and cosine components), once again with $(k/j) = (1/1)$, $f_1 = 1$, $f_2 = f_1 + \delta$, and $\delta = -0.1$. Note that here, too, the envelopes $\mathrm{env}_1(x)$ and $\mathrm{env}_2(x)$ are mirror-imaged, due to the negative value of δ.

Appendix B: The connection between the two beating phenomena

In this appendix we express formally the connection between the beating effect which occurs when sampling a periodic signal, and the beating effect which occurs in the continuous world in the sum (or difference) of two mistuned instances of a periodic signal.

The main result we have obtained in Sec. 3.3 can be reformulated more formally as follows:

Proposition B.1: Suppose we are sampling with sampling frequency f_s a continuous signal $g(x) = \cos(2\pi f x)$ whose frequency f is close to $\frac{m}{n} f_s$, i.e. $f = \frac{m}{n} f_s - \varepsilon$. The (m/n)-order sub-Nyquist artifact we obtain in the resulting sampled signal is simply the sampled version of the continuous-world beating modulation effect that appears in the continuous cosine sum $g_A(x) = \frac{1}{2}\cos(2\pi f_1 x) + \frac{1}{2}\cos(2\pi f_2 x)$ whose two frequencies are $f_1 = \frac{m}{n} f_s - \varepsilon$ and $f_2 = \frac{n-m}{n} f_s + \varepsilon$. ■

In other words, this proposition says that although the two continuous-world functions $g(x) = \cos(2\pi f x)$ with frequency $f = \frac{m}{n} f_s - \varepsilon$ and $g_A(x) = \frac{1}{2}\cos(2\pi f_1 x) + \frac{1}{2}\cos(2\pi f_2 x)$ with frequencies $f_1 = \frac{m}{n} f_s - \varepsilon$ and $f_2 = \frac{n-m}{n} f_s + \varepsilon$ are obviously different, their *sampled* versions when using the sampling frequency f_s are identical:

$$g(x_k) = g_A(x_k) \qquad \text{at all the sampling points } x_k$$

The proof of this result is explained in Sec. 3.1 and Fig. 6 for the particular case of $(m/n) = (1/2)$; the general (m/n) case, which is illustrated in rows (a), (a′) and (b) of Fig. 11, can be easily demonstrated in the same manner (see also Sec. 3.3).

Figures B1, B2 and B3 illustrate this result for the cases of $(m/n) = (1/2)$, $(1/3)$ and $(2/5)$, respectively.

Now, since Proposition B.1 bounces us back to the sum of two continuous-world cosines, we can apply here Theorem A.1. But in order to do so, we first need to express k, j and δ of Theorem A.1 in terms of the values m, n and ε that are used in Proposition B.1. The connection between the two can be easily obtained by comparing Eq. (A.5) of Theorem A.1 with Eq. (10), which gives:

$$\begin{aligned} k &= n - m \\ j &= m \\ \delta &= \frac{n}{m}\varepsilon \end{aligned} \qquad \text{(B.1)}$$

or in the converse direction:

$$\begin{aligned} m &= j \\ n &= k + j \\ \varepsilon &= \frac{j}{k+j}\delta \end{aligned} \tag{B.2}$$

We thus obtain:

Theorem B.1: Suppose we are sampling with sampling frequency f_s a continuous signal $g(x) = \cos(2\pi fx)$ whose frequency f is close to $\frac{m}{n}f_s$, i.e. $f = \frac{m}{n}f_s + \varepsilon$ (where ε may be positive or negative). Then the successive sampled points $g(x_i) = \cos(2\pi fx_i)$, $i = 0, 1, 2,\ldots$ fall intermittently on $k + j = (n - m) + m = n$ interlaced periodic curves (called envelopes), each of which being a stretched and shifted version of $g(x)$. These envelopes are expressed by:

$$\begin{aligned} \text{env}_1(x) &= \cos(2\pi\varepsilon x) \\ \text{env}_2(x) &= \cos(2\pi\varepsilon[x + a]) \\ \text{env}_3(x) &= \cos(2\pi\varepsilon[x + 2a]) \\ &\ldots \\ \text{env}_n(x) &= \cos(2\pi\varepsilon[x + (n-1)a]) \end{aligned} \tag{B.3}$$

where the envelope frequency is ε, and the shift a equals $\frac{m}{n}$ of the envelope's period $1/\varepsilon$, i.e. $a = \frac{m}{n\varepsilon}$. ■

The formal proof of this result can be obtained by following the same lines as in our informal discussion in Sec. 3.3. The cosine amplitudes of 2 in Eq. (A.6) have been cancelled out in (B.3) since the cosine sum $g_A(x)$ in Proposition B.1 is defined with half of the cosine amplitudes. The intermittence, i.e. the fact that successive sampled points $g(x_i)$ fall intermittently on successive envelopes, can be easily demonstrated as follows:

Our sampling is performed at the points 0, Δx, $2\Delta x,\ldots$ namely, 0, $1/f_s$, $2/f_s,\ldots$

At the first sampling point, $x = 0$, we have:

$$g(0) = \cos(0) = 1$$

$$\text{env}_1(x) = \cos(0) = 1$$

meaning that the first sampled point of $g(x)$ falls on $\text{env}_1(x)$.

At the second sampling point, $x = 1/f_s$, we have:

$$g(1/f_s) = \cos(2\pi[\tfrac{m}{n}f_s + \varepsilon]/f_s) = \cos(2\pi[\tfrac{m}{n} + \varepsilon/f_s])$$

$$\text{env}_2(1/f_s) = \cos(2\pi\varepsilon[1/f_s + \tfrac{m}{n\varepsilon}]) = \cos(2\pi[\varepsilon/f_s + \tfrac{m}{n}])$$

meaning that the second sampled point of $g(x)$ falls on $\text{env}_2(x)$.

Similarly, at the n-th sampling point, $x = (n-1)/f_s$, we have:

(a) *Discrete-world configuration (results of sampling):*

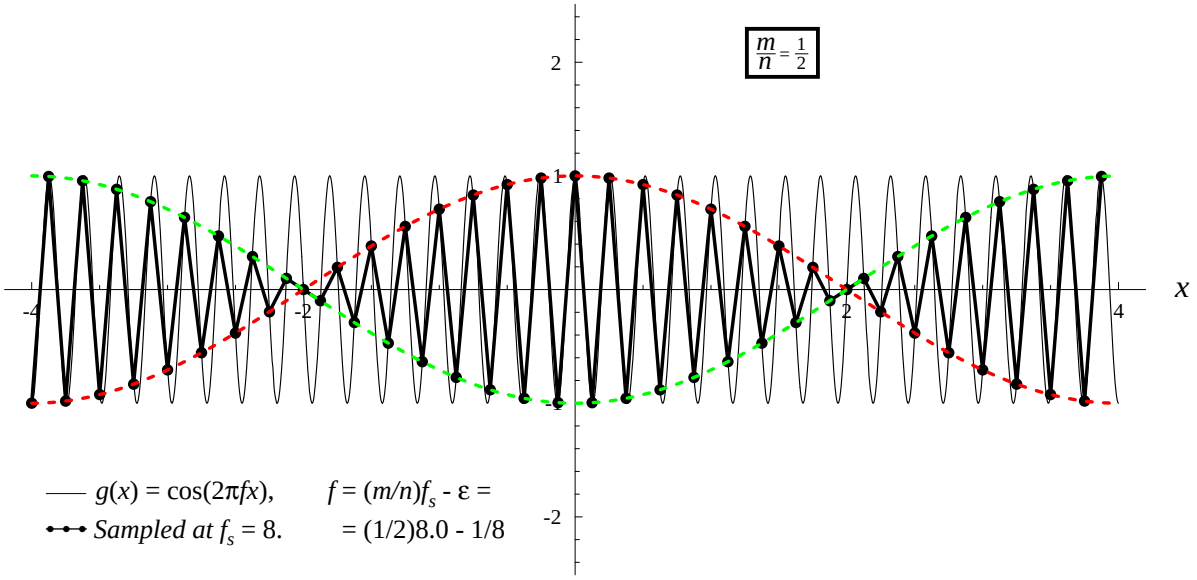

(b) *Continuous-world configuration (sum of mistuned cosines):*

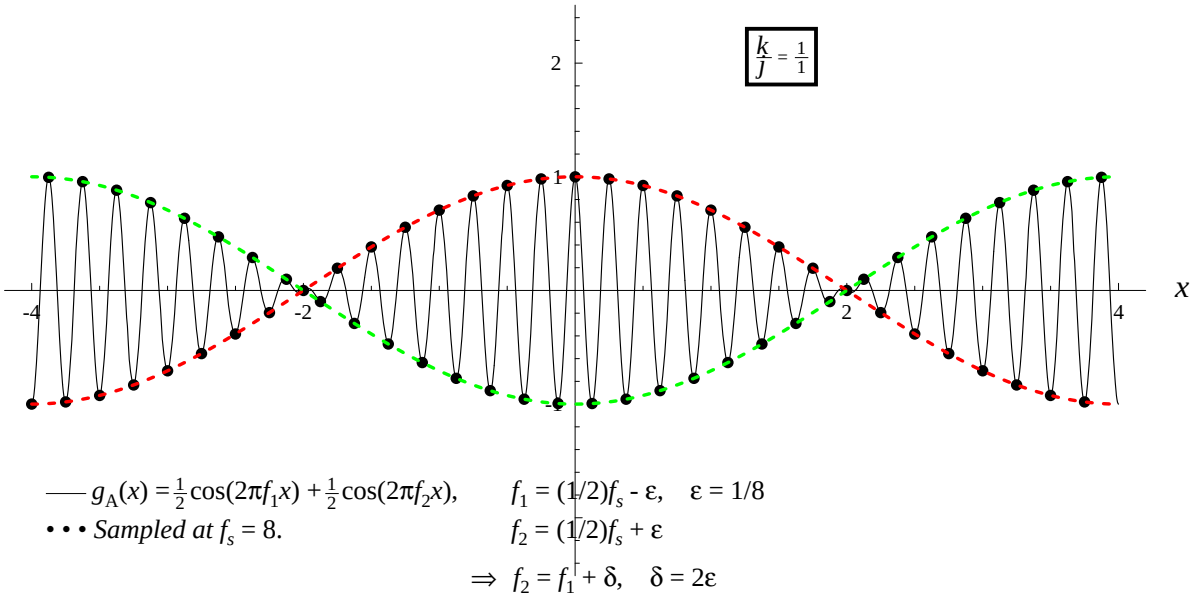

Figure B1: Illustration of Proposition B.1 for the case of $(m/n) = (1/2)$, i.e. a (1/2)-order sub-Nyquist artifact. (a) The continuous cosine $g(x) = \cos(2\pi fx)$ with frequency $f = \frac{1}{2}f_s - \varepsilon$, where $\varepsilon = 1/8$, plotted by a thin, continuous line. Its sampled version $g(x_k)$ with sampling frequency $f_s = 8$ is represented by black dots. These dots have been connected by thicker line segments in order to better convey their correct order. Note that (a) is simply a magnification of Fig. 3(d). (b) The continuous cosine sum $g_A(x) = \frac{1}{2}\cos(2\pi f_1 x) + \frac{1}{2}\cos(2\pi f_2 x)$ with frequencies $f_1 = \frac{1}{2}f_s - \varepsilon$ and $f_2 = \frac{1}{2}f_s + \varepsilon$, plotted by a thin, continuous line. Its sampled version $g_A(x_k)$ after being sampled with the same sampling frequency $f_s = 8$ is represented by black dots. Note that in rows (a) and (b) the sampled points as well as their envelope curves are identical, although the original continuous signals $g(x)$ and $g_A(x)$ are different.

(a) *Discrete-world configuration (results of sampling):*

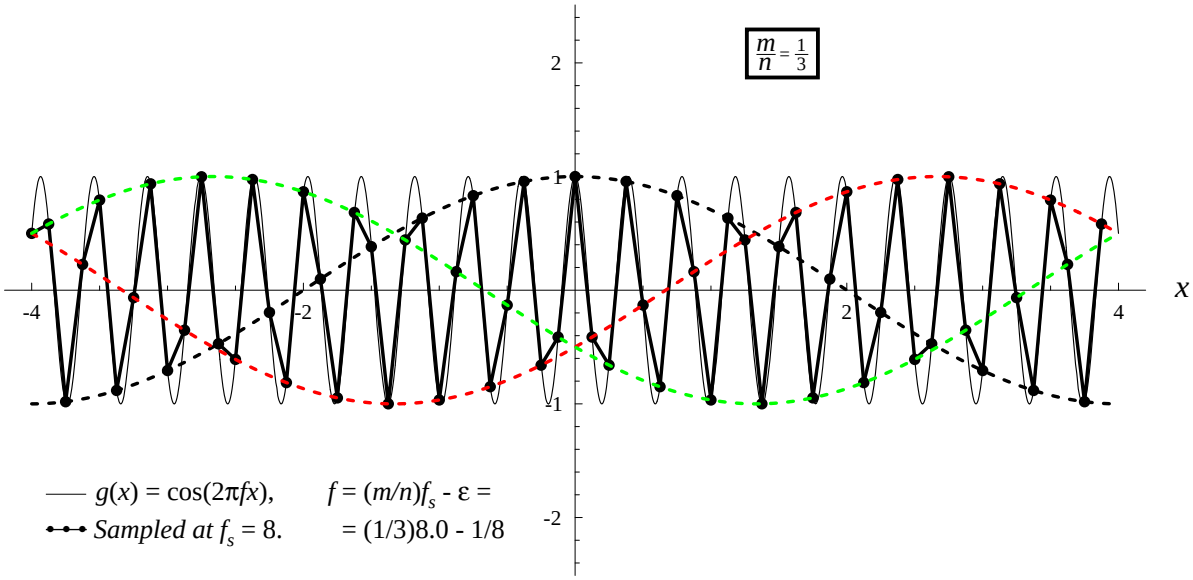

(b) *Continuous-world configuration (sum of mistuned cosines):*

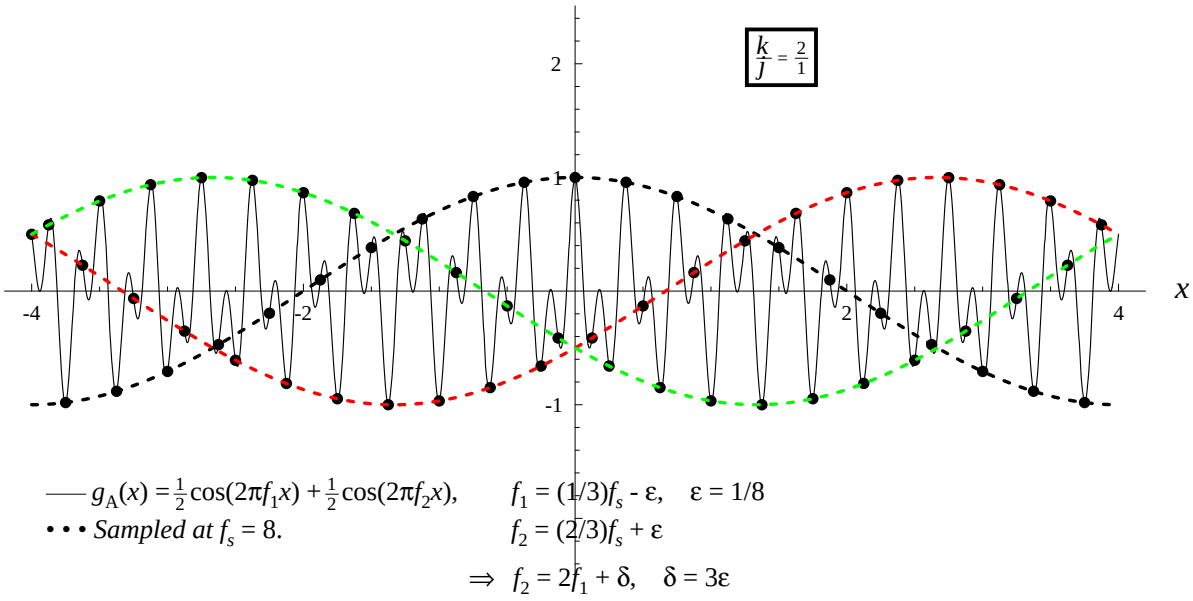

Figure B2: Illustration of Proposition B.1 for the case of $(m/n) = (1/3)$, i.e. a (1/3)-order sub-Nyquist artifact. (a) The continuous cosine $g(x) = \cos(2\pi fx)$ with frequency $f = \frac{1}{3}f_s - \varepsilon$, where $\varepsilon = 1/8$, plotted by a thin, continuous line. Its sampled version $g(x_k)$ with sampling frequency $f_s = 8$ is represented by black dots. These dots have been connected by thicker line segments in order to better convey their correct order. Note that (a) is simply a magnification of Fig. 4(d). (b) The continuous cosine sum $g_A(x) = \frac{1}{2}\cos(2\pi f_1 x) + \frac{1}{2}\cos(2\pi f_2 x)$ with frequencies $f_1 = \frac{1}{3}f_s - \varepsilon$ and $f_2 = \frac{2}{3}f_s + \varepsilon$, plotted by a thin, continuous line. Its sampled version $g_A(x_k)$ after being sampled with the same sampling frequency $f_s = 8$ is represented by black dots. Note that in rows (a) and (b) the sampled points as well as their envelope curves are identical, although the original continuous signals $g(x)$ and $g_A(x)$ are different.

(a) *Discrete-world configuration (results of sampling):*

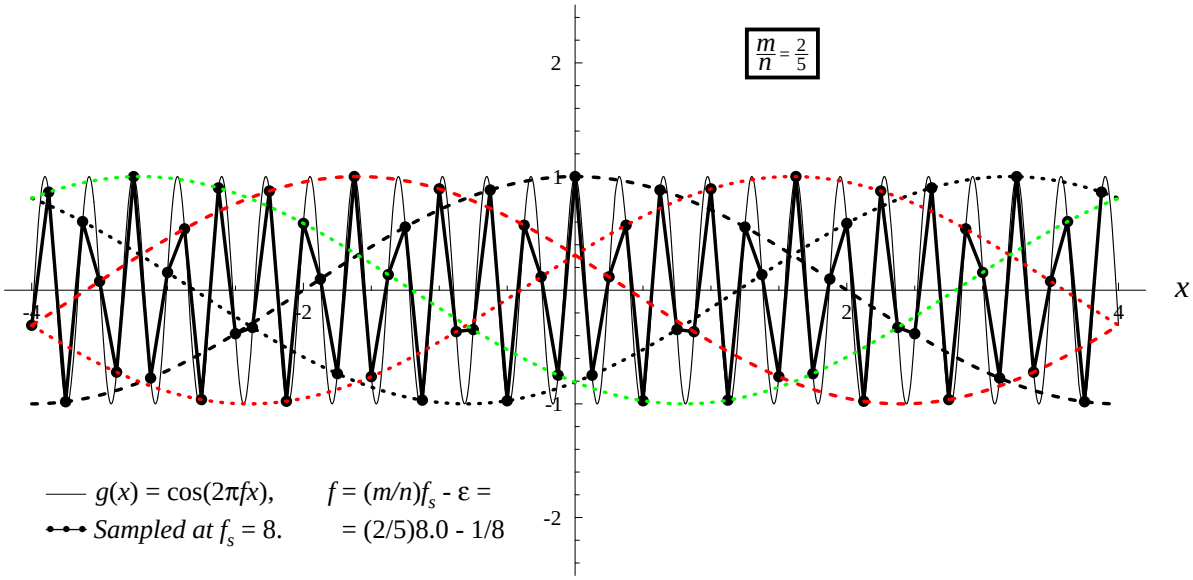

(b) *Continuous-world configuration (sum of mistuned cosines):*

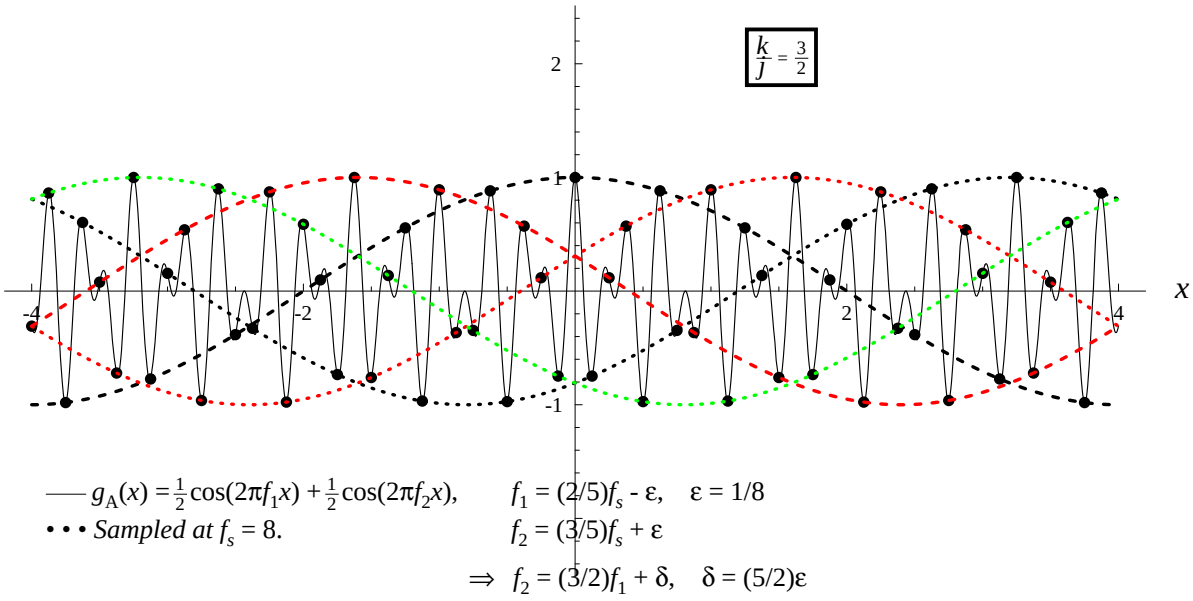

Figure B3: Illustration of Proposition B.1 for the case of $(m/n) = (2/5)$, i.e. a (2/5)-order sub-Nyquist artifact. (a) The continuous cosine $g(x) = \cos(2\pi fx)$ with frequency $f = \frac{2}{5}f_s - \varepsilon$, where $\varepsilon = 1/8$, plotted by a thin, continuous line. Its sampled version $g(x_k)$ with sampling frequency $f_s = 8$ is represented by black dots. These dots have been connected by thicker line segments in order to better convey their correct order. Note that (a) is simply a magnification of Fig. 5(d). (b) The continuous cosine sum $g_A(x) = \frac{1}{2}\cos(2\pi f_1 x) + \frac{1}{2}\cos(2\pi f_2 x)$ with frequencies $f_1 = \frac{2}{5}f_s - \varepsilon$ and $f_2 = \frac{3}{5}f_s + \varepsilon$, plotted by a thin, continuous line. Its sampled version $g_A(x_k)$ after being sampled with the same sampling frequency $f_s = 8$ is represented by black dots. Note that in rows (a) and (b) the sampled points as well as their envelope curves are identical, although the original continuous signals $g(x)$ and $g_A(x)$ are different.

$$g((n-1)/f_s) = \cos(2\pi[\tfrac{m}{n}f_s + \varepsilon](n-1)/f_s) = \cos(2\pi[\tfrac{m}{n}(n-1) + \varepsilon(n-1)/f_s])$$

$$\mathrm{env}_n\,((n-1)/f_s) = \cos(2\pi\varepsilon[(n-1)/f_s + (n-1)\tfrac{m}{n\varepsilon}]) = \cos(2\pi[\varepsilon(n-1)/f_s + (n-1)\tfrac{m}{n}])$$

so that the n-th sampled point of $g(x)$ falls on $\mathrm{env}_n(x)$.

Finally, for n+1 and on a new cycle begins, and the successive sampled points fall again on $\mathrm{env}_1(x)$, $\mathrm{env}_2(x)$, etc.

Very similar results exist also for the sine function:

Proposition B.2: Suppose we are sampling with sampling frequency f_s a continuous signal $g(x) = \sin(2\pi fx)$ whose frequency f is close to $\frac{m}{n}f_s$, i.e. $f = \frac{m}{n}f_s - \varepsilon$. The (m/n)-order sub-Nyquist artifact we obtain in the resulting sampled signal is simply the sampled version of the continuous-world beating modulation effect that appears in the continuous sine difference $g_A(x) = \frac{1}{2}\sin(2\pi f_1 x) - \frac{1}{2}\sin(2\pi f_2 x)$ whose two frequencies are $f_1 = \frac{m}{n}f_s - \varepsilon$ and $f_2 = \frac{n-m}{n}f_s + \varepsilon$. ■

Now, since Proposition B.2 bounces us back to the difference of two continuous-world sines, we can apply here Theorem A.2, using the connections provided by Eqs. (B.1) and (B.2). We thus obtain:

Theorem B.2: Suppose we are sampling with sampling frequency f_s a continuous signal $g(x) = \sin(2\pi fx)$ whose frequency f is close to $\frac{m}{n}f_s$, i.e. $f = \frac{m}{n}f_s + \varepsilon$ (where ε may be positive or negative). Then the successive sampled points $g(x_i) = \sin(2\pi fx_i)$, $i = 0, 1, 2,\ldots$ fall intermittently on $k + j = (n - m) + m = n$ interlaced periodic curves (called envelopes), each of which being a stretched and shifted version of $g(x)$. These envelopes are expressed by:

$$\begin{aligned}
&\mathrm{env}_1(x) = \sin(2\pi\varepsilon x)\\
&\mathrm{env}_2(x) = \sin(2\pi\varepsilon[x + a])\\
&\mathrm{env}_3(x) = \sin(2\pi\varepsilon[x + 2a])\\
&\qquad\ldots\\
&\mathrm{env}_n(x) = \sin(2\pi\varepsilon[x + (n-1)a])
\end{aligned} \tag{B.4}$$

where the envelope frequency is ε, and the shift a equals $\frac{m}{n}$ of the envelope's period $1/\varepsilon$, i.e. $a = \frac{m}{n\varepsilon}$. ■

Finally, as shown in Sec. 4, it turns out that an extended version of these results still holds for any periodic continuous signal $g(x)$. These generalized results can be formulated as follows:

Proposition B.3: Let $g(x)$ be a continuous periodic signal of frequency 1 and period 1. Suppose we are sampling with sampling frequency f_s the continuous periodic signal $g(fx)$ whose frequency f is close to $\frac{m}{n}f_s$, i.e. $f = \frac{m}{n}f_s - \varepsilon$. The (m/n)-order sub-Nyquist artifact we obtain in the resulting sampled signal is simply the sampled version of the continuous-world beating modulation effect that appears in the continuous "signed sum"

$g_A(x) = \frac{1}{2}(\text{even}[g(f_1x)] + \text{even}[g(f_2x)]) + \frac{1}{2}(\text{odd}[g(f_1x)] - \text{odd}[g(f_2x)])$ whose two frequencies are $f_1 = \frac{m}{n}f_s - \varepsilon$ and $f_2 = \frac{n-m}{n}f_s + \varepsilon$. ■

Figures B4, B5 and B6 illustrate this result for the case of $(m/n) = (1/2)$: Fig. B4 shows an example with an even periodic function (whose Fourier series decomposition consists of cosine components only). Fig. B5 shows an example with an odd periodic function (i.e. with sine components only). And Fig. B6 shows an example with a general periodic function (that is composed of both sine and cosine components).

Now, since Proposition B.3 bounces us back to the "signed sum" of two mistuned instances of a continuous-world periodic function, we can apply here Theorem A.3, using the connections provided by Eqs. (B.1) and (B.2). We thus obtain:

Theorem B.3: Let $g(x)$ be a continuous periodic signal of frequency 1 and period 1. Suppose we are sampling with sampling frequency f_s the continuous periodic signal $g(fx)$ whose frequency f is $f = \frac{m}{n}f_s + \varepsilon$ (where ε may be positive or negative). Then the successive sampled points $g(fx_i)$, $i = 0, 1, 2,\ldots$ fall intermittently on $k + j = (n - m) + m = n$ interlaced periodic curves (called envelopes), each of which being a stretched and shifted version of $g(x)$. These envelopes are expressed by:

$$\begin{aligned} \text{env}_1(x) &= g(\varepsilon x) \\ \text{env}_2(x) &= g(\varepsilon[x + a]) \\ \text{env}_3(x) &= g(\varepsilon[x + 2a]) \\ &\ldots \\ \text{env}_n(x) &= g(\varepsilon[x + (n-1)a]) \end{aligned} \qquad \text{(B.5)}$$

where the envelope frequency is ε, and the shift a equals $\frac{m}{n}$ of the envelope's period $1/\varepsilon$, i.e. $a = \frac{m}{n\varepsilon}$. ■

The formal proof of this result can be obtained by following the same lines as in our informal discussion in Secs. 3.3 and 4. The amplitudes of 2 in Eq. (A.12) have been cancelled out in (B.5) since the sum $g_A(x)$ in Proposition B.3 is defined with half of the function amplitudes. The intermittence, i.e. the fact that successive sampled points $g(x_i)$ fall intermittently on successive envelopes, can be easily demonstrated as in Theorem B.1:

Our sampling is performed at the points $0, 1/f_s, 2/f_s,\ldots$ At the first sampling point, $x = 0$, we have:

$$\text{env}_1(x) = g(0)$$

meaning that the first sampled point of $g(x)$ falls on $\text{env}_1(x)$.

At the second sampling point, $x = 1/f_s$, we have:

(a) *Discrete-world configuration (results of sampling):*

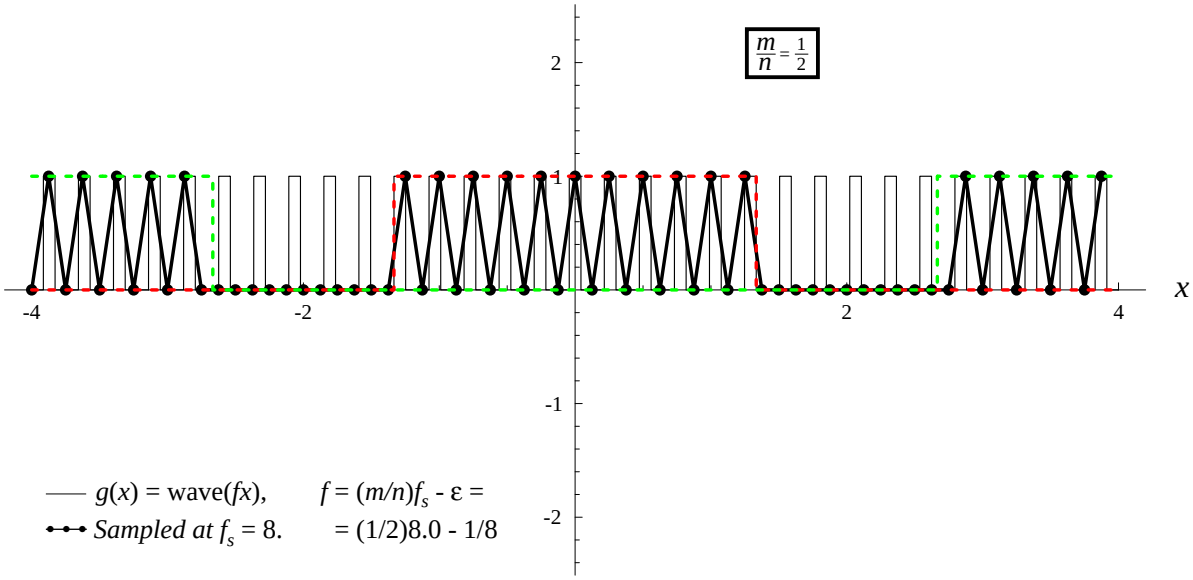

(b) *Continuous-world configuration (sum of mistuned square waves):*

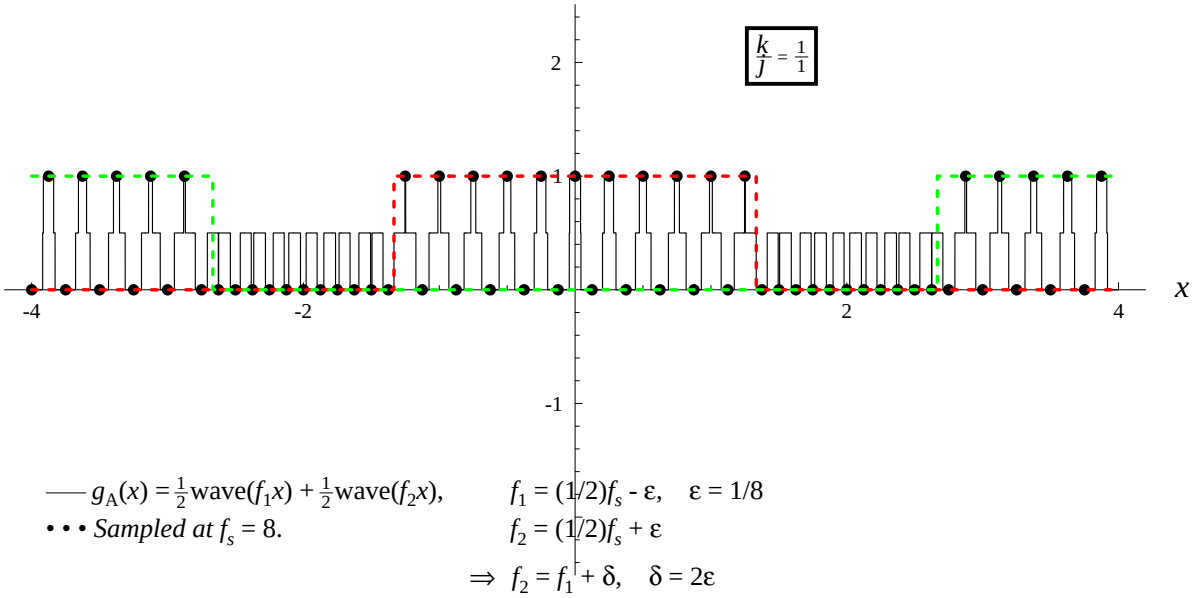

Figure B4: Illustration of Proposition B.3 for the case of $(m/n) = (1/2)$, i.e. a (1/2)-order sub-Nyquist artifact. (a) The continuous-world square wave $g(x) = \text{wave}(fx)$ with frequency $f = \frac{1}{2}f_s - \varepsilon$, where $\varepsilon = 1/8$, plotted by a thin, continuous line. Its sampled version $g(x_k)$ with sampling frequency $f_s = 8$ is represented by black dots. These dots have been connected by thicker line segments in order to better convey their correct order. Note that (a) is simply a magnification of Fig. 10(d). (b) The continuous-world wave sum $g_A(x) = \frac{1}{2}\text{wave}(f_1x) + \frac{1}{2}\text{wave}(f_2x)$ with frequencies $f_1 = \frac{1}{2}f_s - \varepsilon$ and $f_2 = \frac{1}{2}f_s + \varepsilon$, plotted by a thin, continuous line. Its sampled version $g_A(x_k)$ after being sampled with the same sampling frequency $f_s = 8$ is represented by black dots. Note that in rows (a) and (b) the sampled points as well as their envelope curves are identical, although the original continuous signals $g(x)$ and $g_A(x)$ are different.

(a) *Discrete-world configuration (results of sampling):*

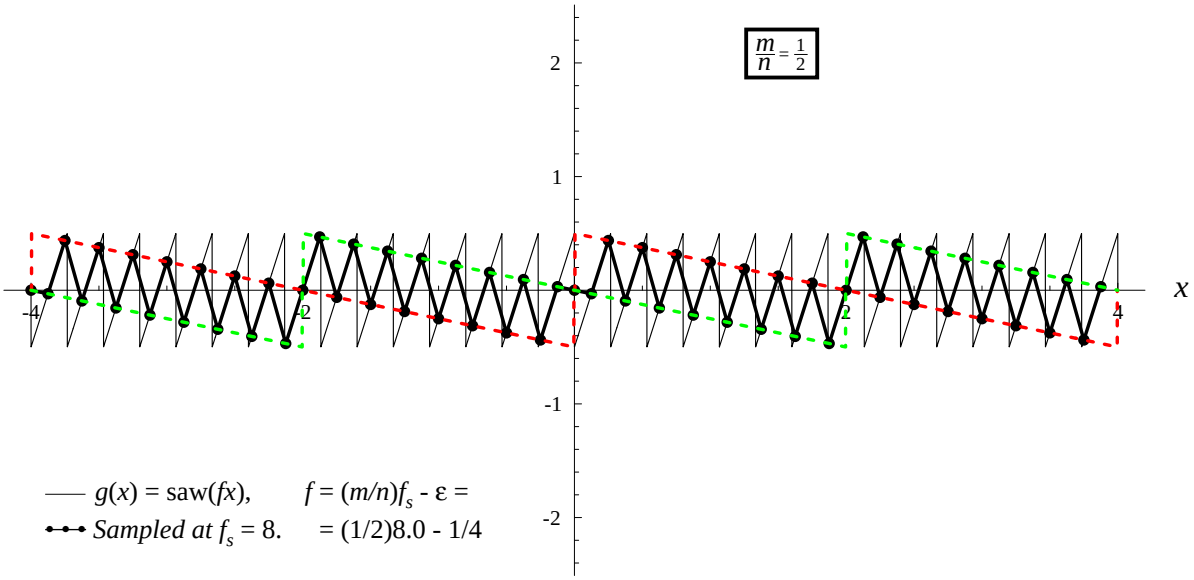

(b) *Continuous-world configuration (difference of mistuned sawtooth waves):*

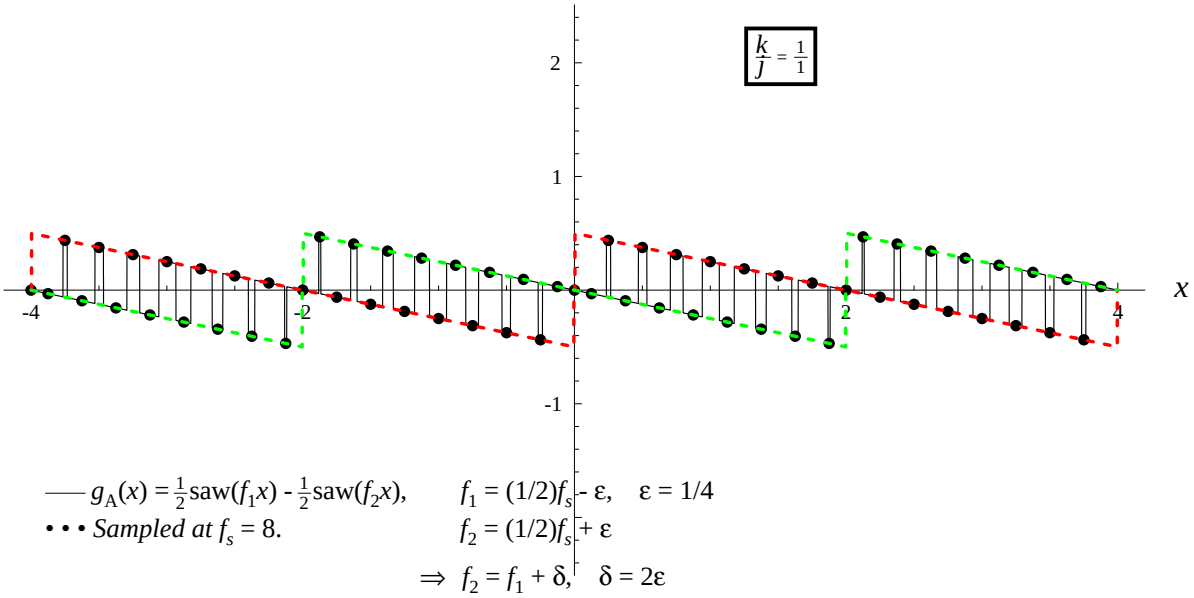

Figure B5: Illustration of Proposition B.3 for the case of $(m/n) = (1/2)$, i.e. a (1/2)-order sub-Nyquist artifact. (a) The continuous-world sawtooth wave $g(x) = \text{saw}(fx)$ with frequency $f = \frac{1}{2}f_s - \varepsilon$, where $\varepsilon = 1/4$, plotted by a thin, continuous line. Its sampled version $g(x_k)$ with sampling frequency $f_s = 8$ is represented by black dots. These dots have been connected by thicker line segments in order to better convey their correct order. (b) The continuous-world wave difference $g_A(x) = \frac{1}{2}\text{saw}(f_1x) - \frac{1}{2}\text{saw}(f_2x)$ with frequencies $f_1 = \frac{1}{2}f_s - \varepsilon$ and $f_2 = \frac{1}{2}f_s + \varepsilon$, plotted by a thin, continuous line. Its sampled version $g_A(x_k)$ after being sampled with the same sampling frequency $f_s = 8$ is represented by black dots. Note that in rows (a) and (b) the sampled points as well as their envelope curves are identical, although $g(x)$ and $g_A(x)$ are different.[16]

[16] Note that a Fourier series development assigns to any discontinuity point of $g(x)$ the midvalue at that point [7, pp. 235-236]. Because Theorem A.3 and hence Theorem B.3 rely on the Fourier series development of $g(x)$, we must use here a definition of saw(x) that satisfies this rule. Further details and references on the midvalue rule can be found in [5, Sec. 8.2].

(a) *Discrete-world configuration (results of sampling):*

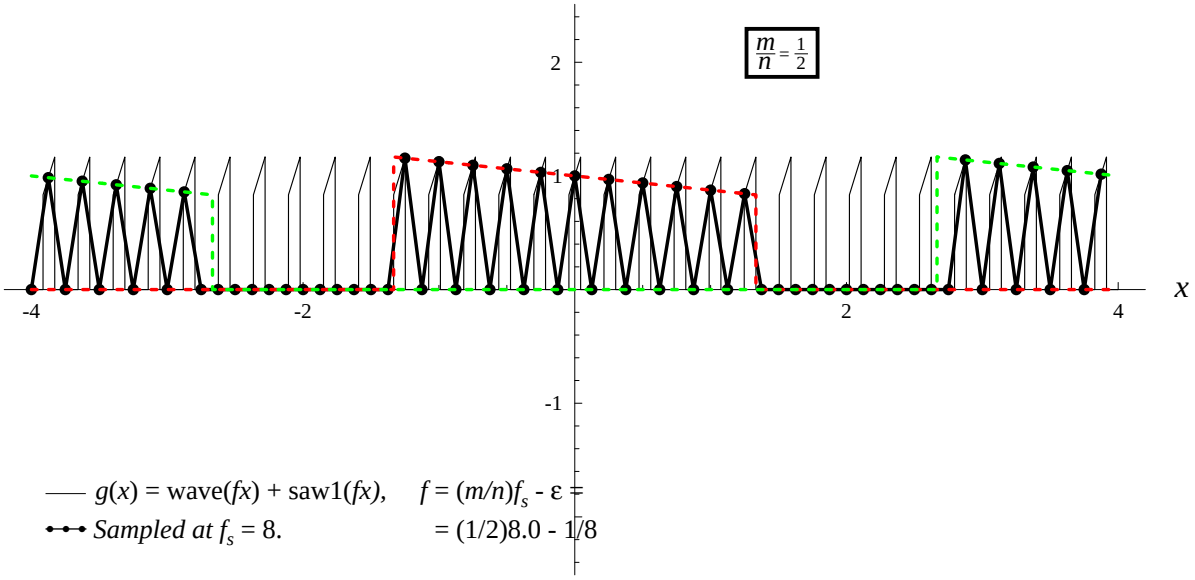

(b) *Continuous-world configuration (sum of mistuned complex periodic waves):*

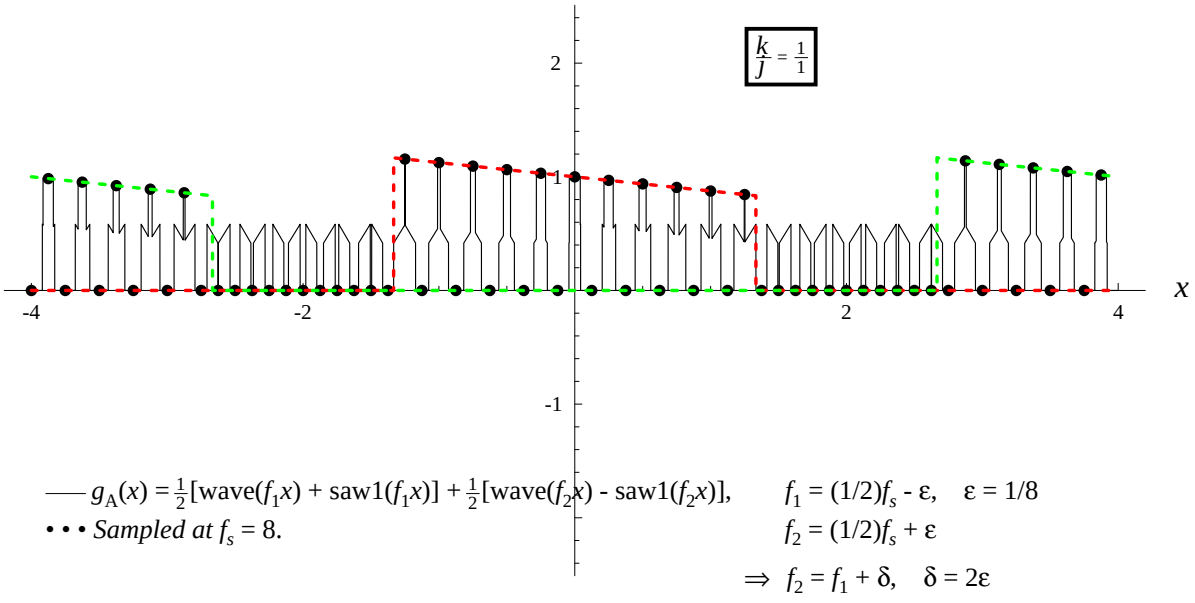

Figure B6: Illustration of Proposition B.3 for the case of $(m/n) = (1/2)$, i.e. a (1/2)-order sub-Nyquist artifact. (a) The continuous-world asymmetric wave $g(x) = \text{even}[g(x)] + \text{odd}[g(x)] = \text{wave}(fx) + \text{saw1}(fx)$, where saw1$(x)$ is a sawtooth wave that is shifted by half a period and truncated to the pulse-width of the square wave. The function $g(x)$ with frequency $f = \frac{1}{2}f_s - \varepsilon$, $\varepsilon = 1/8$, is plotted here by a thin, continuous line. Its sampled version $g(x_k)$ with sampling frequency $f_s = 8$ is represented by black dots. These dots are connected by thicker line segments in order to better convey their correct order. (b) The continuous-world "signed sum" wave $g_A(x) = \frac{1}{2}\text{wave}(f_1x) + \frac{1}{2}\text{wave}(f_2x) + \frac{1}{2}\text{saw1}(f_1x) - \frac{1}{2}\text{saw1}(f_2x)$ with frequencies $f_1 = \frac{1}{2}f_s - \varepsilon$ and $f_2 = \frac{1}{2}f_s + \varepsilon$, plotted by a thin, continuous line. Its sampled version $g_A(x_k)$ after being sampled with the same sampling frequency $f_s = 8$ is represented by black dots. Note that in rows (a) and (b) the sampled points as well as their envelope curves are identical, although the original continuous signals $g(x)$ and $g_A(x)$ are different.

$$g(f/f_s) = g([\tfrac{m}{n}f_s + \varepsilon]/f_s) = g(\tfrac{m}{n} + \varepsilon/f_s)$$

$$\mathrm{env}_2(1/f_s) = g(\varepsilon[1/f_s + \tfrac{m}{n\varepsilon}]) = g(\varepsilon/f_s + \tfrac{m}{n})$$

meaning that the second sampled point of $g(x)$ falls on $\mathrm{env}_2(x)$.

Similarly, at the n-th sampling point, $x = (n–1)/f_s$, we have:

$$g((n–1)f/f_s) = g([\tfrac{m}{n}f_s + \varepsilon](n–1)/f_s) = g(\tfrac{m}{n}(n–1) + \varepsilon(n–1)/f_s)$$

$$\mathrm{env}_n((n–1)/f_s) = g(\varepsilon[(n–1)/f_s + (n–1)\tfrac{m}{n\varepsilon}]) = g(\varepsilon(n–1)/f_s + (n–1)\tfrac{m}{n})$$

so that the n-th sampled point of $g(x)$ falls on $\mathrm{env}_n(x)$.

Finally, for n+1 and on a new cycle begins, and the successive sampled points fall again on $\mathrm{env}_1(x)$, $\mathrm{env}_2(x)$, etc.

Note that Theorems B.1 and B.3 are equivalent (up to some formulation details) to Theorems 1 and 2 in [1], which have been proved there in a completely different way, based on signal-domain considerations only.

Appendix C: Miscellaneous remarks

In this appendix we provide some further remarks that may shed new light on various aspects of our discussion.

Remark 6 (*cases with n = 1, i.e. true moiré effects*):

It is interesting to ask now whether the spectral-domain approach we presented here still works in cases with $n = 1$. As we have seen in [1, Sec. 3], in such cases all the sampled points $g(x_k)$ fall on a single envelope, which corresponds to a *true* moiré effect: there are no interlaced envelopes, and the sampled points no longer jump intermittently from one curve to another as they do in a sub-Nyquist artifact. Formally, in cases with $n = 1$ Theorem A.1 gives us $k + j = (1–m) + m = 1$ modulating envelopes, whose frequency is $f_{\mathrm{env}} = \frac{j}{k+j}\delta = m\delta = m(1/m)\ \varepsilon = \varepsilon$, which is indeed correct (see for example the true sampling moiré effects with $n = 1$ in Figs. 1 and 2). But this resulting envelope curve turns out to be irrelevant to the cosine sum in question (namely, it is not a true envelope thereof). The reason is, as we can see in Remark 4 in Appendix A, that Theorem A.1 deals with sums of continuous cosines; such sums can only give modulations – but never true moirés, which correspond to new low frequencies. Therefore, Theorem A.1 cannot handle situations where a true moiré effect is generated, such as the first-order moiré shown in Figs. 1 and 7(a), or the second-order moiré shown in Figs. 2 and 7(b). And indeed, true sampling moiré effects are explained by the spectral approach in the classical way, i.e. by the presence in the spectrum of new low-frequency impulses that are introduced by the sampling-induced replicas (see, for example, rows (a) and (b) in Fig. 7). The spectral approach *only* recurs to Theorem A.1 for the explanation of pure or hybrid sub-Nyquist artifacts (like in rows (c)-(e) of Fig. 7 or in Fig. 8). ■

Remark 7 (*moiré effects due to higher harmonics*):

In cases where the original continuous periodic function $g(x)$ contains only the fundamental frequency f but no higher harmonics, sampling moiré effects may only occur when an impulse $mf_s - f$ happens to fall close to the spectrum origin. This configuration can only give $(m,-1)$ moiré effects (see, for example, the (1,-1) moiré in Figs. 7(a) and 1, and the (2,-1) moiré in Figs. 7(b) and 2). However, when the original continuous periodic function $g(x)$ contains the n-th harmonic of f, too, sampling moiré effects may also occur whenever an impulse $mf_s - nf$ falls close to the origin. This may give rise to an $(m,-n)$ sampling moiré effect (see, for example, the (1,-2) moiré in Figs. 8(b) and 9). In the first case, where $n = 1$, all the sampled points $g(x_k)$ fall on a single envelope, which corresponds indeed to a pure moiré effect in the sampled signal (see Figs. 1 and 2). But in the second case, when $n > 1$, the sampled points oscillate between n intermittent envelopes, giving a hybrid moiré effect (like in Fig. 9). ■

Remark 8 (*omnipresence of modulating envelopes*):

We saw in Theorems A.1-A.3 that two mistuned instances of a continuous periodic function having frequencies f_1 and f_2, where $f_2 \approx (k/j)f_1$, may give rise to a modulation effect. It is important to note that modulating envelopes can be traced along our continuous-world signal $s(x)$ in all circumstances, whether the frequency f_2 is close to $(k/j)f_1$ or not (note that Theorems A.1-A.3 hold for *any* value of δ, be it small or large). Moreover, for any given f_1 and f_2, different sets of modulating envelopes belonging to different k, j values can be always traced along the very same signal $s(x)$ (see Fig. C2).[17] Nevertheless, these modulating envelopes only become relevant and truly visible when f_2 is sufficiently close to $(k/j)f_1$, i.e. when $\delta = f_2 - (k/j)f_1$ is close to zero (so that the (k/j)-order modulation effect is close to its singular state; see Remark 3 in Sec. A.1).[18] Furthermore, the larger the integer numbers k,j (and hence the number $k+j$ of interlaced envelopes), the less visible and prominent the envelopes become (see Fig. C1). The reason is that when several envelopes are intermingled together it becomes more difficult for the eye to detect and follow each of the envelopes separately, i.e. to detect a visible order within the oscillations of the signal $s(x)$. Thus, although modulating envelopes are always present in the signal $s(x)$, in practice the resulting beating effect is only visible for relatively low values of k, j and δ. In fact, the signal $s(x)$ is simultaneously modulated by various sets of interlaced envelopes, each set corresponding to different k, j, δ values (see Fig. C2); but the envelopes truly become visible only when the values of k, j and δ are relatively low. ■

Remark 9 (*the main theorem of* [1]):

For the sake of completeness, we repeat here Theorem 2 from [1]. Note that this theorem was proved there using signal-domain considerations only:

---

[17] Note that for any given f_1 and f_2 there exist infinitely many values of k,j and δ that satisfy Eq. (A.5), $f_2 = (k/j)f_1 + \delta$. For any chosen k and j, there exists a corresponding δ value that satisfies the equation.

[18] Note that when the k,j values are ill-adapted and give a δ value that is too far from zero, each of the interlaced envelope curves "skims" $s(x)$ within shorter intervals, that are also spaced farther apart. For example, consider Fig. C2 and compare there row (a), in which $\delta = 0.1$, with rows (b) and (c), in which $\delta = 1.1$ and $\delta = -0.9$, respectively.

The (k/j)-order modulation effect in $s(x) = \cos(2\pi f_1 x) + \cos(2\pi f_2 x)$ with:

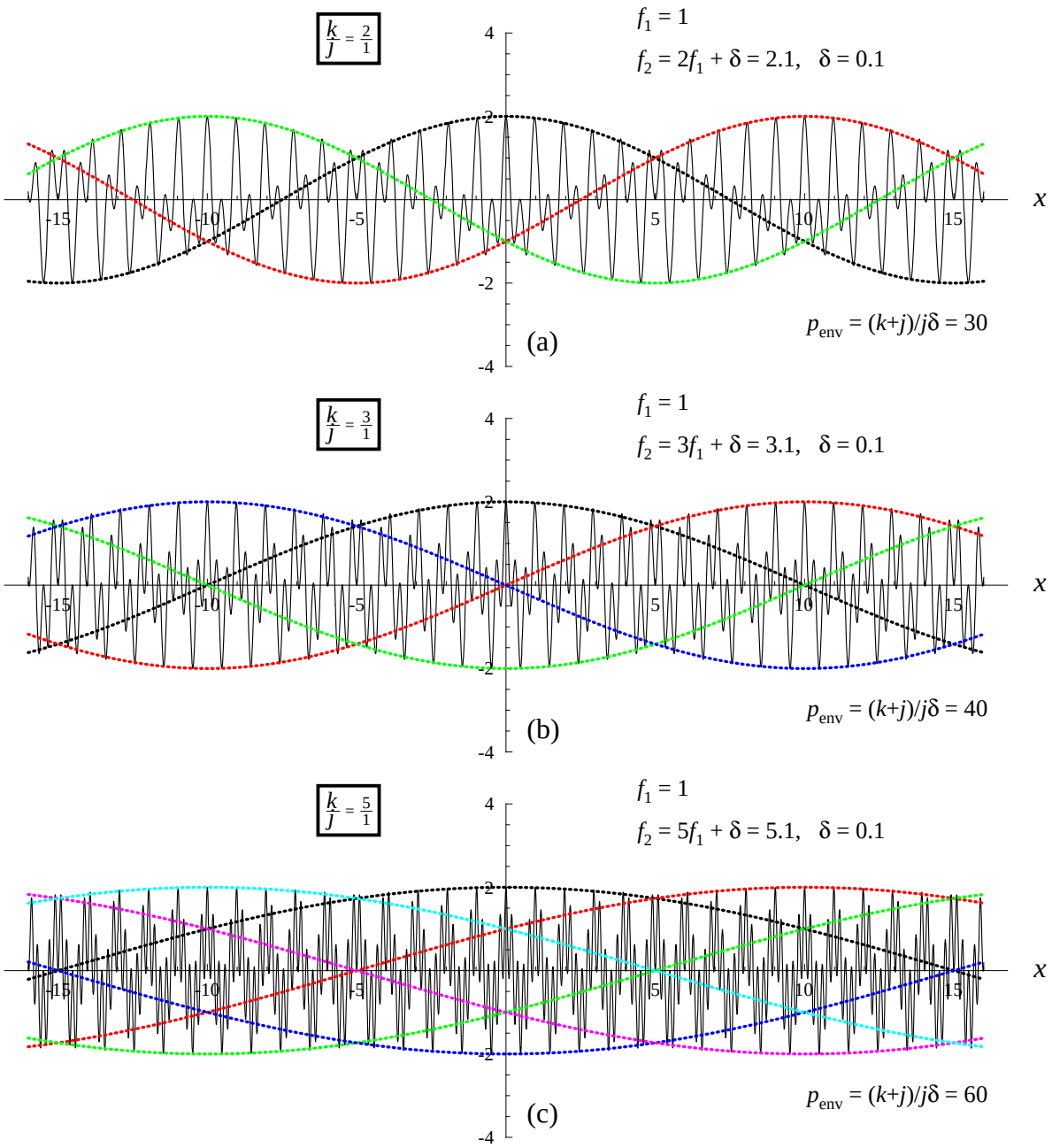

Figure C1: Illustration of Remark 1, Appendix A: The transition between "*modulation-shaped*" cases of type (3) and "*riding-shaped*" cases of type (2) is not abrupt, but rather smooth. Each row shows the sum $s(x)$ of two continuous cosinusoidal waves with frequencies $f_1 = 1$ and $f_2 = kf_1 + \delta$, with $\delta = 0.1$: (a) $k = 2$ (compare with Fig. A3). (b) $k = 3$. (c) $k = 5$. Case (a) is clearly of type (3), but case (c) is already closer to type (2), just like Fig. A2(a). In cases of type (2) the modulation described by Theorem A.1 is already too weak to be noticed, but formally the theorem still holds (see row (c)).

The (k/j)-order modulation effect in $s(x) = \cos(2\pi f_1 x) + \cos(2\pi f_2 x)$ with:

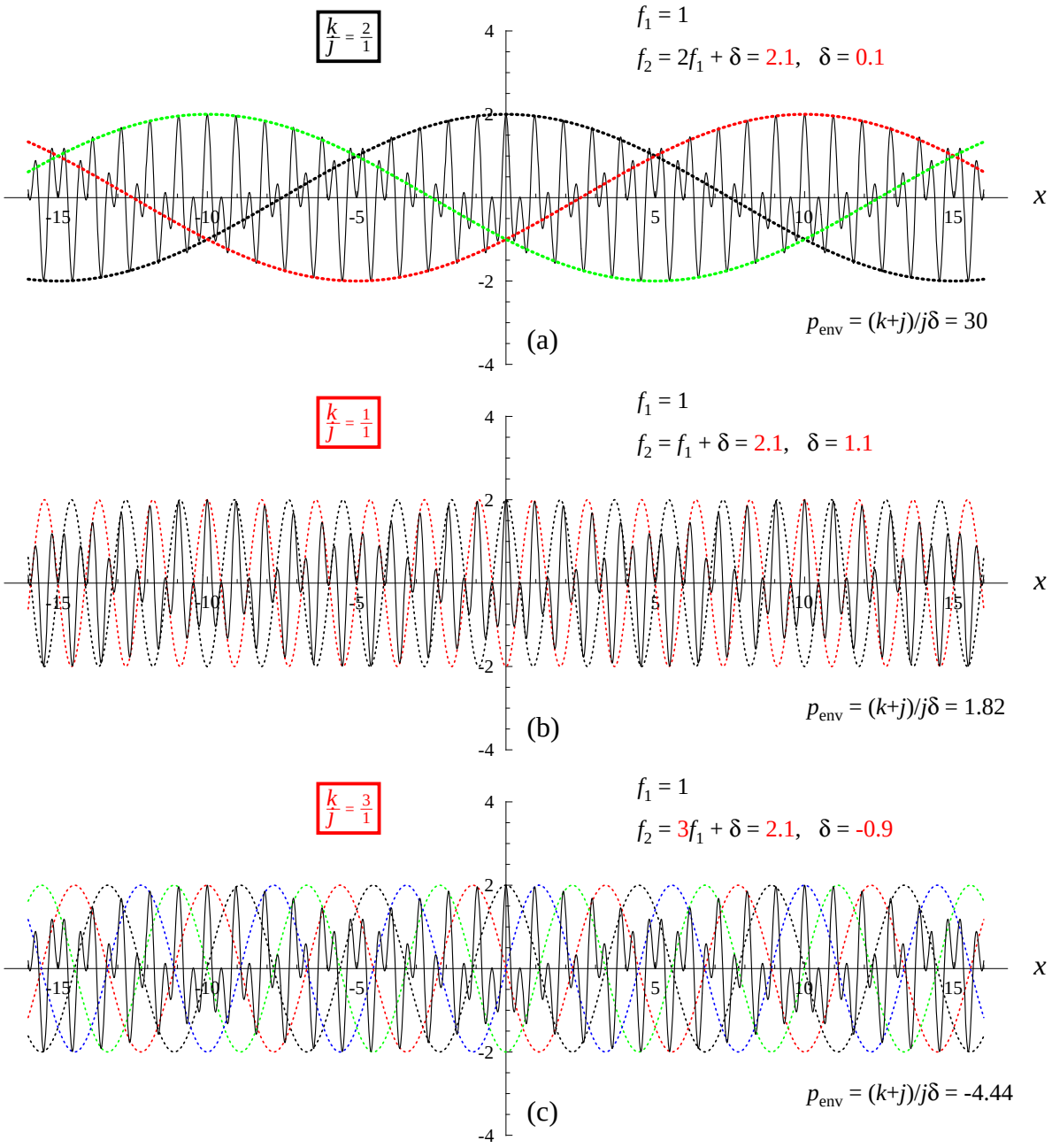

Figure C2: Illustration of Remark 8, Appendix C: All rows show the very same sum $s(x)$ of two continuous cosines with the same frequencies $f_1 = 1$ and $f_2 = 2.1$. And yet, different sets of modulating envelopes belonging to different k, j, δ values can be always traced along the very same sum $s(x)$: (a) $k = 2, j = 1$, $\delta = 0.1$, so that $f_2 = 2f_1 + \delta = 2.1$. (b) $k = 1, j = 1$, $\delta = 1.1$, so that $f_2 = f_1 + \delta = 2.1$. (c) $k = 3, j = 1$, $\delta = -0.9$, so that $f_2 = 3f_1 + \delta = 2.1$. Note that f_1 and f_2 do not vary from row to row, so that $s(x)$ remains identical. Although all the modulating envelopes in all rows "envelop" the signal $s(x)$ correctly, the modulating envelopes only become relevant and truly visible for k,j values that give δ close to zero, i.e. when $f_2 \approx (k/j)f_1$, as is the case in (a).

Suppose we are given a continuous periodic function $g(x)$ having frequency f and period $p = 1/f$, and that we sample this function at the sampling frequency f_s, i.e. with a sampling step of $\Delta x = 1/f_s$. If the frequency f of our given function $g(x)$ differs by ε from the singular frequency $\frac{m}{n}f_s$ for some integers m and n:

$$f = \frac{m}{n}f_s + \varepsilon$$

(where ε may be positive or negative), then the successive sampled points of our original function, $g(x_k)$, $k = 0, 1, 2,...$ fall intermittently on one of n low-frequency envelopes, which are simply expanded (stretched) versions of $g(x)$ having the frequency ε and period $1/\varepsilon$, and which only differ from each other in their phase. Any two successive envelopes are displaced from each other by $\frac{m}{n}$ of their period $1/\varepsilon$, i.e. by a shift of $a = \frac{m}{n\varepsilon}$. ■

References

[1] I. Amidror, "Tutorial: Sub-Nyquist artifacts and sampling moiré effects," Technical Report No. 203756, EPFL, Lausanne, 2014. Available online at: http://infoscience.epfl.ch/record/203756 (accessed March 18, 2015). A significantly shortened version of this article has been published in: I. Amidror, "Sub-Nyquist artifacts and sampling moiré effects," *Royal Society Open Science*, 2: 140550, 2015, pp. 1-15. Available online at: http://dx.doi.org/10.1098/rsos.140550 (accessed March 18, 2015).

[2] G. L. Williams, "Sub-Nyquist distortions in sampled data, waveform recording, and video imaging," NASA Technical Memorandum TM-2000-210381, Ohio, 2000.

[3] J. D. Foley, A. van Dam, S. K. Feiner and J. F. Hughes, *Computer Graphics: Principles and Practice.* Addison-Wesely, Reading, Massachusetts, 1990 (second edition).

[4] D. P. Mitchell and A. N. Netravali, "Reconstruction filters in computer graphics," Proceedings of SIGGRAPH 1988, *Computer Graphics*, Vol. 22, No. 4, 1988, pp. 221–228.

[5] I. Amidror, *Mastering the Discrete Fourier Transform in One, Two or Several Dimensions: Pitfalls and Artifacts*. Springer, NY, 2013.

[6] S. W. Smith, *Digital Signal Processing: A Practical Guide for Engineers and Scientists*. Newnes, Amsterdam, 2003.

[7] R. N. Bracewell, *The Fourier transform and its Applications*. McGraw-Hill, Boston, 2000 (third edition).

[8] E. O. Brigham, *The Fast Fourier Transform and Its Applications.* Prentice-Hall, NJ, 1988.

[9] R. Plomp, "Beats of mistuned consonances," *Journal of the Acoustical Society of America*, Vol. 42, No. 2, 1967, pp. 462–474.

[10] J. W. Harris and H. Stocker, *Handbook of Mathematics and Computational Science*. Springer, NY, 1998.

[11] T. D. Rossing, F. R. Moore and P. A. Wheeler, *The Science of Sound*. Addison Wesley, San Francisco, 2002 (third edition).

[12] J. G. Roederer, *The Physics and Psychophysics of Music: An Introduction*. Springer, NY, 2008 (fourth edition).

[13] E. J. Heller, *Why You Hear What You Hear*. Princeton University Press, NJ, 2013.

[14] T. D. Rossing and K. Dols, "Second-order beats between complex tones," *The Catgut Acoustical Society Newsletter*, No. 25, 1976, pp. 17–18. Available online at: http://purl.stanford.edu/gt654mx8229 (accessed July 4, 2014).

[15] I. Amidror and R. D. Hersch, "The role of Fourier theory and of modulation in the prediction of visible moiré effects," *Journal of Modern Optics*, Vol. 56, No. 9, 2009, pp. 1103–1118.

[16] I. Amidror, *The Theory of the Moiré Phenomenon, Volume I: Periodic Layers*. Springer, NY, 2009 (second edition).

[17] I. N. Bronshtein and K. A. Semendyayev, *Handbook of Mathematics*. Springer, Berlin, 1997 (reprint of the third edition).

[18] W. M. Hartmann, *Signals, Sound and Sensation*. American Institute of Physics, NY, 2004 (corrected 5th printing).